Nano Research
2019, 12(10): 2407–2436
ISSN 1998-0124 CN 11-5974/O4
https://doi.org/10.1007/s12274-019-2441-5

Review Article

Unlocking the door to highly efficient Ag-based nanoparticles catalysts for $NaBH_4$-assisted nitrophenol reduction

Guangfu Liao[1], Yan Gong[2], Liu Zhong[1], Jiasheng Fang[3], Li Zhang[4], Zushun Xu[5] (✉), Haiyang Gao[1] (✉), and Baizeng Fang[6] (✉)

[1] *School of Materials Science and Engineering, Key Laboratory for Polymeric Composite and Functional Materials of Ministry of Education, Guangdong Laboratory of High-Performance Polymer Composites, Sun Yat-sen University, Guangzhou 510275, China*
[2] *Department of Biomaterials, College of Materials, Xiamen University, Xiamen 361005, China*
[3] *School of Environment and Civil Engineering, Dongguan University of Technology, Dongguan 52308, China*
[4] *Department of Chemistry, City University of Hong Kong, Hong Kong 999077, China*
[5] *Hubei Collaborative Innovation Center for Advanced Organic Chemical Materials, Ministry of Education Key Laboratory for The Green Preparation and Application of Functional Material, Hubei University, Wuhan 430062, China*
[6] *Department of Chemical & Biological Engineering, University of British Columbia, 2360 East Mall, Vancouver, BC, V6T 1Z3, Canada*

Received: 2 March 2019 / **Revised:** 28 April 2019 / **Accepted:** 17 May 2019

ABSTRACT

Ag-based nanoparticles (NPs) catalysts have recently attracted increasing attention in $NaBH_4$-assisted nitrophenol reduction, especially in 4-nitrophenol (4-NP) reduction. Moreover, Ag-based NPs catalysts are considered to be very promising for practical applications because of their fascinating advantages, e.g., easy preparation, relatively low cost and less toxicity, high activity and good stability. Basically, the size and shape of Ag NPs are well known as the key factors for achieving highly efficient catalytic reduction of 4-NP. In this review, three highly efficient Ag-based NPs catalysts (supported Ag NPs, anisotropic Ag NPs and bimetallic Ag NPs) are highlighted for the 4-NP reduction, including the catalytic mechanism and reaction rate caused by their adjustments in size and shape. Although high catalytic activity has been demonstrated by several Ag-based NPs catalysts, further improvement in the catalytic performance is still desired. In terms of the most recent progress in Ag-based NPs catalysts for 4-NP reduction, this review provides a comprehensive assessment on the material selection, synthesis and catalytic characterizations of these catalysts. Moreover, this review aims to correlate the catalytic performance of Ag-based NPs catalysts with their size and shape, guiding the development of novel cost-effective and high-performance catalysts.

KEYWORDS

Ag-based nanoparticles catalysts, catalytic reduction, 4-nitrophenol, catalytic activity, stability

1 Introduction

During recent decades, the conversion of pernicious aqueous phase organic wastes into recyclable products with low toxicity has become a hot research topic [1–6]. Nitrophenol (NP), especially 4-nitrophenol (4-NP) with high toxicity and carcinogenic nature, has been regarded to be one of the most common refractory water contaminants and environmentally hazardous materials. Interestingly, 4-aminophenol (4-AP) with low toxicity nature, which is the corresponding reduction product, has shown its great value in various areas such as corrosion inhibition, anticorrosion lubrication, drying agent, photographic development, etc. [7, 8]. Therefore, developing cost-effective, stable, and highly active catalysts for 4-NP reduction is highly desirable. The most commonly used but highly efficient strategy for the catalytic reduction of 4-NP to 4-AP is effectively utilizing metal NPs such as Ag NPs [9], Au NPs [10], Pd NPs [11], and Pt NPs [12] as catalysts and $NaBH_4$ as a reductant. Among these metal NPs catalysts, Ag NPs have been widely used as one of the most effective catalysts due to their several unique advantages. For example, the easy regulation in the catalytic activity by tuning the particle size, shape, and temperature [13], the low temperature requirement for the activation of Ag NPs catalysts [14], the relatively low price for practical application, namely, less than 1/50 of Au or Pt, and about 1/25 of Pd [15], and the relatively low toxicity for environmental application [16].

Despite Ag NPs are an ideal catalyst for $NaBH_4$-assisted 4-NP reduction, single Ag NPs used as a catalyst have many issues such as easy oxidation and aggregation, poor stability, and low catalytic activity [17]. Three approaches have been reported so far to solve these problems. First, the incorporation of Ag NPs into various substrates can effectively reduce Ag NPs aggregation because of the strong interaction between them, thus improving their catalytic activity [18, 19]. Second, anisotropic Ag NPs with more active surface sites are used instead of common spherical Ag NPs due to the fact that the small molecule reactants are easy to be absorbed on the anisotropic Ag NPs surface because of their sharp edges and corners [20, 21]. Third, bimetallic Ag NPs are applied to replace their corresponding monometallic Ag NPs because of the composition-dependent property and synergistic effect of the bimetallic Ag NPs [22]. These three approaches can not only effectively increase catalytic performance of Ag-based catalysts, but also endow them with some new functions such as magnetic recoverability and environmental benignity. Remarkably, since the first reported by Pal's group [23, 24], the research interest in Ag-based catalysts-catalyzed 4-NP reduction

Address correspondence to Zushun Xu, zushunxu@hubu.edu.cn; Haiyang Gao, gaohy@mail.sysu.edu.cn; Baizeng Fang, bfang@chbe.ubc.ca

has risen rapidly, and particularly, the number of published papers has increased considerably since 2013.

Although various applications of Ag-based catalysts [15, 25–29] have been reported, there is not systematic review articles specifically focused on the Ag-based NPs catalysts for $NaBH_4$-assisted 4-NP reduction. This review will focus on the reaction mechanism and latest developments on highly efficient Ag-based catalysts for $NaBH_4$-assisted 4-NP reduction. The main focus will be the investigation of different methods for improved catalytic activity, including the utilization of various substrates for loading Ag NPs (such as polymers, carbons, oxides, metal-organic frameworks, porous organic polymers, etc.) to effectively reduce Ag NPs aggregation, and a series of anisotropic Ag NPs (such as Ag nanodisks, Ag nanocages, hollow Ag nanospheres, etc.) and bimetallic Ag NPs (alloy, core-shell and anisotropic bimetallic Ag NPs), which possess much higher catalytic activity compared to commonly used bulk Ag NPs.

2 Reaction mechanism

The reaction pathway for the catalytic reduction of 4-NP to 4-AP through Ag-based NPs catalysts with $NaBH_4$ is shown in Fig. 1 [14]. $NaBH_4$ is firstly converted to $B(OH)_4^-$ and active hydrogen species via hydrolysis reaction. The generated active hydrogen species and 4-NP is then adsorbed on Ag NPs surface. Next, the active hydrogen species adsorbed on Ag NPs surface will further react with 4-NP to produce 4-AP. To make it clear, the catalytic mechanism of 4-NP reduction Ag-based NPs catalysts with $NaBH_4$ is illustrated in Fig. 2. In step A, 4-NP is firstly reduced to 4-nitrosophenol, which is then rapidly converted into 4-hydroxylaminophenol (Hx). Among them, the Hx is a stable intermediate. It is then converted into the final compounds (4-AP) as shown in step B, which is the rate-determining step. Notably, all reduction reactions are carried out on Ag NPs surface with an adsorption-desorption equilibrium [30].

The 4-NP reduction through using $NaBH_4$ as reducing agent in aqueous solution and catalyzed by Ag-based NPs catalysts can be light-monitored through UV–vis spectroscopy, and the decrease rate of the absorption peak of 4-NP at 400 nm is considered as a common evaluation criterion for comparing the catalytic property of various Ag-based NPs catalysts. For this kind of catalytic reaction, the diffusion of the reactants to Ag NPs is expeditious when compared to the rate-determining step (step B). The competition between mass transport and chemical reaction can be estimated by the second Damköhler number (DaII), which reflects the ratio of the reaction rate to the diffusion rate

$$\mathrm{DaII} = \frac{kc^{n-1}}{\beta a} \quad (1)$$

where k is the reaction rate constant, c is the reactants concentration, n is the reaction order, β is the mass transport coefficient, and a is the total area of the interface [31–33]. When DaII << 1, the diffusion of the reactants to or from the Ag NPs surface is faster than that of chemical reaction on Ag NPs surface. When DaII > 1, the diffusion control must be considered. Generally, DaII can be estimated easily once the kinetic constant has been calculated so that the problem of possible diffusion control can be solved without any restriction. Moreover, the reduction of 4-NP cannot be controlled by diffusion because DaII is in the order of 10^{-3} via the analysis of the model reactions [32].

Langmuir-Hinshelwood model elucidates in details the reaction kinetics if all steps are envisaged to conduct solely on Ag NPs surface [34]. Both reactants (BH_4^- and 4-NP) are firstly adsorbed on Ag NPs surface before the reaction occurs. The adsorption of BH_4^- and 4-NP is expeditious, and it is modeled by an equilibrium process depicted by the Langmuir isotherm. The adsorbed reactant species then react with each other, and finally the compounds are decomposed

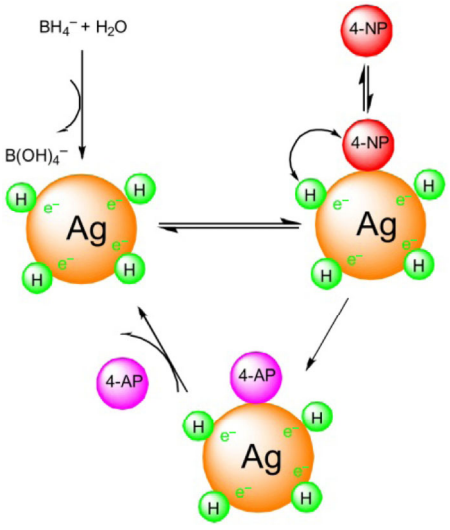

Figure 1 The Langmuir-Hinshelwood mechanism model for 4-NP reduction via Ag-based NPs catalysts with $NaBH_4$.

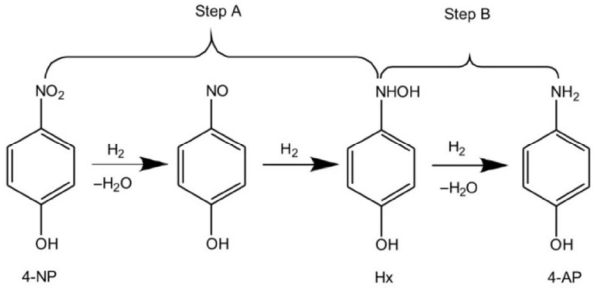

Figure 2 Proposed mechanism of 4-NP reduction via Ag-based NPs catalysts with $NaBH_4$.

from the Ag NPs surface. This model gives an accurate illustration of the reaction kinetics. Usually, the concentration of $NaBH_4$ is greater than the concentration of Ag-based NPs catalysts and 4-NP, and the catalytic reaction rates can be assumed to rely solely on the concentration of 4-NP [35]. Therefore, the reaction rate constant (k) can be measured directly by the slope of the linear correlation of $\ln(A/A_0)$ with time t according to first-order rate law. The k is calculated to vary directly as the total surface area (S) available in the Ag NPs [36]. Thus, two kinetic constants k and k_1 can be derived by Eq. (2)

$$\frac{-\mathrm{d}c_t}{\mathrm{d}t} = kc_t = k_1 S c_t \quad (2)$$

where c_t is the concentration of 4-NP at time t, k_1 is the rate constant normalized to S, and S is the total surface area of Ag NPs. The reaction rate constant k is a key parameter for evaluating catalytic activity, generally, the higher the k value the higher the catalytic activity.

3 Substrates-supported Ag NPs for 4-NP reduction

It is well known that single Ag NPs used as a catalytic material suffer from easy oxidation and aggregation issues. A very effective strategy to solve these issues is to incorporate Ag NPs into or onto different matrixes [37]. Recently, many materials such as polymers, carbons, oxides, metal-organic frameworks (MOFs) and porous organic polymers (POFs), have already been employed as common matrixes to construct Ag-based NPs catalysts.

3.1 Polymer-supported Ag NPs for 4-NP reduction

Polymers including polystyrene (PS), conductive polymer, cellulose,

dendrimers, etc., have recently been widely used as promising catalyst supports for supporting Ag NPs because of their fantastic merits, e.g., high chemical/thermal/environmental stability and strong interaction with Ag NPs, and tunable morphology as well as low cost and easy preparation [38]. Here, the comparison of various polymer-supported Ag NPs catalysts for 4-NP reduction is summarized (Table 1).

3.1.1 *PS-supported Ag NPs*

PS is proverbially used as templates for supporting Ag NPs due to its controllable sizes and uniform spherical shapes. Li's group [39] reported that Ag NPs could be loaded on the PS microspheres surface by a facile and controllable strategy on the basis of colloid thermodynamics. Surface pretreatments of PS microspheres endowed the obtained Ag NPs with small size and uniform distribution. Analogously, meta-stable state PS microspheres were firstly synthesized in presence of azodiisobutyronitrile (AIBN) and polyvinyl pyrrolidone (PVP), and then $NaBH_4$ was used as a reducing agent to reduce the Ag precursor to hydrophilic Ag NPs [40]. However, the size of Ag NPs prepared in these works is relatively large (~ 54 nm) because of the weak interaction force between Ag NPs and PS microspheres, and thus leading to a relatively low catalytic activity ($k = 3.49 \times 10^{-3}$·s^{-1}).

To further decrease the supported Ag NPs size, functional PS was found to be an ideal substrate to load Ag NPs due to their stronger interaction force with Ag NPs [41–44]. The strong interaction forces endowed the obtained Ag-based catalysts with high stability and recyclability. Mao's group [45] proposed a simple two-step strategy to develop sesame sticks-like Fe_3O_4@PS/polydopamine (PDA)-Ag nanocomposite tubes with controllable size and highly dispersed Ag NPs (Fig. 3). Fe_3O_4@PS nanocomposite tubes were first simply

Table 1 Comparison of catalytic activity for various polymer-supported Ag NPs catalysts

Catalyst	Concentrations		Catalyst (mg)/Ag loading (wt.%)	Ag NPs size (nm)	k[a] ($\times 10^{-3}$ s^{-1})	Ref.
	4-NP (mM)	$NaBH_4$ (mM)				
Ag/PS	0.1	10	—/—	30	3.49	[39]
Fe_3O_4@PS/PDA-Ag	0.2	50	0.3/—	10	6.55	[45]
PSMAA-Ag	0.1	60	2/9.66	16	8.17	[44]
Ag-PAL-PANI	0.14	—	0.03/—	2.6	35.8	[57]
PHM-Ag	10	100	6/—	40	1.56	[90]
Ag-PANI	10	100	0. 05/—	—	0.93	[65]
BDP@Ag	1	3	0.06/48.95	10	3.23	[66]
Ag@PPy	0.12	100	0. 25/29.4	130	0.18	[67]
Ag-PEDOT	0.1	15	—/—	12.5	—	[68]
Ag@PEDOT	0.005	0.05	0.01/—	130	1.09	[69]
Ag-PDMAEMA	0.1	10	—/—	15	0.47	[71]
Ag-PVP	2	30	—/—	30	2.2	[74]
Ag/Cellulose	0.4	400	0.3/3	5.55	13	[78]
CNC@PDA-Ag	0.12	38	0.00016/80	10	4.26	[83]
Ag@PGMA-SH	1	9,000	0.5/0.18	10.06	4.38	[88]
Ag@PGMA-PAM	0.067	200	0.16/0.0135	9.7	11.05	[89]
PS@PAMAM-Ag	0.108	105.7	10/1.35	—	0.84	[91]
Ag-GR-GPAMAM	10	100	5/—	20	21.7	[92]
Ag-chitosan	0.1	10	2.1/1.37	5	1.33	[93]
Ag-PG	5	100	—/—	65	5.5	[94]

[a] k represents the reaction rate constant, which is calculated from the equation: $\ln(C_t/C_0) = -kt$.

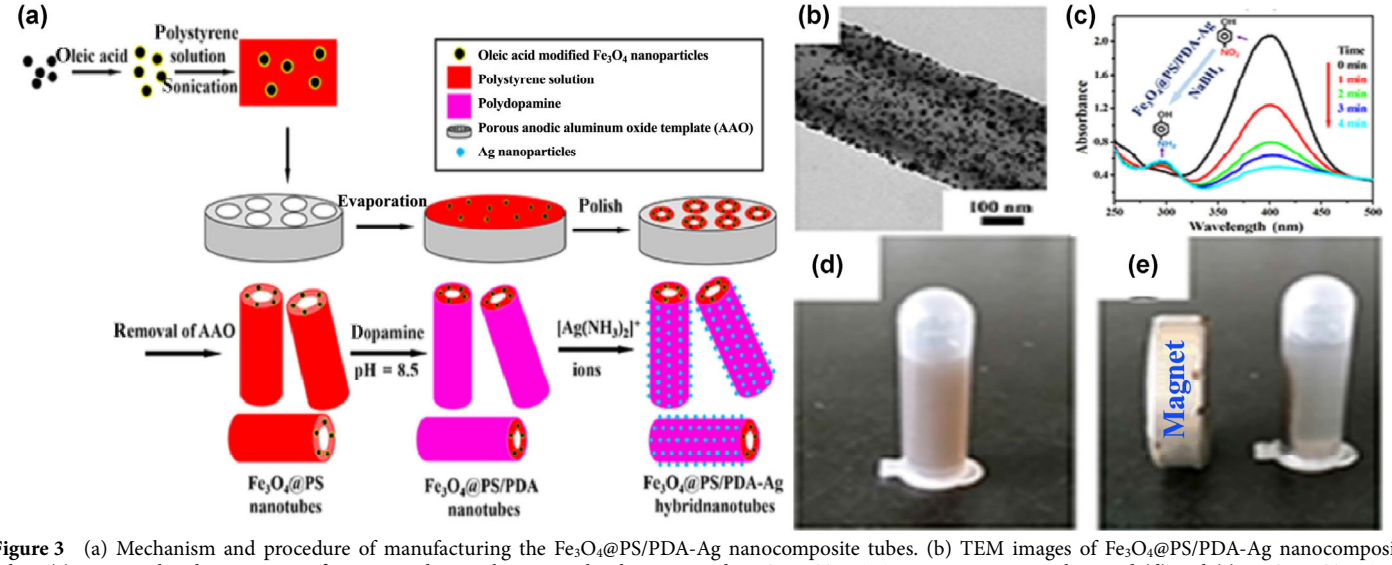

Figure 3 (a) Mechanism and procedure of manufacturing the Fe_3O_4@PS/PDA-Ag nanocomposite tubes. (b) TEM images of Fe_3O_4@PS/PDA-Ag nanocomposite tubes. (c) UV–vis absorbance spectra for 4-NP reduction by $NaBH_4$ by the recovered Fe_3O_4@PS/PDA-Ag nanocomposite tubes, and (d) and (e) Fe_3O_4@PS/PDA-Ag nanocomposite tubes separated from aqueous dispersion using an external magnet. Reproduced with permission from Ref. [45], © Peng, F. et al. 2016.

prepared through using PS/toluene solution with highly dispersed oleic acid modified Fe_3O_4 nanoparticles in a commercial anodic aluminum oxide (AAO) template. Next, highly dispersed Ag NPs with uniform particle size (~ 10 nm) were *in situ* generated and firmly adsorbed on substrate's surface due to abundant amine functional groups on PDA [46–51]. The large specific surface area endowed the hybrid nanotubes with excellent catalytic activity for 4-NP reduction. Besides, the as-prepared catalysts can be separated easily by an external magnet from the aqueous phase.

Generally, the construction of traditional functional PS usually requires complicated experiment steps, expensive materials, dangerous and toxic chemical reagents. It is very meaningful to seek a facile and green route to prepare functional PS. Recently, our group developed a facile and environmentally friendly method to construct poly(styrene-methyl acrylic acid)-silver (PSMAA-Ag) nanocomposites [44]. Emulsifier-free emulsion polymerization firstly involved the synthesis of PSMAA spheres using styrene and MAA. Afterwards, the strong electrostatic interaction prompted $[Ag(NH_3)_2]^+$ ions to adsorb onto the surface of PSMAA spheres because of the existing abundant functional –COOH groups, and then formed metallic Ag in the presence of PVP (Fig. 4(a)). The prepared PSMAA-Ag nanocomposites possessed highly dispersed Ag NPs with a small size ranging from 8 to 24 nm (Fig. 4(b)). Moreover, the prepared PSMAA-Ag catalysts also exhibited higher catalytic activity than the previous work based on Ag/PS ($k = 8.17 \times 10^{-3}$·s^{-1}) [39, 45] (Fig. 4(c)).

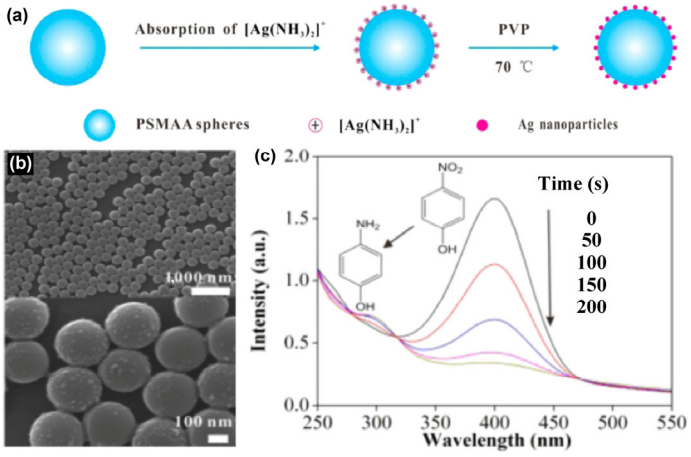

Figure 4 (a) The detailed preparation process of PSMAA-Ag nanocomposites. (b) FESEM images of PSMAA-Ag nanocomposites. (c) Time-dependent UV–vis spectra for the 4-NP catalytic reduction through PSMAA-Ag catalysts in the presence of $NaBH_4$. Reproduced with permission from Ref. [44], © American Chemical Society 2016.

3.1.2 *Conductive polymer-supported Ag NPs*

Conductive polymers are naturally conductive because of their inherent structures with a conjugated electron system inside. During the past years, polyaniline (PANI), polypyrrole (PPy), polythiophene (PTH) and their derivatives, have attracted increasing interest in various areas [52–56]. It is noteworthy that conductive polymer hybrids have become a hot research field, especially the combination of conductive polymer with metal NPs, such as Ag [57], Au [58], Pd [59], Pt [60], etc. Among these conductive polymer-metal NPs hybrids, conductive polymer-Ag NPs hybrids have been widely researched because of their unique chemical, physical, and biological property and relatively low price. Usually, a stabilizer such as amines, alkanethiols, and polymers [61] would be used to cap Ag NPs by following the basic principle of the construction of Ag-based hybrids to avoid the agglomeration caused by the van der Waals force [62]. There are four strategies reported for the preparation of these kinds of conductive polymer-Ag NPs hybrids [63]: (1) simple physical blending of pre-synthesized conductive polymer and Ag NPs; (2) *in-situ* reduction of Ag^+ to Ag^0 by conductive polymer; (3) *in-situ* polymerization of specific monomers like aniline, pyrrole and thiophene in the presence of Ag NPs; (4) simultaneous formation of conductive polymer and Ag NPs.

Since the conjugated electrons or heteroatoms (N or S) existed in conductive polymer chains could be combined with metal atoms, conductive polymers are considered as a promising support for supporting Ag NPs [64]. Moreover, the conductive polymer-Ag NPs composites possess a great potential for 4-NP catalytic reduction due to their easy preparation and controllable doping process, excellent thermal and environmental stability, low cost, etc. Tian et al. [57] prepared a multifunctional palygorskite-polyaniline-Ag NPs (PAL-PANI-Ag) nanocomposites by a facile one-pot *in-situ* polymerization reaction between aniline monomers and the surface adsorbed Ag^+ on natural PAL nanorods at room temperature (Fig. 5). In this way, Ag^+ was utilized as oxidant and Ag precursor, which initiated the polymerization of aniline monomers and simultaneously was reduced to metallic Ag. The catalytic performance evaluation indicated that the prepared PAL-PANI-Ag nanocomposites could act as an efficient catalyst to quickly catalyze the reduction of 4-NP. Dai's group [65] developed Janus structured Ag-PANI NPs and

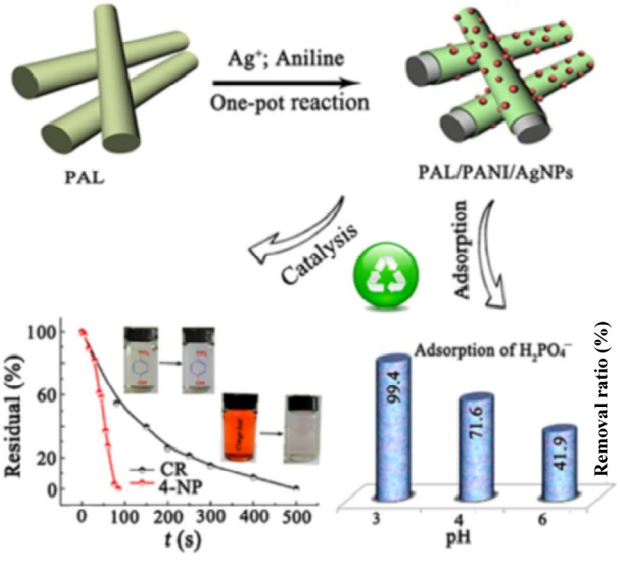

Figure 5 Diagrammatic sketch of the synthetic process for PAL/PANI/Ag nanocomposites with good catalytic performance. Reproduced with permission from Ref. [57], © Elsevier B.V. 2016.

core-shell structured Ag@PANI NPs by using a simple hydrothermal route at different hydrothermal temperatures. For Ag@PANI core-shell NPs, the outer PANI shell could be accessible to the lipophilic nitrobenzene, and thus improving the catalytic property at the same time. Notably, the catalytic property of the core-shell structured Ag@PANI NPs for hydrophilic 4-NP reduction was regulatable by adjusting the PANI shell from undoped states to doped states. However, these features were not found for the Ag-PANI Janus NPs. Moreover, Malik's group [66] has successfully synthesized benzene tetracarboxylic acid-doped PANI-Ag (BDP@Ag) composites using a simple solution-dipping method. In this way, high-aspect-ratio BDP fiber acted as a stabilizer and reducing agent, as well as a good substrate to support Ag NPs with a controllable loading by regulating the molar concentration of $AgNO_3$. The as-developed catalyst exhibited highly effective catalytic performance for 4-NP reduction.

In addition to PANI-Ag hybrids, other conductive polymer-Ag hybrids have also been reported. For example, Zhang et al. [67] have achieved encapsulation of Ag on polypyrrole (PPy) via a simple and direct reduction reaction between $AgNO_3$ and PPy in the existence of sodium dodecyl sulfate. The prepared Ag@PPy nanocomposites showed a great potential as a highly efficient catalyst

for the reduction of 4-NP. Chen et al. [68] prepared a novel Ag-poly(3,4-ethylenedioxythiophene) (PEDOT) nanocomposite (Ag-PEDOT) via one-pot method in acidic condition by choosing polystyrene sulfonate (PSS^-) as both a dopant and particle stabilizer, and 3,4-ethylenedioxythiophene (EDOT) as a reductant. Ag NPs were uniformly distributed around PEDOT polymer with a size ranging from 10 to 15 nm and the obtained Ag-PEDOT nanocomposite also possessed high catalytic activity toward the reduction of 4-NP.

The configuration of conductive polymer/Ag hybrids plays a critical role in catalytic activity [64]. Normally, conductive polymer/Ag hybrids are divided into two categories. One is Ag NPs supported on conductive polymer's surface, the other is Ag NPs deeply embedded in conductive polymer. In the former case, the short pathway between reactants and Ag NPs surface may result in high catalytic activity, but Ag NPs tend to agglomerate due to the insufficient isolation, exhibiting relatively poor stability or recyclability. Although a high stability can be realized in the latter case, the outer organic shells hinder the attachment of reactants to Ag NPs surface, and thus resulting in relatively unsatisfactory catalytic activity. Consequently, it is highly desirable to fabricate conductive polymer/Ag NPs hybrids with both improved catalytic activity and stability. As a novel core/shell structured composite, hollow conductive polymer micro/nanospheres functionalized with movable Ag NPs cores (yolk/shell structures) could combine the advantages of good stability and high catalytic activity. If the reagents can reach Ag NPs core by permeating the conductive polymer shell, it would be easier to obtain an enhanced catalytic activity. Meanwhile, the stability can also be improved since segmental structure change of shells will not lead to the leakage of inside Ag NPs cores. Xu et al. [69] have successfully prepared a yolk/shell structured Ag@PEDOT by a simple and direct penetration and reduction approach. The experimental results indicated that the prepared Ag@PEDOT yolk/shell structure exhibited higher catalytic activity, stability and recyclability compared to core/shell structured catalysts because the cores are usually packed by the shell, so the core surface is directly hindered through the outer shell, greatly suppressing the reaction rate.

3.1.3 *Other polymer-supported Ag NPs*

Besides the two types of polymers mentioned above, other polymers (such as poly(ethylene glycol) (PEG), polyvinylpyrrolidone (PVP), cellulose, poly(glycidyl methacrylate) (PGMA), dendrimers, etc.) have also been used to support Ag NPs. These polymers could become an attractive and promising matrix for the preparation of Ag-based catalysts due to their own unique characteristics.

PEG and their derivatives, the most commonly used hydrophilic polymers, have been utilized as an ideal reductant and stabilizer for Ag NPs preparation, mainly due to their good water solubility and biocompatibility [70]. Lang's group [71] successfully prepared amphiphilic star-shaped copolymer stabilized Ag NPs (Fig. 6). These amphiphilic copolymers consisted of 2-(dimethylamino)ethyl methacrylate (DMAEMA), poly(ε-caprolactone) (PCL) and oligo(ethylene glycol)monomethyl ether methacrylate (OEGMA) segments, which would be able to self-assemble into amphiphilic micelles and act as nanoreactors for the synthesis of Ag NPs. Due to the existed tertiary amine groups on PDMAEMA chain, PDMAEMA could be used as a stabilizer and reducing agent, and the stability of Ag NPs could be further improved because of the highly hydrated ability of POEGMA. When Ag^+ was diffused to the nanoreactor, it could be spontaneously reduced to Ag NPs in the shell of the micelles. The obtained Ag NPs were spherical with a diameter of 10–20 nm and could also be an efficient catalyst for the reduction of 4-NP.

PVP has become one of most commonly used polymers for stabilizing and protecting Ag NPs because of its good affinity to Ag NPs. Moreover, PVP/Ag hybrids possess excellent catalytic property toward large numbers of organic dyes catalytic reduction [72, 73]. Yang's group [74] has synthesized well-dispersed, hydrophilic, and colloidal Ag NPs. These Ag NPs were 10–50 nm in diameter, sphere-like, and passivated with the stabilizer PVP via a simple alternating voltage induced electrochemical synthesis strategy. Herein, PVP played a vital role in stabilizing and protecting colloidal Ag

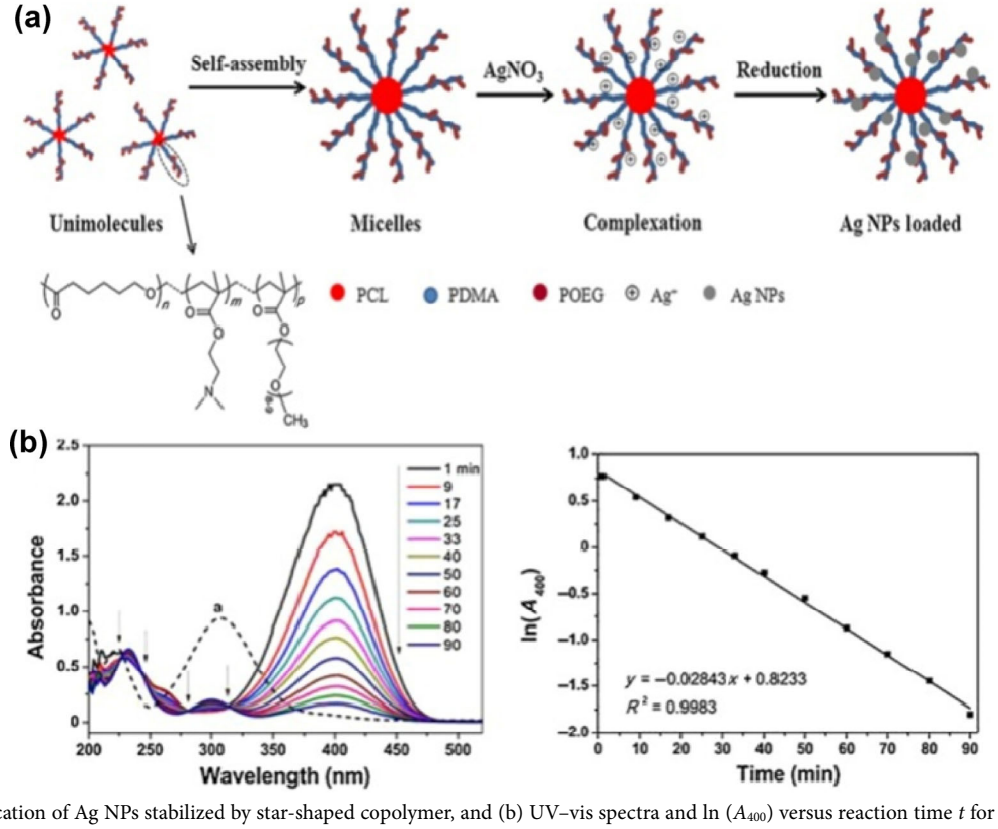

Figure 6 (a) The fabrication of Ag NPs stabilized by star-shaped copolymer, and (b) UV–vis spectra and ln (A_{400}) versus reaction time t for 4-NP catalytic reduction by Ag NPs with $NaBH_4$. Reproduced with permission from Ref. [71], © Elsevier B.V. 2011.

NPs, thus showing excellent catalytic performance for the reduction of 4-NP.

Cellulose, one of the richest and most commonly exploited natural biomass materials, has attracted more and more interests both in scientific and industrial applications [75]. Moreover, cellulose is also an ideal matrix for supporting Ag NPs because of the presence of a great deal of hydroxyl and ether groups on cellulose chain which can effectively stabilize Ag NPs via strong interactions. In addition, cellulose is easily to form porous structure which can regulate the size and shape of Ag NPs [76, 77]. Wu et al. [78] used a sol-gel method to fabricate porous cellulose microspheres as micro-reactors as well as reducing reagents for controllable generation of Ag NPs, of which total amounts, size and size distribution could be easily adjusted by the initial concentration of $AgNO_3$. Moreover, the prepared cellulose/Ag composite microspheres showed higher catalytic activity than hydrogel/Ag NPs composites towards 4-NP catalytic reduction.

Cellulose nanocrystals (CNCs), extracted from wood, cotton and other cellulose sources by the acid hydrolysis, possess many unique features due to their size and surface functionalities [79–81]. Making full use of the advantages of the large surface area and functionalities, the incorporation of Ag NPs onto the surface of CNCs should be an efficient method for the synthesis of Ag-based NPs catalyst for the reduction of 4-NP [82]. Tang et al. [83] proposed a green approach to decorate Ag NPs onto CNCs surface via PDA coating at room temperature without using any stabilizer and reducing agent (Fig. 7). The dopamine self-polymerization first formed a PDA coating in the presence of CNCs, and then the Ag NPs were generated on the CNC@PDA surface by catecholamine oxidation. The prepared CNC@PDA-Ag nanohybrids possessed unique core-shell structure with innumerable Ag NPs "satellites" supported on the surfaces of CNCs. Moreover, it also showed excellent catalytic activity (the k is up to 4.26×10^{-3} s^{-1}) for the 4-NP reduction.

Poly(glycidyl methacrylate) (PGMA) microsphere has been considered to be a promising support for supporting Ag NPs due to its many advantages such as simplicity in synthesis process, easy separation and abundant active sits on the surface [84–87]. Recently, Zhang's group [88] proposed a novel strategy for facile preparation of Ag NPs loaded sulfhydryl-functionalized poly(glycidyl methacrylate) (Ag@PGMA-SH) microspheres. The obtained Ag NPs possessed a good monodispersity and stability with a diameter ~ 16.97 nm and the prepared Ag@PGMA-SH composite showed high catalytic activity (the k is up to 4.38×10^{-3} s^{-1}) for the 4-NP catalytic reduction. Later, they also prepared Ag NPs supported on PAM-modified PGMA (Ag@PAM-PGMA) microspheres, in which PAM acted as a robust anchor due to the existed amide functional groups in the polymer chains and then monodispersed Ag NPs (~ 9.7 nm) were generated on the surface of PGMA-PAM microspheres. More importantly, Ag@PGMA-PAM exhibited an outstanding catalytic performance (the k is up to 11.05×10^{-3} s^{-1}) for 4-NP catalytic reduction [89]. Other polymer-supported Ag NPs also revealed promising catalytic performance for 4-NP reduction [90–94].

Dendrimers, which are well-defined 3D polymers synthesized either by a convergent or divergent strategy, have been widely exploited as promising substrates to synthesize Ag-based NPs catalysts [95–99]. Main reasons include (1) dendrimers possess a uniform structure and thus can produce well-defined Ag NPs; (2) the Ag NPs can be embedded within the dendrimers, and agglomeration of the Ag NPs will reduce; (3) the embedded Ag NPs surface would not be easily passivated, thus the reactants could contact the majority of the Ag NPs surface; (4) the unique structure can act as controllable "gates" for the reactants to access the embedded Ag NPs; (5) the terminal groups on the periphery can link the Ag NPs with surfaces or polymers. Shi's group [91] first prepared cross-linked PS microspheres through dispersion copolymerization of styrene, acrylic acid and crosslinking monomer 1,2-divinylbenzene. Afterwards, the polyamidoamine (PAMAM) dendrimer shell was successfully grafted onto cross-linked PS microspheres surface by repetitive Michael addition reaction using methyl acrylate (MA) and amidation of the esters with superfluous ethylenediamine (EDA). Finally, Ag NPs were embedded directly inside the PAMAM shell and the

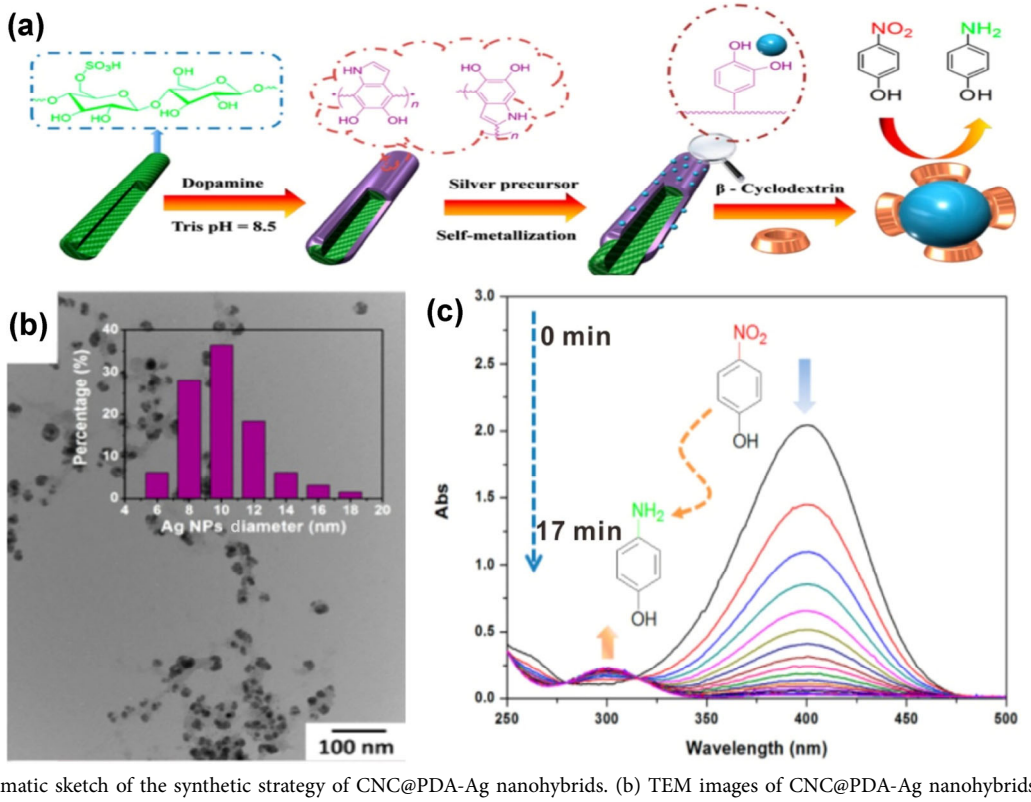

Figure 7 (a) Diagrammatic sketch of the synthetic strategy of CNC@PDA-Ag nanohybrids. (b) TEM images of CNC@PDA-Ag nanohybrids. (c) Time-dependent UV–vis absorption spectra of 4-NP catalyzed by CNC@PDA-Ag nanocomposites with $NaBH_4$. Reproduced with permission from Ref. [83], © American Chemical Society 2015.

prepared PS@PAMAM-Ag nanocomposites exhibited good catalytic activity for the reduction of 4-NP. Rajesh et al. [92] fabricated Ag NPs within the graphite grafted hyperbranched PAMAM dendrimer templates. The obtained catalysts showed amazing catalytic property for 4-NP catalytic reduction with a high reaction rate constant at 21.7×10^{-3} s^{-1} for the PS@PAMAM-Ag (G3) nanocomposites.

Murugadoss et al. [93] reported a Ag NPs/chitosan nanocomposites by an environmental friendly method using chitosan as stabilizer and simultaneously as reducing agent to synthesize Ag NPs with a diameter < 5 nm. The results showed that the prepared Ag NPs/chitosan nanocomposites possessed excellent catalytic property towards 4-NP catalytic reduction. Baruah et al. proposed a facile one-pot single-phase method for the synthesis of norbornene type cationic polymers (polyguanidino oxanorbornenes (PG) and polyamino oxanorbornenes (PA) stabilized Ag NPs [94]. The results showed that both of the prepared catalysts exhibited efficient catalytic reduction for 4-NP, and the catalytic performance of Ag NPs-PG was higher than Ag NPs-PA.

3.2 Carbon-supported Ag NPs for 4-NP reduction

Carbon materials including graphene, carbon dots (CDs) and carbon nanotubes (CNTs), etc., have been widely researched in the catalytic fields for a long time. They can act as direct catalysts or promising catalyst supports due to their fascinating properties including high specific surface area, tunable porosity, easy functionalization, high chemical and thermal stability, easy recovery from the reaction mixture [100–103]. Based on the unique properties of carbon materials, carbon-supported Ag NPs catalysts have been investigated as the most important and common catalysts for 4-NP reduction due to their low cost of manufacture, high specific surface area, good electrical and thermal conductivity [104, 105]. The comparison of various carbon-supported Ag NPs catalysts for 4-NP reduction is summarized (Table 2).

3.2.1 *Graphene-supported Ag NPs*

Graphene, one of the most promising carbon nanomaterials, is a 2D monolayer of sp^2-hybridized carbons and possesses unique electrical, chemical and mechanical properties [106]. Moreover, it has large specific surface area (ca. 2,630 $m^2 \cdot g^{-1}$), tunable surface property, remarkable electrical property, and good chemical and thermal stability, which makes it a promising candidate for supporting Ag NPs [107]. Mao's group [108] prepared graphene oxide (GO) nanosheets supported Ag NPs (Ag/GO) by using a liquid-liquid two phase strategy at room temperature. These Ag NPs with a diameter of ~ 10 nm were uniformly coated on GO nanosheets, which were flexible and could form stable suspensions in various organic phases. Moreover, Ag/GO could serve as highly active (the k is up to 14.5×10^{-3} s^{-1}) catalysts to activate the 4-NP reduction. Similarly, Li et al. [109] reported a facile solid-state synthetic method to synthesize GO supported Ag NPs (Ag/GO). The Ag NPs were uniformly loaded on the surface of GO nanosheets with a size ~ 50 nm and the prepared Ag/GO nanocomposites showed a high stability and catalytic activity for 4-NP catalytic reduction.

Developing homogeneous graphene-based Ag catalysts with a good distribution and controllable loading remains a great challenge because graphene tends to aggregate and the interaction between Ag NPs and graphene is too weak [110, 111]. To solve this problem, both electrostatic stabilization and chemical functionalization could be very useful in reducing aggregation and increasing the interaction between Ag NPs and graphene. Wang et al. [112] reported a green strategy for the preparation of tea polyphenols (TPs) modified reduced graphene oxide/Ag NPs (TPs-modified-RGO/Ag NPs) hybrids using TPs as both stabilizer and reducing agent (Fig. 8). First, TPs were adsorbed on RGO surface and then *in situ* generated Ag NPs due to the reduction and stabilization of TPs. The prepared TPs-modified-RGO nanohybrids showed outstanding water dispersity because of the TPs stabilization, and could be as highly efficient catalyst to reduce 4-NP. Jeon et al. [113] proposed a facile and green way to synthesize Ag NPs (~ 7.7 nm) loaded dopamine-functionalized GO nanosheets in the absence of reductants and stabilizers at room temperature (Fig. 9). In order to functionalize the GO surface with dopamine small molecules, the catechol group in dopamine was protected via acetonide group (Dopa*), which can effectively impede undesirable side reactions, such as, self-polymerization of dopamine. After the synthesis of Dopa*, the reaction between the free amine group of Dopa* with the carboxylic acid and the epoxide groups of GO surface led to the formation of GO-Dopa. The results showed that the prepared Ag/GO-Dopa hybrid catalyst possessed good water dispersity and outstanding catalytic performance for 4-NP reduction.

The incorporation of heteroatoms, e.g., B, S, N, and P into the skeleton of graphene to obtain doped graphene is a very efficient method to ameliorate the electron-donor property and thus further improve the catalytic performance of Ag/grapheme [114, 115]. Doped graphene has currently become a promising substrate for the construction of Ag nanocomposites due to its large specific surface area, plentiful functional groups, good electrical conductivity and unique electron-donor property. More importantly, the active sites of doped graphene can be selected to load Ag NPs and strengthen the interaction between Ag and graphene, and thus leading to an improved stability [116–119]. Tian et al. [120] deposited Ag NPs on

Table 2 Comparison of catalytic activity for various carbon-supported Ag NPs catalysts

Catalyst	Concentrations		Catalyst (mg)/Ag loading (wt.%)	Ag NPs size (nm)	k^a ($\times 10^{-3}$ s^{-1})	Ref.
	4-NP (mM)	$NaBH_4$ (mM)				
Ag/GO	0.2	15	—/—	10	14.5	[108]
Ag/GO	0.03	0.1	3/—	50	8.22	[109]
TPs-modified-RGO-Ag	0.1	10	1/—	4	3.35	[112]
Ag/GO-Dopa	0.05	100	—/2.4	7.71	6.06	[113]
Ag/N-RGO	0.2	200	1/54.2	17.5	8.17	[120]
CNT/PiHP/Ag	50	400	—/—	16.2	19.8	[127]
Ag@MWCNTs-polymer	0.1	5	10/0.25	3	7.88	[129]
Ag@CACDs	0.2	200	0. 04/10.8	12.5	23	[135]
PGNFs-Ag	5	300	—/—	19	4.2	[137]
Ag NPs/C	0.05	100	1/55.2	10	1.69	[138]
Ag/mC	10	45	—/13.6	< 5	120	[141]
Ag/mNC	0.12	—	0.00005/4.28	6	14.1	[143]

[a] k represents the reaction rate constant, which is calculated from the equation: $\ln(C_t/C_0) = -kt$.

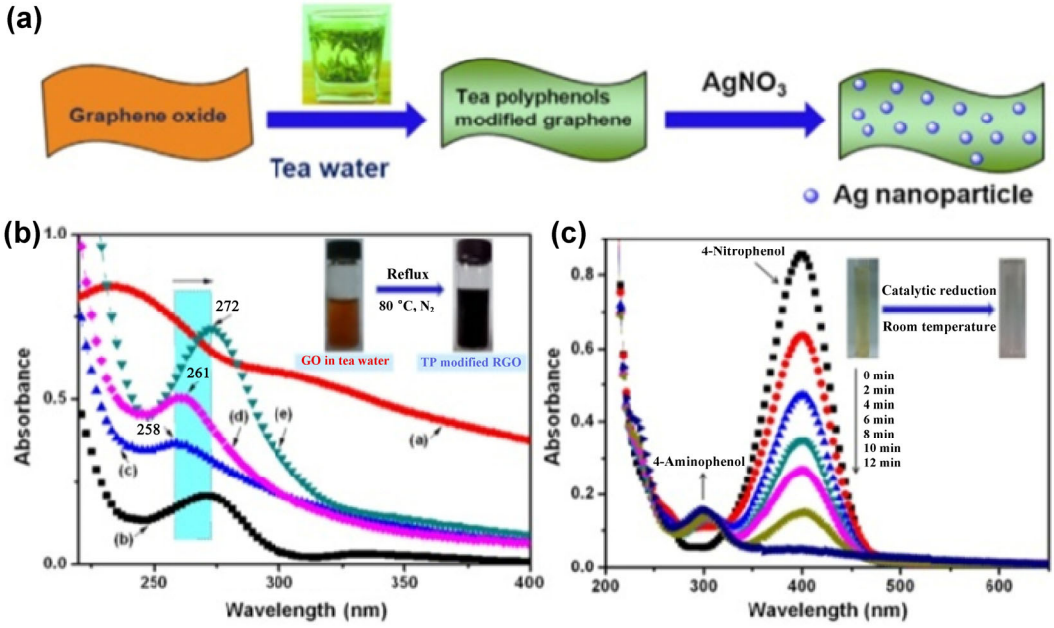

Figure 8 (a) Diagrammatic sketch of the synthetic strategy of TPs-modified-RGO nanohybrids. (b) UV–vis tracks the green reduction of GO to TPG by reflux in tea water at 80 °C, the inset shows the photographs of the reduction process, and (c) UV–vis spectra of 0.1 mM 4-NP with 10 mM $NaBH_4$ in the existence of TPs-modified-RGO catalyst. Reproduced with permission from Ref. [112], © Elsevier B.V. 2015.

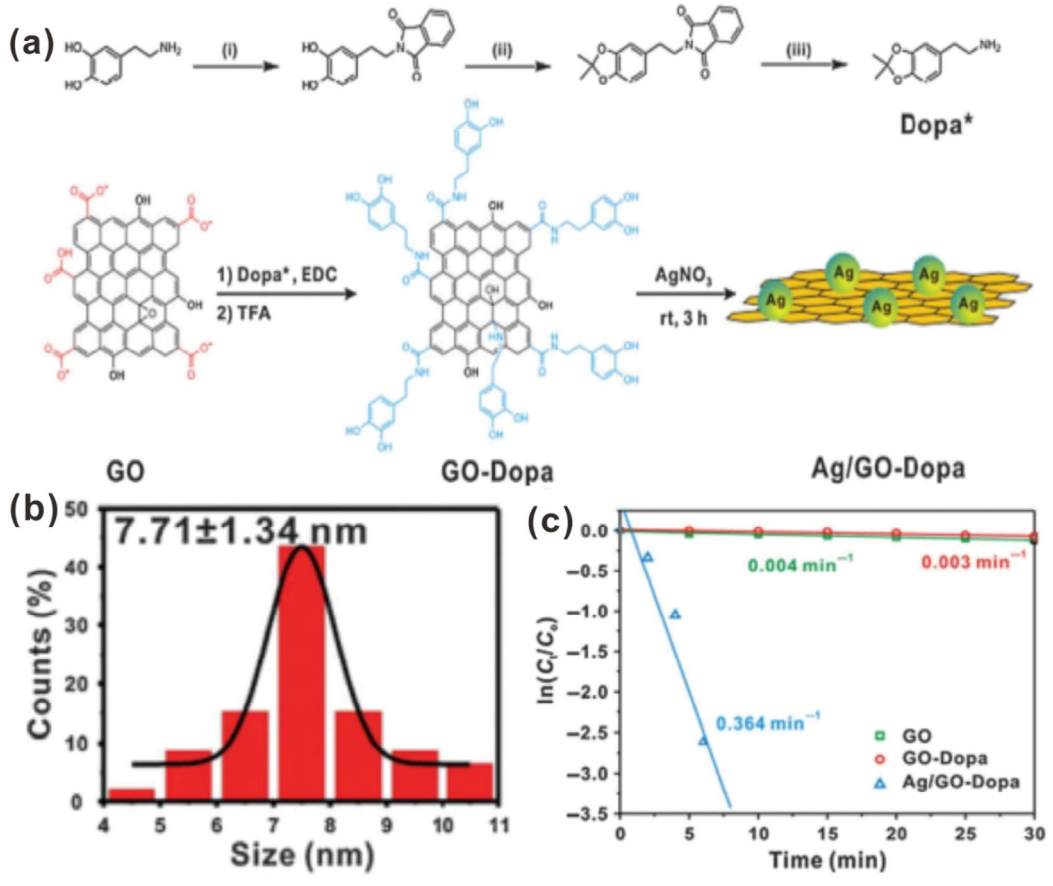

Figure 9 (a) Diagrammatic sketch of the synthesis route of Ag/GO-Dopa nanocomposites. (b) Size distribution histogram of the Ag NPs, and (c) plot of $\ln(C_t/C_0)$ versus time t for 4-NP reduction with three different catalysts. Reproduced with permission from Ref. [113], © The Royal Society of Chemistry 2013.

N-doped RGO (Ag/N-RGO) through a solvothermal and microwave-polyol strategy. The obtained Ag/N-RGO nanocomposites exhibited a better dispersion, smaller Ag NPs size, stronger interactions between Ag NPs and graphene and a better durability when compared to the undoped RGO (Ag/RGO), thus resulting in a higher catalytic performance for the reduction of 4-NP.

3.2.2 *CNTs-supported Ag NPs*

CNTs, a cylindrical form rolled up from graphene layers, have recently been used as a promising catalyst support because of their unique merits such as high ratio of surface area to volume, excellent stability under chemical/thermal/mechanical treatment, chemically

controllable topography, lower raw material cost and facile reclaim of various metals [121, 122]. The use of CNTs as substrates for supporting Ag NPs has received much attention because they are consistent materials and show excellent catalytic property. Moreover, CNTs also increase the electron transfer rate of many redox reactions and can stabilize transient higher oxidation states of supported Ag NPs. These unique features make CNTs especially attractive as a support for depositing Ag NPs with excellent dispersion and excellent catalytic property. To make full use of CNTs, it is necessary to integrate a variety of functional materials (polymers, inorganic materials, biomolecules, etc.) [123, 124] onto the surfaces of CNTs to achieve functionalized CNTs via covalent and/or non-covalent process. Kim's group [125] firstly used a non-covalent process to prepare dendritic pyrenyl-moiety-supported hyperbranched polyglycidol (pHBP) functionalized CNTs, and then the Ag NPs were *in situ* generated onto the hybrid CNT/pHBP surface. The prepared CNT/pHBP/Ag exhibited outstanding catalytic performance for 4-NP reduction, which may be because external CNTs surface was mostly exposed to the Ag NPs, making it accessible to reactants. Moreover, the hydrophilic polymer functionalized CNTs showed an improved water solubility, which also would improve their catalytic properties. In addition, hyperbranched polyglycidol possessed 3D void-containing architectures with electronegative inner environments, which made it an ideal medium for supporting and stabilizing Ag NPs [126]. For example, Li et al. [127] first synthesized 1-pyrenemethanol initiated hyperbranched polyglycerol (PiHP) and used it to functionalize CNTs, and then Ag NPs were randomly generated on the sidewalls, forming CNT/PiHP/Ag hybrids (Fig. 10). The prepared CNT/PiHP/Ag hybrids possessed improved catalytic property for 4-NP reduction.

In addition, the functionalized CNTs should be ideal substrates for supporting Ag NPs because surface modification is an effective method to impede the aggregation and thus obtain better water-dispersed and stabilized CNTs [128]. Ahamad's group [129] prepared a novel catalyst by the combination of –COOH group functionalized multi-walled carbon nanotubes (MWCNTs), chitosan and Ag NPs, which could offer superior properties including larger ratio of surface area to volume and better stability. The Ag NPs were generated though reduction of $AgNO_3$ in the MWCNTs-polymer nanocomposites, showing a very small Ag NPs size (~ 3 nm). The prepared Ag@MWCNTs-polymer composites could be recycled and reused for many times with a high catalytic activity ($k = 7.88 \times 10^{-3}$ s^{-1}) for 4-NP reduction.

3.2.3 *Other carbon-supported Ag NPs*

Since the accidental discovery of carbon dots (CDs), the studies on their preparation and application have shown an exponential growth because of their many appealing optical and physical properties, such as large red-edge effects, strong electron donor/acceptor capability, large aqueous solubility, high photostability, low cytotoxity, etc. [130–134]. To improve and extend their functions, CDs are usually combined with other functional nanomaterials (such as Ag NPs) to form nanocomposites. Baker's group [135] reported a mild and environmentally friendly way to synthesize monometallic (Au NPs or Ag NPs) and alloyed bimetallic AuAg NPs utilizing citric acid-derived carbon dots (CACDs) as both stabilizer and reducing agent. Au_xAg_y@CACDs bimetallic NPs could be prepared by the co-reduction of both Au and Ag precursors. The prepared Au_xAg_y@CACDs bimetallic NPs showed remarkable enhancement in the 4-NP catalytic reduction compared with Au@CACDs monometallic NPs because of the synergistic effects derived from Au and Ag.

Platelet-type graphite nanofibers (PGNFs), which are made up of uniform-sized graphene layers (commonly 40–200 nm) stacked along the nanofiber axis with lengths up to a few micrometer, showing better dispersion in a series of solvents than that of other graphitic nanomaterials (such as graphene and CNTs) [136]. The PGNF dispersions could be prepared by magnetically stirring the PGNF

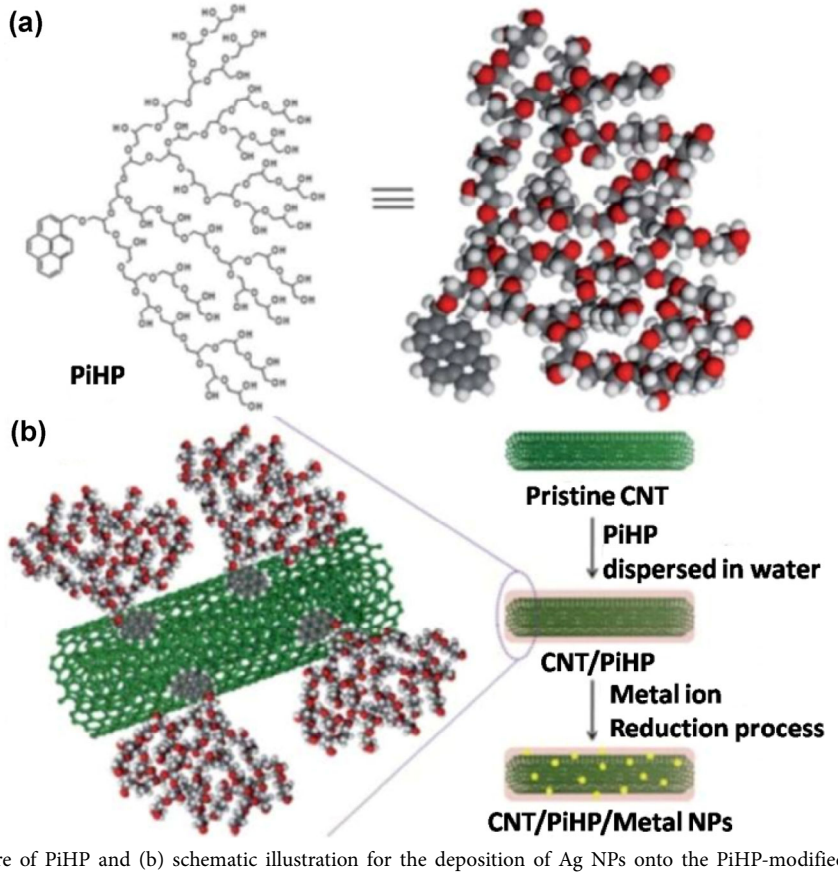

Figure 10 (a) Molecular structure of PiHP and (b) schematic illustration for the deposition of Ag NPs onto the PiHP-modified CNT surfaces by non-covalent functionalization approach. Reproduced with permission from Ref. [127], © The Royal Society of Chemistry 2013.

powder in the solvents and it will be a highly ideal support for supporting Ag NPs. Guardia's group [137] synthesized two carbon nanomaterial supported Ag NPs composites (PGNFs/Ag NPs and GO/Ag NPs) in the liquid-phase using a green photochemical route. The prepared PGNFs-Ag NPs composites exhibited higher catalytic activity than GO-Ag NPs composites for 4-NP reduction.

Carbon spheres (CSs) have also obtained increasing attention in many aspects because of their excellent reactivity, thermal insulation, low density, high compressive strength, large cavity space, etc. A crucial advantage of CSs is that their functionalization may be achieved by encapsulating Ag NPs, which have many unique properties and have been explored as a novel catalyst. Tang et al. [138] reported a fast and high-yield approach to prepare Ag/C composites by microwaving nanoporous CSs suspensions in the presence of aqueous $Ag(NH_3)_2^+$ using PVP as reducing agent. By adjusting the amount of doped Ag NPs, the prepared Ag/C composites showed amazing tunable plasmon resonance shifts and a high catalytic performance for 4-NP reduction. Kao et al. [139] prepared size-tunable hollow CSs containing encapsulated Ag NPs (HCSA) by using a one-pot method for the coupled synthesis and encapsulation. In this way, glucose was utilized as the carbonaceous source and reducing agent. The prepared HCSA exhibited tunable cavity sizes (1.2–2.4 μm), dimensions (0.2–2.7 μm), and morphologies (hollow spherical, bowl-like, ruptured, or solid spherical).

Mesoporous carbon (mC) produced by simply carbonization of biomass (wood, pollen grains, coconut shell and cellulose) is also an ideal support due to its large surface area and reactive surface groups nature, low cost and toxicity, easy preparation, etc. [140]. Zhu's group displayed some interesting works in this respect. They developed a simple chemical-free method to transform cotton fabric into reactive mC by optimized carbonization and oxidation processes. In this work, mC acted not only as catalyst supports, but as reactant which can tune the nucleation/growth of Ag NPs, resulting in Ag NPs (~ 5 nm) uniformly coated on mC surface. As a result, the prepared Ag/mC catalysts could highly efficiently catalyze 4-NP reduction and exhibited outstanding catalytic property (the k is up to 120 × 10^{-3} s^{-1}) [141].

Mesoporous N-doped carbon (mNC) materials have been widely used as a promising catalyst support, this is because the introduction of N atoms into the mesoporous carbon materials framework can greatly enhance the coordination ability with Ag NPs, and thereby enhancing their stability and catalytic activity [142]. Inspired by this, Cui et al. [143] firstly fabricated fluffy-smoke-like mesoporous mNC via a facile one-pot carbonization method employing the cheap melamine and polyacrylonitrile as the trarting materials. The prepared mNC with large specific surface area and high N content was then used as a promising support to synthesize Ag/mNC catalysts. The prepared Ag/mNC catalysts could highly efficiently catalyze 4-NP reduction and exhibited outstanding catalytic property (the k is up to 14.1 × 10^{-3} s^{-1}), mainly because of the small-sized Ag NPs (ca. 6 nm).

3.3 Oxide-supported Ag NPs for 4-NP reduction

Recently, the morphology and catalytic property of oxide-supported Ag NPs have been widely reported. These oxides supports mainly include silica (SiO_2), iron oxides, alumina (Al_2O_3), ceria (CeO_2), and the composites of two or more of the above oxides. Usually, the Ag NPs are supported on oxides surface to form separated "islands" to yield heterointerfaces, and the catalytic property mainly relies on the structure of the supports, and the size and total amount of attached Ag NPs. Herein, the comparison of various oxide-supported Ag NPs catalysts for 4-NP reduction is summarized (Table 3).

Table 3 Comparison of catalytic activity for various oxides-supported Ag NPs catalysts

Catalyst	Concentrations		Catalyst (mg)/Ag loading (wt.%)	Ag NPs size (nm)	k^a (× 10^{-3} s^{-1})	Ref.
	4-NP (mM)	$NaBH_4$ (mM)				
SiO_2@Ag	0.1	60	0.5/—	19.6	9.32	[144]
Ag@hm-SiO_2	0.02	100	0.1/10.29	43	5	[147]
Ag@hm-SiO_2	16	800	2/3.6	20	18	[148]
Dendritic-mSiO_2-NH_2-Ag	0.12	500	0.01/—	—	6.19	[149]
Fibrous SiO_2-Ag	0.12	500	0.0002/8.97	4	10	[150]
Ag-SiO_2	5	200	0.2/—	12	17.6	[156]
SBA-15/PDA/Ag	20	3,000	0.2/3.24	—	14.91	[159]
Fe_3O_4@Ag	5	200	0.4/—	52.2	1.1	[164]
Ag/Fe_3O_4@C	0.2	100	20/—	10	17.17	[165]
Fe_3O_4@Ag/ATO	10	100	1.2/—	—	17.46	[166]
Ag-γ-Fe_2O_3	0.16	68.2	1.15/3.67	7.8	6.4	[167]
Ag@CeO_2	1	10	5/—	180	5.4	[172]
Ag@CeO_2	0.13	20	0.25/28	5	32.6	[173]
RGO/Ag/CeO_2	10	1,500	—/14.6	15	4.48	[174]
Ag@γ-Al_2O_3	0.09	204	0.3/10	7	3.2	[177]
Ag/Al_2O_3	46.4	13.9	0.02/0.6	10.4	—	[179]
Ag-decorated SnO_2	0.14	6.95	1.5/—	5	51.67	[181]
Au@SnO_2@Ag	0.1	300	0.1/24.1	9	37.09	[182]
TiO_2@Ag	1	10	0.1/10	10	7.53	[183]
ZnO/Ag	1	10	—/0.03	10	—	[186]
Fe_3O_4/SiO_2/Ag	1	10	0.039/—	15	—	[190]
Fe_3O_4@SiO_2-Ag	0.12	12	—/0.1	3.65	7.67	[191]
Fe_3O_4@SiO_2-Ag	5	200	3/3.72	10	11.3	[192]
ZnO-SiO_2-Ag	0.01	500	50/2.5	37.5	4	[193]

[a] k represents the reaction rate constant, which is calculated from the equation: $\ln(C_t/C_0) = -kt$.

3.3.1 SiO_2-supported Ag NPs

SiO_2 is one of the most common supports for supporting Ag NPs due to its low cost, excellent stability, and robust surface chemistry. Tzounis et al. [144] reported a novel water-based strategy for the controllable decoration of Ag NPs with a uniform particle size on SiO_2 spheres surface (Fig. 11). Polyethyleneimine (PEI) was first introduced to modify SiO_2 spheres (~ 120 nm) to endow the surface with functional amine groups which could coordinate with Ag^+. Subsequently, Ag seeds (~ 4 nm particle size) were formed by reduction reaction and uniformly distributed on the SiO_2 spheres surface (SiO_2@Ag-seed). Moreover, other two growth steps of Ag were conducted with a diameter change from 12 to 19 nm for further improvement of the catalytic properties and optical responsive ability (SiO_2@Ag-1 and SiO_2@Ag-2). The raspberry-like SiO_2@Ag nanocomposites showed excellent SERS capability and enhanced catalytic property. The major merits of this study include the tunable particle size of Ag NPs, durable colloidal stability and no any organic solvents involved during the preparation process.

Compared to common SiO_2 NPs supports, the hollow mesoporous SiO_2 (hm-SiO_2) with yolk/shell nanostructures (YSNs) exhibit many structure-related advantages such as freely movable active metal core, protective mesoporous-shells, large specific surface area, low density, rapid mass transfer and interstitial hollow space [145, 146], which make them a promising platform for the construction of Ag nanocomposites. Recently, Zhang et al. [147] presented an effective protocol for the synthesis of Ag@hm-SiO_2 YSNs via a facile "ship-in-a-bottle" method. The prepared Ag@hm-SiO_2 YSNs possessed a single Ag core in the interior of hm-SiO_2 nanospheres, where the thickness of hm-SiO_2 outer shell was about 14 nm and the Ag core exhibited an average size of about 43 nm. The prepared Ag@hm-SiO_2 YSNs ($k = 5 \times 10^{-3}$ s^{-1}) exhibited improved catalytic performance for 4-NP reduction compared to the pure Ag NPs ($k = 1.7 \times 10^{-3}$ s^{-1}). Later, they also reported a new Ag@hm-SiO_2 nanocomposite catalyst consisted of a hm-SiO_2 shell and multiple encapsulated Ag NPs yolks by pre-shell/post-core strategy (Fig. 12). There were 5–10 Ag NPs yolks (~ 20 nm) encapsulated in one Ag@hm-SiO_2 and the Ag content was calculated to be about 3.6 wt.%. Interestingly, the Ag NPs yolks showed a decrease in particle size and an increase in the amount treated by a laser ablation, leading to 3-fold-enhanced catalytic performance for 4-NP reduction compared to the pure Ag@hm-SiO_2. Such excellent catalytic property was mainly attributed to the special structural characteristics of the Ag@hm-SiO_2, of which the mesoporous shell provided highly efficient protection for the Ag NPs yolks as well as convenient channel for the rapid transport of reactants to the yolks [148].

In addition, developing an appropriate SiO_2 support with various shapes, endowing it with highly accessible active sites, is also of great significance. Sun et al. [149] prepared a multifunctional dendritic SiO_2-Ag nanocomposite catalyst with large specific surface area and easily accessible active sites via a facile oil-water biphase stratification coating strategy. The resultant nanocatalysts exhibited outstanding catalytic properties (the k is up to 6.19×10^{-3} s^{-1}) for 4-NP reduction because of easily accessible active sites. Moreover, these kinds of novel nanocatalysts could be conveniently separated and reused for at least five times without a significant decrease in the catalytic performance. Dong et al. [150] reported a facile strategy for the fabrication of novel fibrous SiO_2-Ag nanocatalysts, which possessed large specific surface area and easily accessible active sites. In this

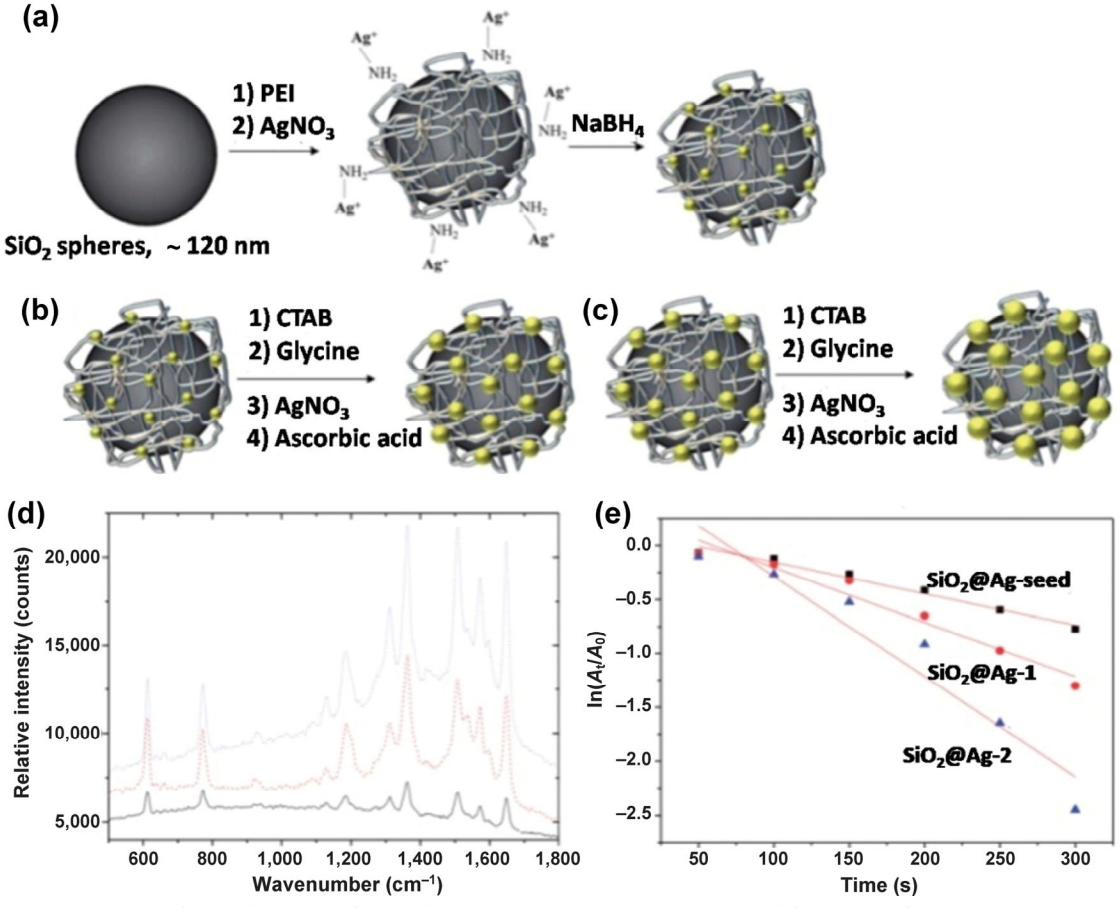

Figure 11 (a) Diagrammatic sketch for the deposition of SiO_2 spheres with Ag seeds using PEI as a ligand for Ag^+, and further Ag growth on the formed Ag seeds using two subsequent growth steps ((b) and (c)), (d) SERS spectra of R6G (10^{-5} M) adsorbed from aqueous solution at SiO_2@Ag-seed (black solid line), SiO_2@Ag-1 (red dashed line) and SiO_2@Ag-2 (blue dotted line), and (e) comparative plots of $\ln(A_t/A_0)$ versus time t towards 4-NP reduction using SiO_2@Ag catalytic systems. Reproduced with permission from Ref. [144], © The Royal Society of Chemistry 2014.

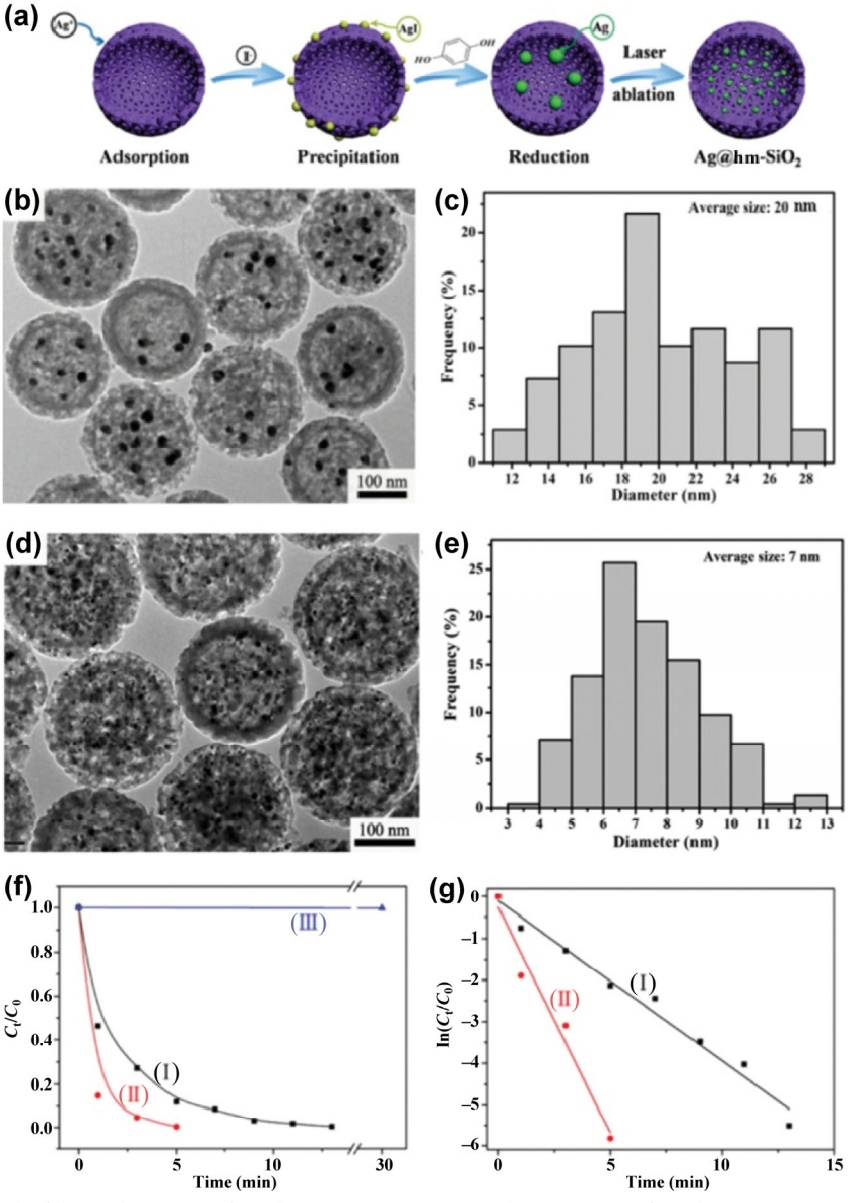

Figure 12 (a) Diagrammatic sketch of the synthetic route of Ag@hm-SiO_2 nanocomposites. (b) TEM image of Ag@hm-SiO_2 nanocomposites and (c) the corresponding size distribution of Ag cores from the TEM image, (d) TEM image of Ag@hm-SiO_2 spheres after the treatment of laser ablation and (e) the size distribution histogram of Ag cores from the TEM image, (f) and (g) C_t/C_0 and the corresponding linear fits versus time with different catalysts: (I) Ag@hm-SiO_2 before laser ablation; (II) Ag@hm-SiO_2 after laser ablation; (III) without any catalyst. Reproduced with permission from Ref. [148], © the Partner Organisations 2016.

way, fibrous SiO_2 with large specific surface area was grafted with $-NH_2$ groups, which served as a promising anchor agent for decorating nano-sized Ag NPs (ca. 4 nm) on fibrous SiO_2 surface. The 10×10^{-3} s^{-1} of k was achieved by the prepared SiO_2-Ag nanocatalysts for 4-NP reduction due to their large specific surface area and easily accessible active sites.

In the past few decades, monodisperse hollow SiO_2 spheres have also attracted increasing interest in catalyst supports area because of their well-defined morphology, homogeneous size, low density, good compatibility and large surface area [151, 152]. Owing to the presence of mesopores on SiO_2 shells, the reactants can be rapidly diffused inside the hollow SiO_2 spheres, and then catalytic reactions are performed within confined small space [153, 154]. Recently, Ag NPs-decorated hollow SiO_2 spheres with mesopores on shells have been widely examined as catalysts for 4-NP reduction. Zhang et al. [155] reported an easy and controllable way to synthesize porous hollow metal-layer@SiO_2 nanoreactors with designed structure, which showed a high catalytic activity and stability. Xiao et al. [156] proposed a one-pot strategy to fabricate hollow Ag-SiO_2 composite spheres with developed porosity by employing monodisperse carboxylic-capped polystyrene (PS-COOH) spheres as a hard template. The well-designed composite spheres possessed thin and spherical SiO_2 shell (~ 10 nm), high surface-to-volume ratio (> 240 $m^2 \cdot g^{-1}$) and small mesopores (6.0–9.0 nm). Moreover, they also showed excellent catalytic performance (the k is up to 17.6×10^{-3} s^{-1}) towards 4-NP reduction.

Due to their controllable mesostructures and enhanced thermal stability, mesoporous SiO_2 supports such as MCM-41, SBA-15, and KIT-6 have been widely used in the field of catalyst supports [157]. Among them, SBA-15 is one of the most common catalyst supports due to its highly organized pore structures and manipulable tubular length [158]. Song et al. [159] reported a novel method to *in situ* prepare Ag NPs by using PDA as biomimetic reducing agents, which were loaded into the rod-like mesoporous SBA-15 channels. The results illustrated a controllable release of Ag NPs from the mesopore structure and the prepared tubular SBA-15/PDA/Ag showed an enhanced catalytic activity (the k is up to 14.91×10^{-3} s^{-1}) towards the degradation of 4-NP when compared to core-shell

structured SiO_2/PDA/Ag.

3.3.2 *Iron oxides-supported Ag NPs*

Recyclability is one of the most important criteria to evaluate the practical application value of catalyst. The majority of the technologies for separation are mainly based on physical separation, such as filtration and centrifugation, but they are time-consuming. Magnetic iron oxide NPs, especially Fe_3O_4 and Fe_2O_3, have been widely used as promising oxide supports because they are easily to synthesize, and possess abundant active surface for adsorption or decoration of Ag NPs. More importantly, the separation of the catalysts could be easily realized only using an extra magnet [160].

Fe_3O_4@Ag nanocomposites not only exhibited high catalytic activity for organic pollutants reduction in wastewater treatment applications [161], but also could be easily recovered only using extra magnet [162]. Moreover, the Fe_3O_4@Ag nanocomposites can also be reused for the degradation of pollutants in succession without obvious loss in the catalytic activity [163]. Sharma et al. [164] presented a facile route for the preparation of Fe_3O_4@Ag core-shell nanocomposites, where Fe_3O_4 microspheres were used as the core and the shell consisted of Ag NPs. The preparation process did not involve any external reducing agent and surface modification of Fe_3O_4. The prepared Fe_3O_4@Ag core-shell nanocomposites were a promising catalyst for 4-NP and methylene blue (MB) catalytic reduction in aqueous solution, and it could also be easily separated only using an extra magnet. Zhu et al. [165] prepared Ag NPs loaded on magnetic Fe_3O_4@C (Ag/Fe_3O_4@C) core-shell nanocomposites, the Fe_3O_4@C composites consisted of a magnetic core (Fe_3O_4 microspheres) and thin C layer prepared via *in-situ* carbonization of glucose (Fig. 13(a)). The prepared Ag/Fe_3O_4@C core-shell nanocomposites showed excellent catalytic property (the k is up to 17.17×10^{-3} s^{-1}) for 4-NP reduction (Figs. 13(d) and 13(e)), and it could also be easily separated only by an extra magnet (Figs. 13(b) and 13(c)).

The introduction of antimony doped tin oxide (ATO) NPs to Fe_3O_4@Ag nanocomposites can significantly increase their adsorption capability. Apart from enhancing the catalytic activity of Fe_3O_4@Ag nanocomposites, the introduction of ATO is also beneficial to boost the adsorption of 4-NP onto Fe_3O_4@Ag nanocomposites. Karki et al. [166] prepared Ag NPs loaded Fe_3O_4 and ATO (Fe_3O_4@Ag/ATO) magnetic nanocomposites by an environmentally friendly and simple *in-situ* one-pot hydrothermal process. The ATO was used for hydrothermal growth of Ag and Fe_3O_4 magnetic NPs, which offered an effective bonding interaction between Ag NPs, Fe_3O_4 NPs and ATO NPs. The prepared Fe_3O_4@Ag/ATO magnetic nanocomposites showed enhanced catalytic activity (the k is up to 17.46×10^{-3} s^{-1}) for 4-NP reduction when compared to the pure Fe_3O_4 and Fe_3O_4@Ag, and the catalyst could be easily separated only through using an extra magnet. The enhancement was mainly attributed to the strong adsorption capacity of ATO NPs.

Like Fe_3O_4, Fe_2O_3 is also an ideal oxide support for supporting Ag NPs due to its magnetical recoverability. Kaloti et al. [167] presented a green method for the preparation of γ-Fe_2O_3-supported Ag NPs (γ-Fe_2O_3@Ag) in an aqueous medium. In this way, glucose showed weak non-covalent interactions with Ag and γ-Fe_2O_3 in the composites through –OH and –C=O functional groups, which not only served as an effective stabilizer but also improved the homogeneous reactive sites in its surface. Therefore, the prepared γ-Fe_2O_3@Ag nanocomposites showed good catalytic property for 4-NP reduction, and were also magnetically separable and recyclable with super paramagnetic features.

3.3.3 *CeO_2-supported Ag NPs*

CeO_2, as a multifunctional rare-earth oxide, has achieved great interest because of its unique chemical, physical, and biological property. Recently, the use of CeO_2 as a support for supporting Ag NPs has been widely researched because of their morphological compatibility with Ag NPs, large interfacial area, greatly enhanced catalytic property [168]. To enhance the stability of Ag-based NPs catalysts, endowing them with an infarctate shell to obtain core-shell or yolk-shell nanostructures will be a good solution [169–171]. Wang et al. [172] prepared Ag@CeO_2 core-shell nanospheres by a facile one-step solvothermal route using $Ce(NO_3)_3{\cdot}6H_2O$, $AgNO_3$, PVP, and ethanol as the starting materials. The prepared Ag@CeO_2 nanospheres consisted of Ag core and CeO_2 shell. Moreover, the prepared Ag@CeO_2 nanospheres exhibited much better catalytic property than the pure Ag NPs for 4-NP reduction. The improved catalytic activity was mainly attributed to the strong interaction between the core surface of Ag NPs and surface defects of the CeO_2

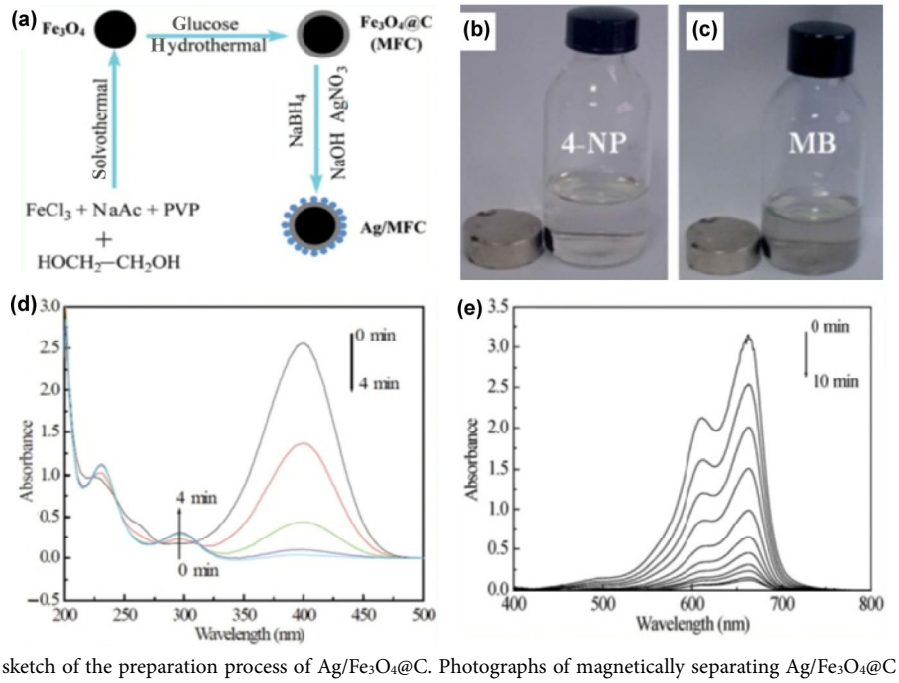

Figure 13 (a) Diagrammatic sketch of the preparation process of Ag/Fe_3O_4@C. Photographs of magnetically separating Ag/Fe_3O_4@C from the reaction media after completion of the reaction, (b) 4-NP; (c) MB. (d) Time-dependent UV–vis spectral variations in 4-NP catalyzed by Ag/Fe_3O_4@C. (e) Time-dependent UV–vis spectral changes in MB catalyzed by Ag/Fe_3O_4@C. Reproduced with permission from Ref. [165], © The Royal Society of Chemistry 2013.

shell. Shi et al. [173] prepared Ag@CeO_2 nanocomposites through the combination of a redox reaction and the reverse micelle technique without any additional reductants or surfactants. Under nitrogen atmosphere, the redox reaction automatically occurred between Ag^+ and Ce^{3+} in an alkaline solution, and finally leading to the formation of Ag@CeO_2 nanocomposites by self-assembly process. The Ag NPs with a diameter of 3–7 nm were loaded on CeO_2 NPs surface. The prepared Ag@CeO_2 nanocomposites showed improved catalytic activity (the k is up to 32.6×10^{-3} s^{-1}) and higher recyclability for 4-NP reduction when compared to the pure Ag NPs.

The incorporation of two or more active components into Ag@CeO_2 nanocomposites with uniform distribution will further improve their catalytic activity. Shen's group [174] prepared a three-component RGO/Ag/CeO_2 nanocomposites via a facile and green route. The Ag NPs and CeO_2 NPs were uniformly distributed on RGO nanosheets surface. Moreover, the prepared RGO/Ag/CeO_2 nanocomposites exhibited excellent catalytic property for 4-NP reduction. The introduction of CeO_2 had a significant impact on the size of the Ag NPs as well as could significantly enhance the catalytic activity and stability.

3.3.4 Al_2O_3-supported Ag NPs

Al_2O_3, especially mesoporous γ-Al_2O_3, has been employed as catalyst supports owing to their high specific surface area, abundant porous structure and good thermal stability [175, 176]. Naik et al. [177] presented a simple chemical reduction approach for the preparation of Ag NPs with average size of ~ 7 nm, which were formed within the mesopores of γ-Al_2O_3 matrix. The prepared Ag@γ-Al_2O_3 nanocomposites exhibited high catalytic activity for 4-NP reduction. In addition, they could have the potential to be an ideal catalyst because of their several unique advantages, such as (i) the reactants got easy access to the active sites because of high specific surface area and porous structure of the mesoporous γ-Al_2O_3 supports; (ii) the growth of Ag NPs within the pores of mesoporous γ-Al_2O_3 supports was beneficial to impede agglomeration; (iii) these kinds of catalysts could easily be separated from the reaction system only by simple filtration or centrifugation.

Murthy et al. [178] firstly prepared size-regulatable Ag NPs through simple *in-situ* reduction between $AgNO_3$ and $NaBH_4$. Subsequently, the prepared small-sized and monodispersed Ag NPs were uniformly loaded on Al_2O_3 surface. The obtained Ag/Al_2O_3 products could be used as a highly efficient catalyst for 4-NP reduction. A similar work was reported by Yamashita's group [179], who prepared Ag/Al_2O_3 nanocomposites via a pH-triggered assembly dispersion control strategy, which ensured the loaded Ag NPs with different sizes and distributions. The prepared Ag/Al_2O_3 nanocomposites could be used as a highly efficient catalyst for 4-NP reduction.

3.3.5 Other oxides-supported Ag NPs

There are a few reports about other oxides-supported Ag NPs catalysts for 4-NP reduction in recent years. SnO_2, a traditional n-type semiconductor, showing large bandgap, high electron mobility, low cost, less toxic and excellent chemical and thermal tability, which reveals an eminent property when it is used as catalyst supports [180]. Hu et al. [181] prepared layered Ag-decorated SnO_2 microspheres via a simple one-pot hydrothermal strategy. As hydrothermal time progresses, SnO_2 NPs self-assembled into SnO_2 nanosheets and then Ag NPs were loaded onto the surface of SnO_2 nanosheets. The prepared hierarchical Ag-decorated SnO_2 microspheres showed excellent catalytic activity (the k is up to 51.67×10^{-3} s^{-1}) and good recyclability for 4-NP reduction. Lei et al. [182] prepared ternary Au@SnO_2@Ag yolk-shell-shell (YSS) NPs through a SiO_2 seeds-mediated hydrothermal strategy, where SnO_2 was located between the Au NPs and Ag NPs. The prepared ternary Au@SnO_2@Ag YSS NPs showed enhanced catalytic activity for 4-NP reduction compared to the bare Au NPs and Ag NPs, which was attributed to the synergistic effect of Au NPs and Ag NPs in the ternary YSS NPs.

Like SnO_2, TiO_2 is also an important transition metal oxide semiconductor with high chemical and physical stability, and thus has recently become a promising catalyst support. Ma et al. [183] reported TiO_2@Ag core-shell nanocomposites, which consisted of the anatase TiO_2 spheres core and Ag NPs shell, and were prepared through Ag nanoseeds-mediated photochemical reduction strategy. The Ag NPs (~ 10 nm particle size) were uniformly coated on Ag nanoseed modified TiO_2 spheres surface under UV radiation. The prepared TiO_2@Ag core-shell composites exhibited higher catalytic activity for 4-NP reduction than that of the pure Ag NPs. Shoaib et al. [184] reported a new versatile strategy to prepare noble metals (Au, Ag, and Cu) nanoclusters supported on TiO_2 nanosheets with exposed (001) facets and controlled size, crystalline interface, and loading amount. The prepared Au, Ag, and Cu nanoclusters supported on TiO_2 could be used as a promising catalyst for 4-NP reduction, photocatalytic H_2 evolution, etc.

Compared to other oxides supports, ZnO, with controllable morphology and high stability, is well known to induce a strong metal-support interaction when it is used as a support for metal catalysts, which offers an opportunity for the supported catalysts to improve the catalytic property and tune their catalytic behavior [185]. Zhang et al. [186] prepared sub-micrometer sized ZnO/Ag composite spheres by a simple photodeposition route. The photochemical reduction method needed no other reductant or surfactant, which was a promising method to ensure the uniform distribution of Ag NPs (~10 nm) on ZnO spheres surfaces (~ 480 nm). The prepared ZnO/Ag composites showed excellent catalytic performance for the catalytic reduction of 4-NP.

3.3.6 Composites of two or more oxides-supported Ag NPs

Besides the above-mentioned examples of single oxides as supports for supporting Ag NPs, some multiple oxides-supported Ag NPs nanocomposites have also been widely researched. These kinds of nanocomposites show unique hierarchical and multifunctional characteristics. Commonly, magnetic iron oxides provide a magnetic separability, while porous oxides favor the fast mass transport of reactants, and functional oxides serve as an effective microreactor and restrain Ag NPs agglomeration [187–189].

Kim's group [190] reported a facile, economical and green sonochemical method for the preparation of Fe_3O_4/SiO_2/Ag core-shell nanocubes and SiO_2/Ag core-shell nanospheres. The microjet and shock waves were a key factor for promoting the surface functionalization of Fe_3O_4 in SiO_2 shell as well as Ag NPs (Fig. 14(a)). The prepared Fe_3O_4/SiO_2/Ag nanocubes showed higher activity for 4-NP reduction than both the bare Ag NPs and SiO_2/Ag nanospheres (Figs. 14(b)–14(d)). It could also be recirculated at least fifteen times without an obvious decrease of catalytic property (Fig. 14(e)) and separated from the reaction solution only by using an extra magnet (Fig. 14(f)).

Chi et al. [191] reported a facile *in situ* wet chemistry strategy to produce magnetic Fe_3O_4@SiO_2-Ag core-shell structure nanocomposites using PVP as reducing agent as well as stabilizer. This way could effectively restrain Ag NPs aggregation, producing uniformly dispersed and ultrasmall-sized Ag NPs. The prepared Fe_3O_4@SiO_2-Ag nanocomposites could be used as a highly efficient recyclable catalyst for 4-NP reduction. Fe_3O_4@SiO_2-Ag contained a magnetic Fe_3O_4 core for highly efficient magnetic separation, a SiO_2 interlayer for preventing the Fe_3O_4 core and Ag NPs from aggregation, and ultrasmall-sized and uniformly dispersed Ag NPs for improving catalytic performance. Similarly, Du et al. [192] presented a novel route for the construction of Ag-deposited SiO_2-coated Fe_3O_4 (Fe_3O_4@SiO_2-Ag) magnetic nanocomposites with a SiO_2 coated magnetic core and active Ag NPs shell by using n-butylamine as

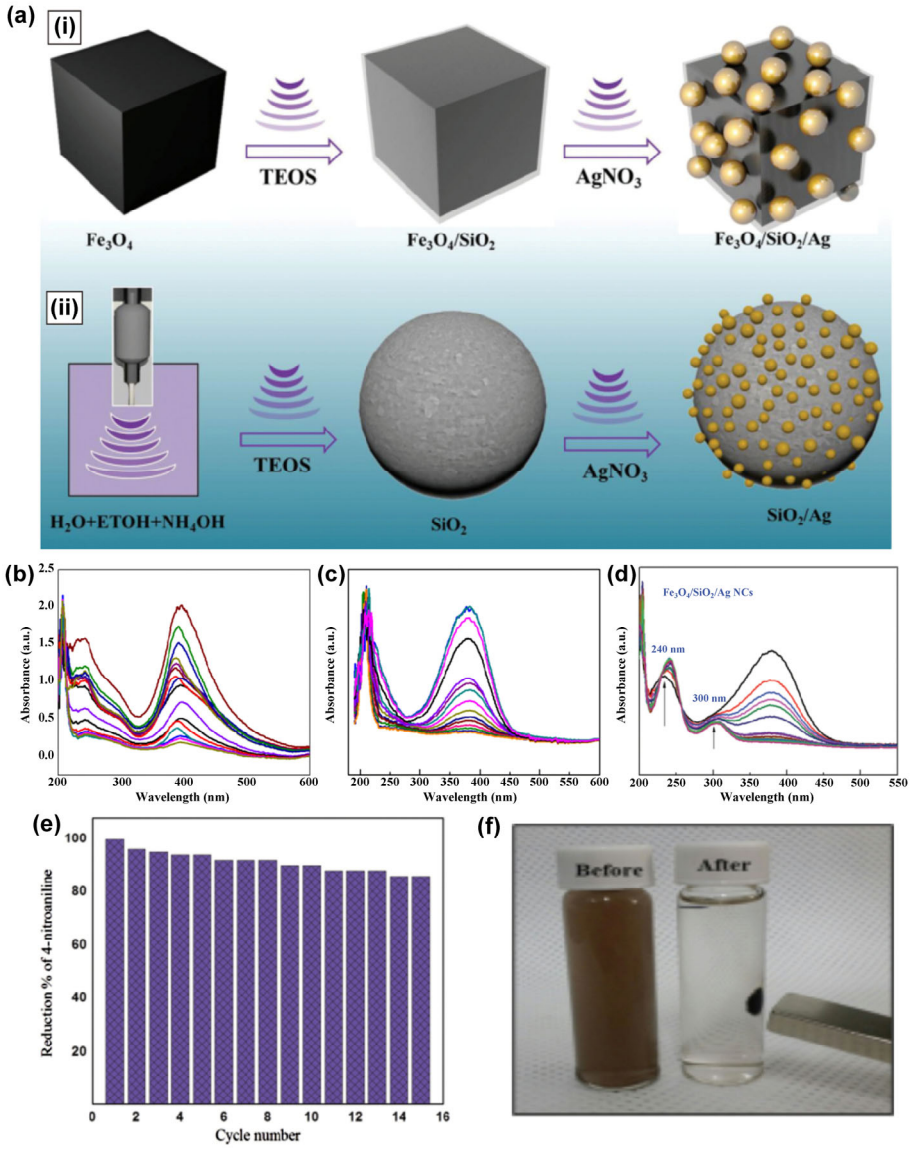

Figure 14 (a) Schematic diagram illustrating the synthesis process of (i) $Fe_3O_4/SiO_2/Ag$ nanocubes and (ii) SiO_2/Ag nanospheres. UV–vis spectra for the 4-NP reduction by (b) SiO_2/Ag, (c) Ag NPs, and (d) $Fe_3O_4/SiO_2/Ag$. (e) The recycling curves of the $Fe_3O_4/SiO_2/Ag$ nanocubes for 15 repetitions. (f) The photograph of $Fe_3O_4/SiO_2/Ag$ nanocubes in water in the absence and presence of an external magnet. Reproduced with permission from Ref. [190], © The Royal Society of Chemistry 2015.

reducing agent. The obtained Fe_3O_4@SiO_2-Ag products showed good mono-dispersity and bifunctionality along with high magnetic separablity and high catalytic activity (the k is up to 11.3×10^{-3} s^{-1}) towards 4-NP reduction.

Although ZnO is an excellent candidate support material for immobilizing Ag NPs, relatively low surface area (10–20 $m^2 \cdot g^{-1}$) seriously restricts its potential application. To solve this issue, other porous oxides such as SiO_2 can be combined with ZnO to act together as a catalyst support. Firstly, SiO_2 possesses high specific surface area because of its porosity, making it an ideal support for uniform distribution of Ag NPs. Secondly, SiO_2 is inert, and cannot take part in catalytic reduction reactions. Thus, the combination of mildly catalytic, low cost support (i.e., ZnO) and high specific surface area porous material (i.e., SiO_2) would improve catalytic efficiency of the resulting products. Kokate et al. [193] prepared ZnO-SiO_2-Ag nanocomposites by a simple one-pot method. ZnO showed mild catalytic activity and antibacterial behavior, and was also an excellent and cheap 3D support for distributing Ag NPs. Ag NPs improved the catalytic and antibacterial property of ZnO. SiO_2 is another important part of the nanocomposites, which not only effectively linked the Ag NPs and ZnO NPs, but also significantly enhanced the specific surface area of the nanocomposites. Thus, the prepared ZnO-SiO_2-Ag nanocomposites showed excellent catalytic performance for 4-NP reduction.

3.4 MOFs-supported Ag NPs for 4-NP reduction

Metal-organic frameworks (MOFs), a novel nanoporous material with high specific surface area, structural diversity, and tailorability, can be used as ideal substrates for the preparation of Ag-based catalysts with tailored size and shape [194–196]. Compared to other substrates, MOFs have many advantages including unique structure and porosity, which provide a tremendous opportunity to engineer a series of advanced functional materials. The stable nanostructures of MOFs with numerous freely accessible active sites offer the supported Ag-based catalysts with enhanced catalytic activity [197]. Acharya's group [198] rationally designed a highly dispersed Ag nanoclusters (NCs) deposited iron based MOFs (AgNC@MIL-101(Fe)) by wet chemical method. The MIL-101 framework $[Fe_3(O)(bdc)_3(Cl)(H_2O)_2]B_{25}H_2O$ held a 3D porous structure that provided a high thermal and chemical stability, large pore size and specific surface area, which was a promising substrate for supporting Ag NCs [199]. The Ag precursor was impregnated and chemically

reduced to Ag NCs with less than 1 nm in the particle size on the iron-based MIL-101. The Ag NCs possessed good stability without further aggregation. Moreover, the prepared AgNC@MIL-101(Fe) showed the higher catalytic activity for 4-NP reduction than that of the PVP-stabilized Ag NPs. The MIL-101 framework with magnetic property also enabled it to be separated from the reaction solution only through a simple magnetic separation.

As one of the most important MOFs, Prussian blue (PB), which consists of a mixed-valence iron(III) hexacyanoferrate(II) compound of composition $Fe_4[Fe(CN)_6]_3$ with a face-centered-cubic (fcc) crystal structure [200], is considered to be a potential precursor for nanoporous Fe_2O_3 with high surface area. Firstly, Ag NPs were loaded on PB surface by *in-situ* reduction. Next, Ag NPs were successfully dispersed on nanoporous Fe_2O_3 (Ag/Fe_2O_3) microboxes via simply annealed process. The prepared Ag/Fe_2O_3 microboxes exhibited good magnetic separability and excellent catalytic activity towards 4-NP reduction. The excellent catalytic property of the Ag/Fe_2O_3 microboxes was mainly attributed to their high specific surface area and the rapid electron transfer from Ag NPs to Fe_2O_3 microboxes [201]. Here, the comparison of various MOFs-supported Ag NPs catalysts for 4-NP reduction is summarized in Table 4.

3.5 POFs-supported Ag NPs for 4-NP reduction

Porous organic frameworks (POFs) are another novel porous materials, which are fabricated solely from organic building blocks [202]. It is classified as covalent organic frameworks (COFs), polymers of intrinsic microporosity (PIMs), and conjugated micro- and meso-porous polymers (CMPs), representing a extensively researched family of porous organic materials, which are commonly fabricated by organic coupling reactions [203]. POFs with permanent porosity, which are different from zeolites [204, 205] or other porous materials [206], exhibit excellent design flexibility as the choice of organic building units can be regulated [207]. In addition, catalytic reactions occurred in confined space may exhibit enhanced catalytic property because of the confinement effect [208].

CMPs networks, one of the most important POFs, are a promising catalyst support because they are relatively thermally robust and chemically stable, and have a tunable micropore size distribution and surface area, which can be controlled by the length of the rigid organic linkers [209]. Cao et al. [210] reported a CMP material with pore function of cyano and pyridyl groups which served as potential binding sites for Ag^+ ion capture. Ultrasmall Ag NPs (~ 3.9 nm) (Fig. 15(c)) were successfully supported on the pre-prepared CMPs, yielding Ag^0@CMP composites via a simple liquid impregnation and light-induced reduction strategy (Fig. 15(a)). The prepared Ag^0@CMP composites could be used as high-performance nanocatalyst for 4-NP reduction at various temperatures (Figs. 15(b) and 15(d)). This work provided a highly efficient platform to obtain ultrasmall Ag NPs embedded in porous CMPs supports with excellent catalytic property.

COFs, as a novel porous crystalline materials, which are prepared through organic building blocks by covalent bonds [211]. The open porous structures and eminent stability of COFs make them become a promising host substrate for the preparation of metal-based catalysts. Shi et al. [212] presented a simple encapsulation strategy for incorporation of Au NPs with different sizes (3.8–100 nm) and shapes (sphere and rod) into a 2D COFs material prepared via reacting 1,3,5-tris(4-aminophenyl)benzene (TAPB) with 2,5-dimethoxyterephthaldehyde (DMTP). The prepared composite catalysts showed high crystallinity, excellent thermal stability, large specific surface area, open mesopores, and good catalytic property for 4-NP reduction. The comparison of various POFs-supported Ag NPs catalysts for 4-NP reduction is also presented in Table 4.

4 Anisotropic Ag NPs for 4-NP reduction

As we know, the particle size and morphology dominate the catalytic activity of Ag-based NPs catalysts, thus it is urgently needed to control

Table 4 Comparison of catalytic activity for various MOFs-supported Ag NPs and porous organic frameworks (POFs)-supported Ag NPs catalysts

Catalyst	Concentrations		Catalyst (mg)/Ag loading (wt.%)	Ag NPs size (nm)	k^a ($\times 10^{-3}$ s^{-1})	Ref.
	4-NP (mM)	$NaBH_4$ (mM)				
AgNC@MIL-101(Fe)	0.2	100	1/0.065	< 1	5.24	[198]
Ag/Fe_2O_3 microboxes	0.1	200	7/2.5	16.8	7	[201]
Ag^0@CMP	10	1000	7.4/0.5	3.9	1.36	[210]

[a] k represents the reaction rate constant, which is calculated from the equation: $\ln(C_t/C_0) = -kt$.

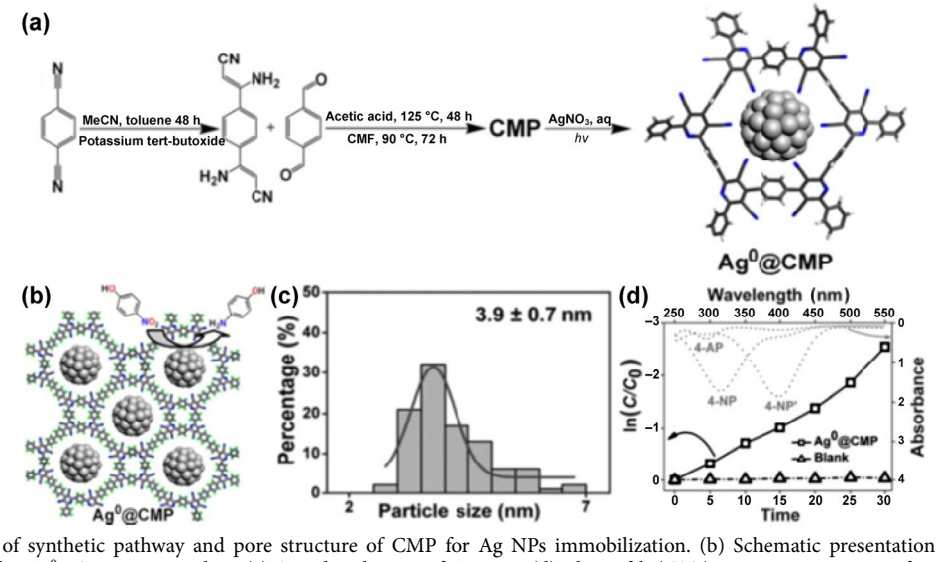

Figure 15 (a) Illustration of synthetic pathway and pore structure of CMP for Ag NPs immobilization. (b) Schematic presentation of the proposed process of nitrophenol reduction on the Ag^0@CMP nanocatalyst. (c) Size distribution of Ag NPs. (d) Plots of $\ln(C/C_0)$ versus reaction time for the Ag^0@CMP nanocatalyst. Reproduced with permission from Ref. [210], © American Chemical Society 2017.

their morphologies for better tailoring the catalytic performance. The total amount of active surface sites in anisotropic Ag NPs is much larger than spherical isotropic Ag NPs, and thus small molecule reactants can be easily adsorbed onto the surface of anisotropic Ag NPs due to the existed sharp edges and corners. The anisotropic Ag NPs exhibited much higher catalytic activity than that of spherical isotropic Ag NPs. Here, the comparison of various anisotropic Ag NPs catalysts for 4-NP reduction is summarized in Table 5.

Recently, various shaped Ag NPs, i.e., plates, rods, wires, disks, triangles, prisms, etc. have been investigated for 4-NP catalytic reduction [213]. For example, Sadeghi's group [214] reported a novel reduction way to convert Ag NPs into Ag nanorods (Ag NRs) and Ag nanoplates (Ag NPTs) in DMF without the supply of external energy. This report paved a way to the shape-controlled synthesis of Ag nanostructures. The prepared Ag NRs and Ag NPTs exhibited higher catalytic activity than that of the spherical Ag NPs. Maiyalagan et al. described a simple method to synthesize Ag NRs using the polyol process, where propylene glycol acted as reducing agent and solvent, and PVP served as capping reagent. The prepared Ag NRs possessed good catalytic property [215]. Kim et al. [216] presented an one-pot photochemical synthesis strategy for the preparation of monodispersed and size-controllable Ag nanodisks (Ag NDs) by using white light from a conventional metal halide lamp. They adjusted the size of the Ag NDs ranging from 15 to 60 nm by a "dilution-control" method. The catalytic study indicated that the catalytic reduction property toward 4-NP was enhanced with the increasing concentration of Ag NDs. Miao et al. [217] prepared monodispersed Ag nanowires (Ag NWs, ~ 10 mm in length and ~ 65 nm in diameter) in high yield using a modified polyol strategy. Their strategy combined the excellent catalytic property of Ag, high specific surface area of NWs, and mechanically stable network-like porous liquid marble shells, resulting in highly efficient catalytic properties. Thus, the prepared catalyst showed excellent catalytic property (the k is up to 6.83×10^{-3} s^{-1}), good recyclability and reusability. Camargo's group [213] investigated systemically the effect of different Ag NPs shapes (quasi-spheres, cubes, triangular, prisms, and wires) and crystalline structures on the catalytic activity. They found the catalytic activities order of these Ag NPs was triangular > prisms and quasi-spheres > wires ≫ cubes, demonstrating the shapes and crystal structures of Ag NPs played a significant role in the catalytic activity.

Apart from the aforementioned structures, dendritic Ag NPs have also recently aroused increasing attention because of their appealing supramolecular structures, high ratio of surface area to volume, and favorable connexity among different sections of the nanostructures [23, 218–220]. Ag nanodendrites (Ag NDDs) are other promising anisotropic Ag NPs with innumerable active points and sharp edges, which could be obtained by an easy and surfactant/template-free approach, and have shown excellent catalytic property for the reduction of 4-NP. Through adjusting the concentration of $AgNO_3$ aqueous solution and the reaction time, various shapes of Ag NDDs were successfully prepared (Figs. 16(a)–16(d)). The prepared Ag NDDs were an ideal catalyst for 4-NPs reduction (Fig. 16(e)) due to the facile synthesis route and high catalytic activity [218]. Similarly, Rashid et al. [221] presented a simple template and surfactant-free wet-chemical way under room temperature for the preparation of different dendritics (DDs) nanostructured Ag NPs. The results revealed the close interrelation between $AgNO_3$ concentration and Ag DDs morphology, and the synthesized Ag DDs exhibited higher catalytic reduction activity toward 4-NP than the spherical Ag NPs.

Hollow structured Ag NPs such as Ag nanocages are another kind of important anisotropic Ag NPs catalyst. These anisotropic Ag NPs possess porous interior and exterior surfaces, and exhibit high catalytic property because of the inside encapsulated reactants, large surface-to-volume ratio and exceedingly thin continuous electrical wall surfaces [222–225]. Jiang's group reported a facile method for the fabrication of well-defined hollow structured and size-controlled Ag nanocages (Ag NCs) using size-tunable NaCl nanocrystals as the templates (Fig. 17). Moreover, Ag@NaCl NPs (NaCl was not washed away), Ag-SCT (Ag NPs prepared by salt-crystal-

Table 5 Comparison of catalytic activity for various anisotropic Ag NPs catalysts

Catalyst	Concentrations		Catalyst (mg)	k^a ($\times 10^{-3}$ s^{-1})	Ref.
	4-NP (mM)	$NaBH_4$ (mM)			
Ag NWs-based liquid marbles	2	200	0.01	6.83	[217]
Ag NDDs	0.1	300	2	5.63	[218]
Ag DDs	0.103	300	0.004	5.19	[221]
Ag NCs	5	100	0.94	3.83	[228]
Hollow Ag NSs	0.5	80	0.085	2.04	[229]

[a] k represents the reaction rate constant, which is calculated from the equation: $\ln(C_t/C_0) = -kt$.

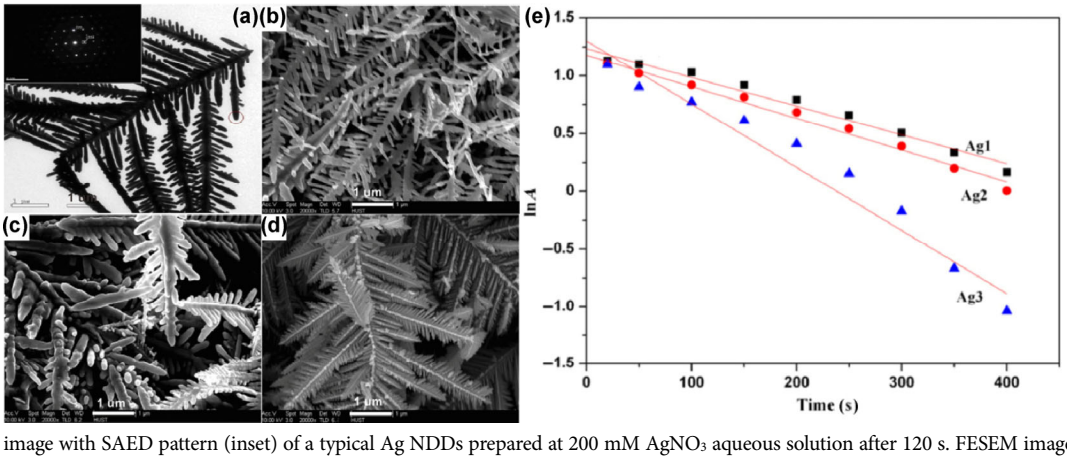

Figure 16 (a) TEM image with SAED pattern (inset) of a typical Ag NDDs prepared at 200 mM $AgNO_3$ aqueous solution after 120 s. FESEM images of the obtained Ag NDDs in the 200 mM $AgNO_3$ aqueous solution for reaction (b) 10 s (Ag1), (c) 60 s (Ag2), and (d) 120 s (Ag3). (e) Plots of ln A vs. time t for the Ag1, Ag2, and Ag3 for 4-NP catalytic reduction at room temperature. Reproduced with permission from Ref. [218], © Elsevier B.V. 2012.

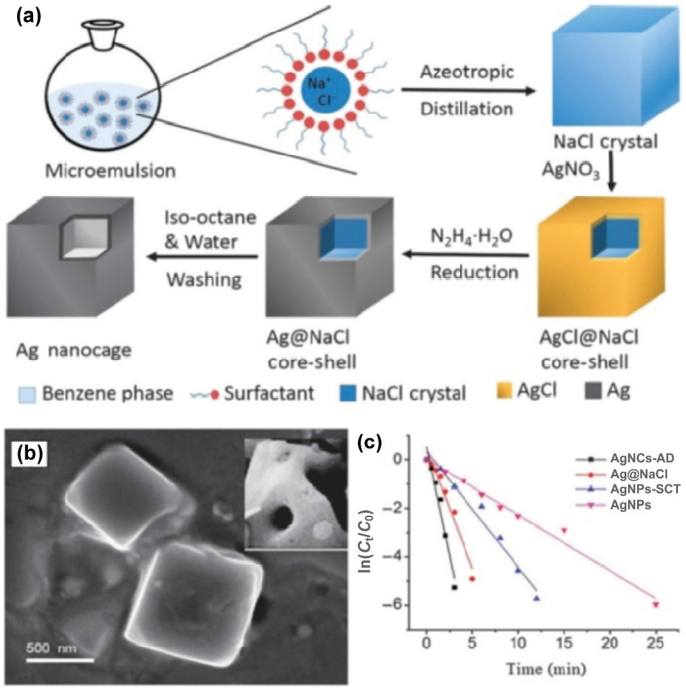

Figure 17 (a) Diagrammatic sketch of the azeotropic distillation assisted route for the preparation of AgNCs. (b) Typical SEM image of AgNCs-AD, the inserted is a magnified image of the sample, showing the hollow interiors of the cubic cages. (c) $\ln(C_t/C_0)$ versus reaction time t for 4-NP reduction with different catalysts. Reproduced with permission from Ref. [222], © American Chemical Society 2015.

template (SCT) method) [226] and Ag NPs (~ 5 nm) were also synthesized for better comparison. It was obvious that the catalytic performance of these catalysts followed an order of AgNCs-AD > Ag@NaCl > Ag-SCT > Ag NPs. From the previous reports, sharper, rougher edges and corners on both the inner and outer surfaces possessed more valency-unsatisfied surface atoms to serve as active sites [227], and thus, anisotropic Ag NPs (such as AgNCs-AD, Ag@NaCl, and Ag-SCT) possessed a higher catalytic property compared to the Ag NPs. Furthermore, the synthesized AgNCs-AD (AgNCs prepared by anazeotropic distillation assisted route) possessed smaller size and narrower size distribution than that of Ag-SCT, which could well explain why the removal of NaCl improved almost doubly the catalytic property [228]. Hollow Ag nanospheres (Ag NSs) are an important hollow structured Ag NPs, which could be prepared through a direct reaction of $AgNO_3$, NaOH and $(NH_2OH)_2{\cdot}H_2SO_4$ with gelatin. The prepared hollow Ag NSs showed excellent catalytic reduction property toward 4-NP, demonstrated by the larger reaction rate constant than other spherical Ag NPs catalysts [229].

5 Bimetallic Ag NPs

Bimetallic NPs commonly composed of various noble metals like Ag, Au, Pd, Pt, etc., have recently received increasing interest especially in catalysis areas. They always showed improved catalytic property when compared to their corresponding monometallic counterparts because of their composition-dependent property and synergistic effect [230, 231]. The catalytic property of bimetallic Ag NPs catalysts mainly depends on the geometric and electronic states of Ag, which can be significantly affected by blended foreign element [231]. For this kind of nanostructure, Ag compounds were combined with Au, Pd, Pt, etc. to fabricate bimetallic Ag NPs with different structures (core-shell, alloy and anisotropic) which showed enhanced catalytic reduction property for 4-NP. Similar to monometallic Ag NPs, various substrates are necessarily used to support the bimetallic Ag NPs in case of aggregation. In this section, Ag NPs will be categorized as alloy, core-shell, anisotropic and mixed bimetallic according to the nature of structures. The comparison of various bimetallic Ag NPs catalysts for the reduction of 4-NP is summarized in Table 6.

5.1 Bimetallic alloyed Ag NPs

During recent decades, researchers have focused on bimetallic alloys that commonly possess improved catalytic activity and stability compared to monometallic Ag NPs, mainly attributed to the combined synergistic effects between Ag NPs and other metals. The bimetallic alloyed Ag NPs are usually obtained through the methods of co-reduction, thermal decomposition, seed-mediated growth, and galvanic replacement reaction (GRR) [232–234].

Among them, Au-Ag alloyed bimetallic NPs have been widely investigated due to their specific composition-tunable plasmons property and can be used as a potential catalyst [235]. The most frequently reported structures of Au-Ag alloyed bimetallic NPs include solid NPs, hollow and porous nanoshell structures (HPNSs) [236, 237]. The wet-chemical approach is often utilized for the preparation of traditional Au-Ag alloyed solid NPs by the co-reduction of $HAuCl_4$ and $AgNO_3$ precursors. Unfortunately, such kind of way possesses two potential issues: the co-precipitation of AgCl in water and phase segregation [238, 239]. To solve AgCl precipitation problems, Rajendra et al. [240] synthesized uniform citrate-stabilized alloyed Au-Ag NPs with an average size < 10 nm using NH_4OH as an additive. This original synthetic process elucidated that the catalytic activity and stability could be influenced by alloy structure. Compared with solid NPs, HPNSs exhibited many unique merits such as larger ratio of surface area to volume, lower aggregation, and widely controllable plasmonics wavelengths [241]. A lot of reports have confirmed that the alloyed Au-Ag HPNSs possessed higher catalytic activity than solid NPs due to the larger ratio of surface area to volume. Wu et al. [242] detailly studied the catalytic performance of some similar-sized HPNSs with different structural openness degrees, and found that the shape and porous structure of HPNSs played a decisive impact on catalytic activity of Au-Ag alloyed HPNSs. Liu's group [243] revealed that the Au/Ag co-existence could greatly affect the physicochemical stabilities, which played a key role in the catalytic property of Au-Ag alloyed HPNSs. Moreover, the simple regulation of sacrificial Ag NPs size would greatly promote the physicochemical stabilities.

Another method is using GRR among Ag NPs and $AuCl_4^-$ to construct Au-Ag alloyed bimetallic NPs because $AuCl_4^-$/Au holds a higher standard reduction potential (1.0 V vs. SHE) than Ag^+/Ag (0.80 V vs. SHE) [244]. Xia et al. [245] reported a novel and green way (i.e., GRR) to prepare Ag-Au alloyed bimetallic NPs (Fig. 18). The NPs were simply fabricated by mixing Au^+ with the as-synthesized Ag NPs seeds in the presence of degraded pueraria starch (DPS) aqueous solution, which served as both a capping agent and reductant. The prepared DPS-capped Au-Ag alloyed bimetallic NPs exhibited a higher catalytic performance (k is up to 53.6×10^{-3} s^{-1}) for the reduction of 4-NP than DPS-reduced AuNPs and DPS-reduced Ag NPs. Lee et al. [246] prepared hollow structured SiO_2-coated Ag-Au nanoboxes through a simple GRR involving SiO_2-coated Ag nanocubes and $AuCl_4^-$, which possessed improved catalytic property and reusability for 4-NP reduction when compared to the SiO_2-coated Ag nanocubes. Guo et al. [247] synthesized heterostructural Ag-Au bimetallic nanocrystals decorated Fe_3O_4@carbon composite microspheres (Fe_3O_4@C@Ag-Au) via a simple and one facile and steerable method, in which the surface loaded Ag nanocrystals acted as a reductant for the GRR. Among them, the carbon acted as a catalyst support for the construction of bimetallic nanocrystals. The catalytic performance tests of Fe_3O_4@C@Ag-Au showed a positive concentration-dependent behavior with the Au contents. Additionally, the magnetic recycling capacity of the Fe_3O_4@C@Ag-Au composite microspheres could be achieved after successive reaction runs.

Table 6 Comparison of catalytic activity for various bimetallic Ag NPs catalysts

Catalyst	Concentrations		Catalyst (mg)/Ag loading (wt.%)	Ag NPs size (nm)	k^a ($\times 10^{-3}$ s^{-1})	Ref.
	4-NP (mM)	$NaBH_4$ (mM)				
Au-Ag HPNSs	7.5	1,000	0.01/26.8	—	32	[243]
DPS-capped Au/Ag	0.2	15	0.3/7.51	26	53.6	[245]
SiO_2-coated Ag/Au	2	100	0.1/—	45.6	5.63	[246]
Fe_3O_4@C@Ag-Au	5	20	0.01/7.65	25	15.8	[247]
Cu/Ag alloyed bimetallic NPs	0.1	300	2/62.6	14.3	3.95	[249]
Ag-Cu NPs	1.2	2,670	10/69.1	—	2.97	[253]
MOFs-supported Au@Ag	0.18	353.5	3.46/2	—	4.97	[254]
Au@Ag core-shell NCs	1	100	—/—	22.5	0.16	[262]
Au@Ag core-shell bimetallic NPs	15	100	1.5/—	10	3.53	[263]
Au@Ag core-shell NPs	0.2	16	0.1/—	3	5.4	[264]
Au@Ag core-shell NCs	1	10	—/19.03	6.5	3	[265]
PEMs-supported Au@Ag	0.2	10	—/22.2	—	3	[266]
Au@Ag@PDA	0.2	15	—/—	10	0.83	[267]
Au/Ag dendrites	0.07	150	0.6/19.1	—	6.07	[269]
Pd-Ag dendrites	1	10	0.1/63.38	—	7.53	[270]
Au-Ag alloy nanoprisms	0.05	50	—/82.52	84	1.7	[271]
Ag-Pd hollow NPs	1	100	0.15/—	100	0.69	[272]
Ag@Ag-Pd NFs	0.2	359.4	0.0026/97.2	39.2	2.13	[282]
Ag@Pd-Ag NCs	200	359.4	—/92.7	39.2	2.81	[281]

[a] k represents the reaction rate constant, which is calculated from the equation: $\ln(C_t/C_0) = -kt$.

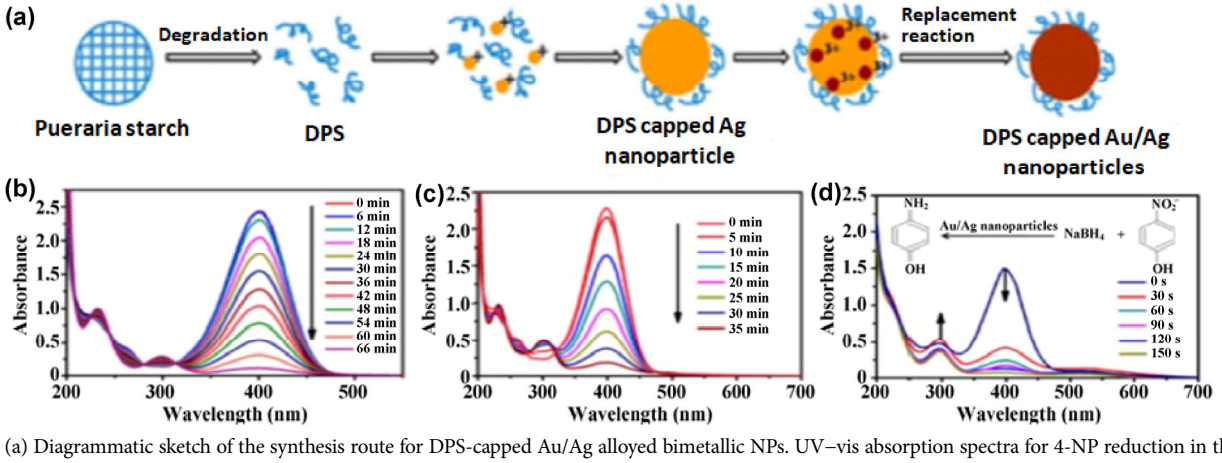

Figure 18 (a) Diagrammatic sketch of the synthesis route for DPS-capped Au/Ag alloyed bimetallic NPs. UV–vis absorption spectra for 4-NP reduction in the existence of (b) DPS-reduced Ag NPs, (c) DPS-reduced Au NPs, and (d) DPS-capped Au-Ag alloyed bimetallic NPs. Reproduced with permission from Ref. [245], © American Chemical Society 2013.

Although many research have been devoted to fabricating alloyed bimetallic Ag NPs including Au-Ag, Pd-Ag, etc., there are very still few reports on Cu-Ag alloyed bimetallic NPs because the difference of lattice constants between Cu (0.409 nm) and Ag (0.361 nm) which makes it difficult to prepare Cu-Ag alloyed bimetallic NPs [248]. In order to overcome these problems, the thermodynamic and kinetic aspects governing the synthesis system can provide effective remedies. Wu et al. [249] proposed a facile one-pot method to synthesize the uniform Cu-Ag alloyed bimetallic NPs. In this way, the low-cost glucose was utilized as reductant, and hexadecylamine was selectively chosen as capping agent for Cu [250, 251]. The prepared Cu-Ag alloyed bimetallic NPs possessed much better catalytic property than monometallic Ag NPs. Moreover, polyol method as a new generation method was also exploited to prepare Cu-Ag alloyed bimetallic NPs. The prepared alloyed nanostructures showed improved physical and chemical properties, and better stability [252]. Verman et al. [253] developed a polyol preparation route to synthesize Ag-Cu bimetallic NPs (Ag-Cu NPs) by a polyol synthesis route, and for the first time studied how the size was changed and morphology of Ag-Cu bimetallic NPs influenced by the precursor salts ingredients. The prepared Ag-Cu NPs exhibited a high catalytic performance and good chemical stability for 4-NP reduction.

5.2 Core-shell bimetallic Ag NPs

Core-shell structured bimetallic Ag NPs received great interests attributed to their specific property and great potential as well as higher catalytic performance for catalyst applications when compared to their monometallic Ag NPs or even alloyed Ag NPs [254, 255].

Among them, bimetallic Au@Ag core-shell NPs have attracted the most interest in catalytic applications. A great number of research groups have presented different methods such as seed-mediated growth [256, 257], microwave-polyol [258], plasmon-mediated growth [259, 260], and sequential loading [261], etc. to fabricate various Au@Ag core-shell NPs. For example, Tsao et al. [262] recently reported a novel Au@Ag core-shell nanocrystal with the Au core size-dependent catalytic activity. On the basis of this report, Haldar et al. [263] paid

a close attention to how the core size of the Au@Ag core-shell bimetallic NPs affected the catalytic activity. The catalytic efficiency varied from 41.8% to 96.5% with the size of core changing from 10 to 100 nm, and the Au_{100}@Ag bimetallic core-shell NPs was found to be about 12 times compared to the 100 nm sized pure Au NPs (Fig. 19). Therefore, the catalytic activity is strongly dependent on the core size of the Au@Ag core-shell bimetallic NPs. Li et al. [264] prepared a narrow-size distributed and water-soluble Au@Ag core-shell NPs with a diameter ranging from 1 to 5 nm by utilizing unmodified apoferritin as template. The thickness of Ag shell could be changed to one or several layers by regulating the loading Ag-precursor concentration and the prepared catalyst showed a highly efficient catalytic performance for the reduction of 4-NP. Besides, a similar Au@Ag core-shell nanocomposite was proposed by Monga et al. [265] which showed a higher catalytic property than monometallic NPs for the reduction of 4-NP.

In addition, many polymers, MOFs, and metal oxides based colloidal or solid scaffolds have also been utilized to support Au@Ag core-shell bimetallic NPs [266, 267]. Xu's group [254] developed the MOF-supported Au@Ag core-shell bimetallic NPs for the first time using a sequential deposition-reduction approach (Fig. 20(a)). The Au@Ag NPs with a small diameter (ca. 2–6 nm) revealed the porous surface structure of MOF, which could provide a steric restriction to hinder the Au@Ag NPs growth (Fig. 20(b)). Moreover, the prepared MOF-supported Au@Ag core-shell bimetallic NPs possessed superior catalytic performance than the alloyed and monometallic NPs (Fig. 20(c)) mainly attributing to the synergistic effects of the Au@Ag NPs core-shell structure. Analogously, polyelectrolyte multilayers (PEMs)-supported Au@Ag core-shell bimetallic NPs also showed much higher catalytic property for the reduction of 4-NP than the monometallic Ag NPs and neat Ag NPs because of the combined Au/Ag synergistic effect [266]. Zhou et al. [267] reported a PDA

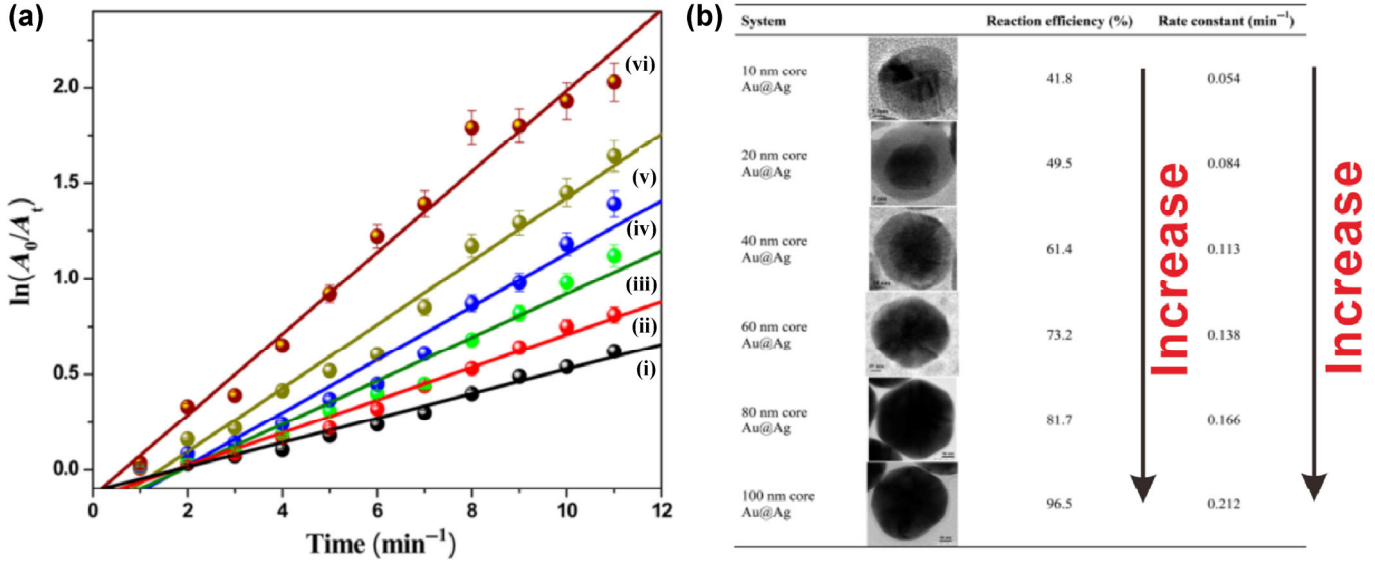

Figure 19 (a) $\ln(A_0/A_t)$ vs. time t plot for determination of rate constants of Au@Ag core-shell bimetallic NPs with core diameter (i) 10, (ii) 20, (iii) 40, (iv) 60, (v) 80, and (vi) 100 nm. (b) Catalytic reaction efficiency and the rate constant of the 4-NP reduction by Au@Ag core-shell bimetallic NPs. Reproduced with permission from Ref. [263], © American Chemical Society 2014.

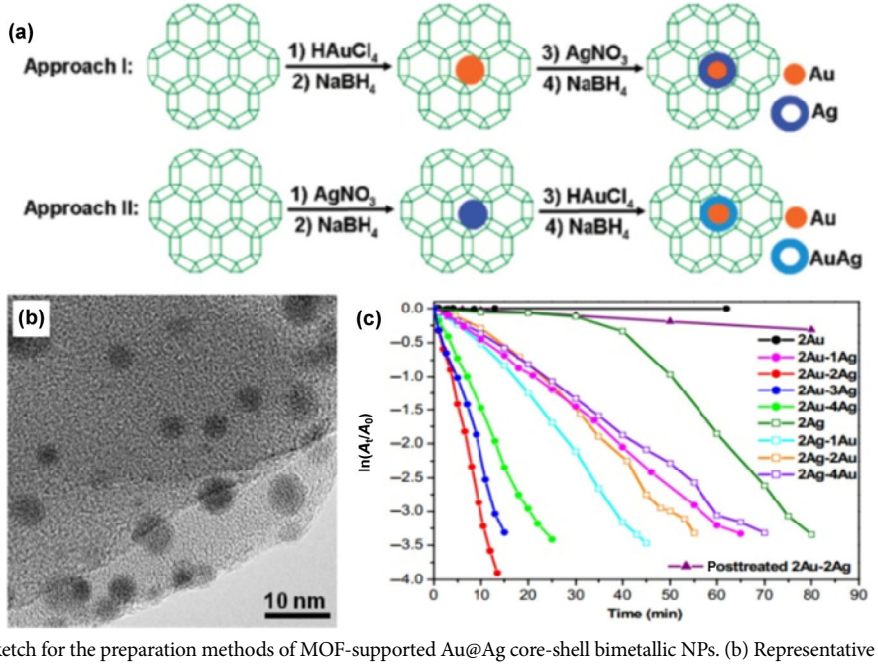

Figure 20 (a) Diagrammatic sketch for the preparation methods of MOF-supported Au@Ag core-shell bimetallic NPs. (b) Representative TEM images of MOF-supported Au@Ag core-shell bimetallic NPs. (c) Plots of $\ln(A_t/A_0)$ versus time t for 4-NP reduction over different catalysts. Reproduced with permission from Ref. [254], © American Chemical Society 2011.

coating-based method for the construction of highly efficient Au@Ag@PDA core-shell NPs. This way involved one-step seeds growth, interface self-assembly, and loading of the densely packed Au@Ag@PDA core-shell NPs on solid substrates. It was noted that the Ag shell seeds with controllable thickness were grown on Au NPs (Figs. 21(b)–21(d)), and then the as-obtained Au@Ag core-shell bimetallic NPs were coated with the PDA (Fig. 21(a)). The PDA coating possessed many advantages for the fabrication of recyclable Au@Ag core-shell NPs catalysts. First, Au@Ag@PDA NPs can self-assemble to a closely packed monolayer structures. Second, the self-polymerized PDA showed very strong adhesion to many organic and inorganic substrates, which facilitated steady binding of the interface self-assembly of Au@Ag core-shell bimetallic NPs on solid substrates. Third, abundant hydrophilic groups endowed PDA coating with porous hydrogel-like structure, which was beneficial to free transportation of reactants to catalyst surfaces. In addition, Au and Ag shell could also be formed on nanocrystal seeds to construct monometallic Au@Au@PDA NPs and Ag@Ag@PDA NPs, respectively (Figs. 21(e) and 21(f)). The rate constant of Au@Ag@PDA core-shell NPs was more than 2 times of those of monometallic Au@Au@PDA NPs and Ag@Ag@PDA NPs, which showed a synergistic effect in the Au@Ag@PDA core-shell nanostructures, improving their catalytic property (Fig. 21(g)).

5.3 Anisotropic bimetallic Ag NPs

Similarly to anisotropic monometallic Ag NPs, anisotropic bimetallic Ag NPs have also attracted increasing interest in many fields because of their superior physical, chemical, biological, and particularly catalytic properties to those of the spherical bimetallic Ag NPs [20]. The catalytic activity of bimetallic Ag NPs relies primarily on their size and shape, and the number of active surface sites in anisotropic

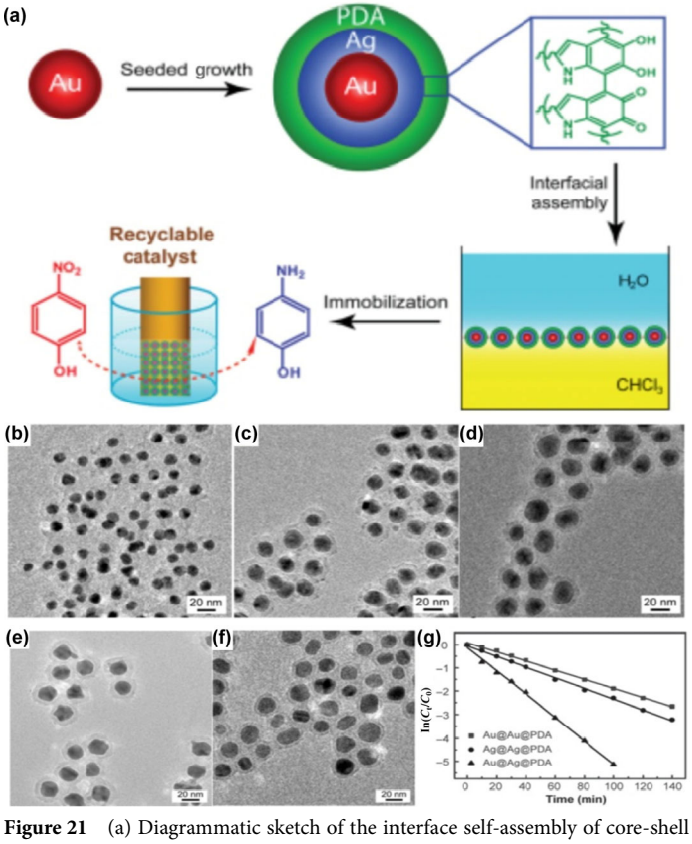

Figure 21 (a) Diagrammatic sketch of the interface self-assembly of core-shell Au@Ag@PDA NPs nanocatalysts. TEM images of Au@Ag@PDA NPs with different thickness of Ag layer ((b)–(d)). TEM images of monometallic Au@Au@PDA NPs (e) and Ag@Ag@PDA NPs (f). (g) The dependence of $\ln(C_t/C_0)$ on reaction time t for 4-NP reduction catalyzed by different catalysts. Reproduced with permission from Ref. [267], © WILEY-VCH Verlag GmbH & Co. KGaA, Weinheim 2013.

bimetallic Ag NPs is much higher than that of the spherical bimetallic Ag NPs, and thus showing enhanced catalytic activity.

Recently, bimetallic dendrites have strong anisotropic shapes and have obtained a growing attention because of their unique chemical, physical, and biological property. The high catalytic property of bimetallic dendrites is mainly attributed to the fact that nanoscaled bimetallic dendrites commonly possess a large specific surface area which causes prominent improvement of surface catalytic activity. Moreover, bimetallic dendrites can integrate the synergistic effect of corresponding monometallic counterparts, which offers an appropriate intermetallic interface where the electronic structures can be adjusted [268]. Meng's group prepared Au-Ag [269] and Pd-Ag [270] bimetallic dendrites through a GRR of Ag dendrites in a Na_2PdCl_4 solution and Ag dendrites in $HAuCl_4$ solution, respectively. The formation mechanism claimed that the original Ag was gradually consumed and then Au or Pd flakes were grown and covered on the substructure. The prepared Au-Ag and Pd-Ag bimetallic dendrites showed enhanced catalytic activity ($k > 6 \times 10^{-3}$ s^{-1}) for 4-NP reduction when compared to monometallic Ag NPs. The improved catalytic activity was mainly attributed to the synergistic effect between bimetallic dendrites. In addition, Au-Ag alloy nanoprisms have also achieved extensive attention. Kim et al. [271] prepared Au-Ag alloy nanoprisms via simultaneous reduction of $HAuCl_4$ and $AgNO_3$ by $NaBH_4$ in aqueous solution. TEM images showed that nearly all of the initial spherical alloy NPs were converted to prismatic structures. This prismatic structures exhibited higher catalytic activity toward 4-NP reduction than that of the initial spherical alloy NPs. Moreover, the prepared Au-Ag alloy nanoprisms showed tunable optical and optoelectronic property.

Similar to bimetallic Au-Ag, Ag-Pd and Ag-Pt bimetallic hollow nanostructures can also be prepared via GRR [272–275]. The Ag-Pd and Ag-Pt bimetallic hollow nanostructures with hollow or porous interiors and open surface nanostructures, i.e., porous nanocages and nanoframes, are particularly interesting as highly efficient nanocatalysts due to their high surface-to-volume ratio, surface accessibility, and nanocage confinement effects [276, 277]. Jing et al. [272] reported a simple GRR between Ag nanocubes and H_2PdCl_4 using mild reducing agents including ascorbic acid and formaldehyde. This reductant-mediated GRR could finely regulate the geometry of the Ag-Pd bimetallic hollow nanostructures with enhanced structural complicacy, and thus tuned the optical characteristic and optimized the catalytic property of Ag-Pd bimetallic nanostructures. Zhang et al. [274] reported the preparation of Pt-Ag bimetallic structures with controllable number of void spaces through a simple GRR. Ag nanocubes (NCs) were used as a template to react with Pt ions in the existence of HCl. The introduction of HCl in the GRR caused rapid precipitation of AgCl, which could grow on Ag NCs surface and served as a portable template for the formation of Pt. The number of nucleation sites could be regulated by changing the amount of HCl or by adding PVP to the reaction system. These Pt-Ag bimetallic nanostructures possessed high specific surface area and improved catalytic activity because of the existence of abundant void space and porous walls.

Bimetallic nanoframes have recently obtained growing attention in catalytic applications because of their large ratio of surface area to volume and highly open nanostructures [278, 279]. Compared to the solid counterparts, bimetallic nanoframes possess more metal atoms, making them feasible to hold highly dispersed active atoms which give a relatively large overall size. Importantly, the overall size raised led to the nanoframes not easy to fall off a catalyst support, thus improving the durability of the catalyst [280]. Qin's group [281] reported a facile route to prepare Ag@Pd-Ag NCs via co-titrating Na_2PdCl_4 and $AgNO_3$ into Ag NCs aqueous suspension in the existence of ascorbic acid (AA) and PVP at room temperature. They found that the Pd and Ag atoms were co-deposited onto the edges, corners,

and side faces of the Ag NCs in a site-by-site fashion. Moreover, the catalytic property of the Ag@Pd-Ag NCs could be optimized by regulating Pd/Ag ratio. Based on previous research, they also reported a novel Ag-enriched Ag-Pd bimetallic nanoframes with ~ 1.7 nm ridges (Fig. 22). The prepared Ag-enriched Ag-Pd bimetallic nanoframes showed significantly improved catalytic performance for 4-NP reduction compared to Ag NCs and Ag@Ag-Pd core-frame NCs as well as excellent mechanical property [282].

6 Conclusions and outlook

Ag-based nanostructured materials are considered to be the most promising catalysts toward $NaBH_4$-assisted 4-NP reduction because of their unique advantages such as tunable shape and size of Ag NPs, high catalytic activity and stability, easy preparation, relatively low cost and toxicity, environmental benignity, etc. Ballauff et al. has stressed the importance of Langmuir-Hinshelwood mechanism and applied it to this catalytic reduction reaction: the reactants can transfer fast to the Ag NPs surface meanwhile the reaction kinetics can be adjusted by reactant's reconstruction on Ag NPs surface. The reaction rate constant (k) is found to be changed in proportion to the total surface area (S) available in the Ag NPs, demonstrating that the catalytic performance is strongly dependent on their sizes

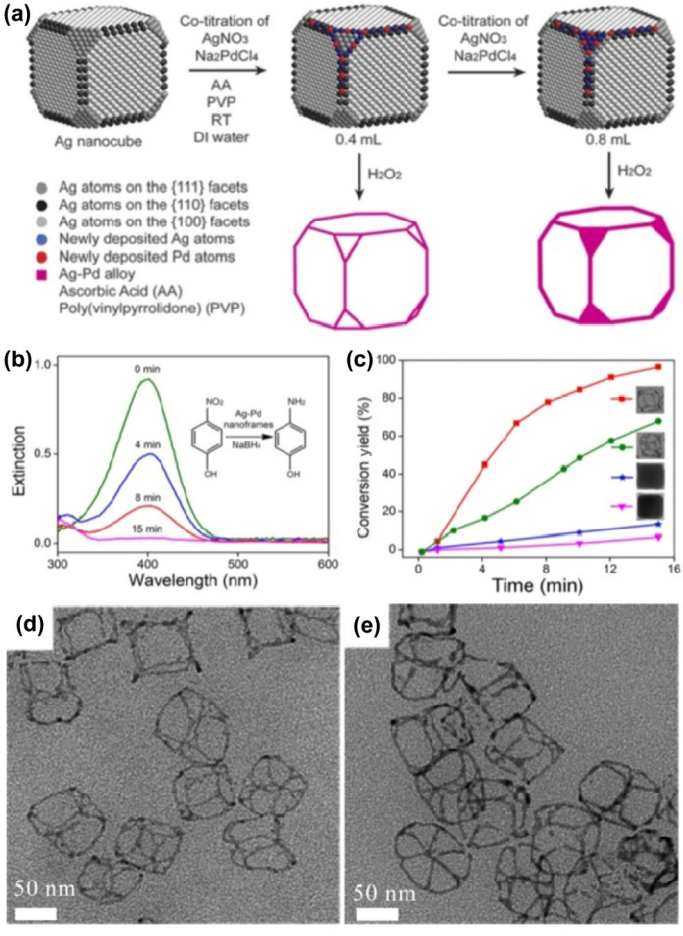

Figure 22 (a) Diagrammatic sketch of Ag-enriched Ag-Pd bimetallic nanoframes and Ag@Ag-Pd core-frame nanocubes prepared by templating with the Ag nanocubes. (b) UV–vis spectra of 4-NP solution at different time after the addition of the Ag-enriched Ag-Pd bimetallic nanoframes. (c) Comparison of 4-NP reduction as a function of time for three different types of catalysts: Ag nanocubes (triangles), Ag@Ag-Pd core-frame nanocubes (stars), and Ag-enriched Ag-Pd bimetallic nanoframes prepared by the co-titration volume of 0.4 mL (squares) and 0.8 mL (circles). (d) TEM images of the Ag-enriched Ag-Pd bimetallic nanoframes. (e) TEM images of the Ag-enriched Ag-Pd bimetallic nanoframes after centrifugation at 55,000 rpm for 30 min. Reproduced with permission from Ref. [282], © Wiley-VCH Verlag GmbH & Co. KGaA, Weinheim 2016.

and shapes. Generally, the presence of a smaller Ag NPs size and sharper edge and corner will help to enhance the total surface area, and accordingly enhance the catalytic property. The incorporation of Ag NPs into various substrates can effectively reduce Ag NPs aggregation due to their strong interaction, thus improving their catalytic activity or even endowing them with some new functions such as good stability, magnetic recoverability, environmental benignity, lower cost, etc. Anisotropic Ag NPs possess many sharp edges and corners which offer more excellent catalytic property compared to the regular spherical Ag NPs. In addition, bimetallic Ag NPs also show improved catalytic property compared to their corresponding monometallic Ag NPs because of their component-dependent characteristic and synergistic effect. These three strategies can effectively enhance the Ag-based NPs catalysts' catalytic performance.

Although a great progress has been achieved regarding Ag-based catalysts for $NaBH_4$-assisted 4-NP reduction, some problems are still not fully addressed and need to be investigated further. One of the most important issues is the inconsistency of catalytic performance tests, such as the different usage amounts of 4-NP, $NaBH_4$, and catalyst, and the disunity of testing temperature (see Tables 1–7), which makes it difficult to fairly compare the catalytic performance of various Ag-based NPs catalysts in detail. Therefore, standardization of catalytic performance tests is well worth consideration. In addition, more significant researches should be focused on the improvement of catalytic property as well as how to endow the catalyst with more functions.

Compared with some representative highly-efficient catalysts summarized in Table 7, the iron oxide-supported Ag NP catalyst has revealed a moderate reaction rate constant (i.e., 17.46) [166], which is about one third of the best one (i.e., 53.6 reported for the bimetallic Ag-Au alloy NPs) [245]. However, considering the much lower cost of iron oxides than Au, iron oxides-supported Ag NP catalysts are much more promising for a large scale industrial application. Besides the easy preparation and low cost, iron oxides-supported catalysts can be easily recovered from the target solution for reuse through a simple magnetic separation technique, which is also particularly favorable in terms of cost and environmental protection. Furthermore, iron oxides are nontoxic and environmentally benign, and thus have better prospect for practical application in industry. Although the many advantages have been demonstrated by iron oxide-supported Ag NP catalysts, a further improvement in the catalytic activity should be realized before they can be commercialized in a large scale. In addition, as evident from Table 7, the supported Ag NPs (i.e., Ag NPs supported on the SnO_2 microspheres) [181] have displayed a comparable reaction rate constant (i.e., 51.67) to that (i.e., 53.6) of the Ag-Au alloy NPs, which is mainly attributed to the highly accessible active sites generated by the uniform dispersion of small Ag NPs on the microspheres assembled with SnO_2 nanosheets. Furthermore, the mesoporous carbon supported Ag NPs demonstrated an extremely high reaction rate constant of 120, which is mainly attributed to the well-controlled particle size of the supported Ag NPs along with an excellent dispersion on the carbon support [141]. Compared with unsupported catalysts, the much higher catalytic activity of the supported Ag NPs also indicates that there is still a large room for the improvement in the catalytic activity of iron oxides-supported Ag NP catalysts. In brief, in order for supported Ag-based catalysts to achieve high catalytic performance, a rational design in the morphology and nanostructure of the support is very important. In selection of advanced catalyst supports from polymers, porous carbons, oxides, MOFs, and COFs, the following considerations should be given: 1) incorporating magnetic oxide(s) for good recoverability; 2) introducing hierarchical nanostructure for fast mass transport; 3) possessing large surface area for more active sites and enhanced catalytic activity; and 4)

Table 7 Summary and comparison of advantages and highest catalytic activity for representative highly efficient Ag-based NPs catalysts

Catalyst	Advantages	Concentrations		Catalyst (mg)/ Ag loading (wt.%)	Highest k [a] ($\times 10^{-3}$ s^{-1})	Ref.
		4-NP (mM)	$NaBH_4$ (mM)			
Supported Ag NPs	Supporter reduces Ag NPs aggregation and endows them with highly accessible active sites and new functions such as excellent chemical and thermal stability, etc.	10	45	—/13.6	120	[141]
PS-supported Ag NPs	PSs have controllable sizes and uniform spherical shapes, providing Ag NPs with a tunable catalytic property	0.1	60	2/9.66	8.17	[44]
Conductive polymer-supported Ag NPs	Easy preparation and controllable doping process, excellent thermal and environmental stability, low cost, and strong binding ability with Ag NPs	0.14	—	0.03/—	35.8	[57]
Other polymer-supported Ag NPs	Polymer acts as a proper reducer and stabilizer; has strong binding ability and uniform structure for immobilizing Ag NPs with low preparation cost, easy separation, and abundant active sites	10	100	5/—	21.7	[92]
Graphene-supported Ag NPs	Graphene has a large specific surface area, tunable surface property, remarkable electrical property, and good chemical and thermal stability	0.03	0.1	3/—	8.22	[109]
CNTs-supported Ag NPs	CNTs have a high ratio of surface area to volume, excellent stability, chemically controllable topography, low cost and facile reclaim of various metals	50	400	—/—	19.8	[127]
Other carbon-supported Ag NPs	Large red-edge effects, strong electron donor/acceptor capability, large aqueous solubility, high photostability, low cytotoxity, excellent reactivity, thermal insulation, low density, high compressive strength, large cavity space, strong binding ability with Ag NPs, etc.	10	45	—/13.6	120	[141]
SiO_2-supported Ag NPs	Freely movable active Ag cores and protective mesoporous SiO_2 shells provide large specific surface area and interstitial hollow space, low density, rapid mass transfer excellent stability, low cost, and robust surface chemistry, etc.	16	800	2/3.6	18	[148]
Iron oxides-supported Ag NPs	Iron oxides are easily to synthesize, and possess abundant active surface for adsorption and decoration of Ag NPs with excellent magnetic recoverability	10	100	1.2/—	17.46	[166]
CeO_2-supported Ag NPs	Morphological compatibility with Ag NPs, enabling them to have large interfacial area and greatly enhanced catalytic property	0.13	20	0.25/28	32.6	[173]
Al_2O_3-supported Ag NPs	High specific surface area, abundant porous structure and good thermal stability	0.09	204	0.3/10	3.2	[177]
Ag-supported SnO_2	Large bandgap, high electron mobility, low cost, less toxic and excellent chemical and thermal tability	0.14	6.95	1.5/—	51.67	[181]
Composites of two or more oxides-supported Ag NPs	Hierarchical and multifunctional characteristics, combined with the advantages of various supports	5	200	3/3.72	11.3	[192]
MOFs-supported Ag	High specific surface area, structural diversity, and tailorability	0.2	100	1/0.065	5.24	[198]
POFs-supported Ag NPs	Thermally robust and chemically stable, tunable micropore size distribution and surface area	0.1	200	7/2.5	7	[201]
Anisotropic Ag NPs	Abundant active surface sites due to the existence of sharp edges and corners	2	200	0.01/—	6.83	[217]
Bimetallic Ag NPs	Composition-dependent property and synergistic effect for enhanced catalytic activity	0.2	15	0.3/7.51	53.6	[245]

[a] The highest catalytic activity among these kinds of catalysts. k represents the reaction rate constant, which is calculated from the equation: $\ln(C_t/C_0) = -kt$.

having strong interaction with the supported Ag NPs for improved chemical stability. As we know from this review, nanostructured supports with a hierarchical porosity are rarely reported, thus further research should be concentrated on the construction of novel hierarchically nanostructured Ag hybrid catalysts due to their excellent catalytic property and high cycling stability. Anisotropic Ag NPs with various shapes such as nanoplates, nanorods, nanowires, nanodisks, nanoprisms, nanodendrites, and nanocages, have demonstrated better catalytic property than the regular spherical Ag NPs because of their sharp edges and corners, providing more active sites. More efforts should be made in future to create anisotropic Ag NPs with sharper edges and corners. Bimetallic Ag NPs including alloyed, core-shell, and anisotropic structures also show significantly improved catalytic property because of their composition-dependent property and synergistic effect. Future work should be focused on choosing a suitable substrate for supporting bimetallic Ag NPs, which will be able to effectively reduce their aggregation, and thus further improving their catalytic property. There is no doubt that rational design of novel Ag-based catalysts with a tailored shape, size and structural characteristics will pave a highly efficient avenue to catalytic reduction of nitrophenol.

Acknowledgements

This work is supported by the National Natural Science Foundation of China (NSFC) (Nos. 21674130, 51873234 and 51573039), the Natural Science Foundation of Guangdong Province (Nos. 2017A030313254 and 2017A030310349), the Fundamental Research Funds for the Central Universities (No. 17lgjc02), PetroChina Innovation Foundation (No. 2017D-5007-0505), and Research Start-up Funds of DGUT (No. GC300501-116). Key Laboratory Opening Fund of PCFM is also gratefully acknowledged.

References

[1] Mika, L. T.; Cséfalvay, E.; Németh, Á. Catalytic conversion of carbohydrates to initial platform chemicals: Chemistry and sustainability. *Chem. Rev.* **2018**, *118*, 505–613.

[2] Gawande, M. B.; Goswami, A.; Felpin, F. X.; Asefa, T.; Huang, X. X.; Silva, R.; Zou, X. X.; Zboril, R.; Varma, R. S. Cu and Cu-based nanoparticles: Synthesis and applications in catalysis. *Chem. Rev.* **2016**, *116*, 3722–3811.

[3] Gao, D. W.; Zhang, X.; Dai, X. P.; Qin, Y. C.; Duan, A. J.; Yu, Y. B.; Zhuo, H. Y.; Zhao, H. R.; Zhang, P. F.; Jiang, Y. et al. Morphology-selective synthesis of active and durable gold catalysts with high catalytic performance in the reduction of 4-nitrophenol. *Nano Res.* **2016**, *9*, 3099–3115.

[4] Xiong, W.; Sikdar, D.; Yap, L. W.; Guo, P. Z.; Premaratne, M.; Li, X. Y.; Cheng, W. L. Matryoshka-caged gold nanorods: Synthesis, plasmonic properties, and catalytic activity. *Nano Res.* **2016**, *9*, 415–423.

[5] Ai, Y. J.; Hu, Z. N.; Shao, Z. X.; Qi, L.; Liu, L.; Zhou, J. J.; Sun, H. B.; Liang, Q. L. Egg-like magnetically immobilized nanospheres: A long-lived catalyst model for the hydrogen transfer reaction in a continuous-flow reactor. *Nano Res.* **2017**, *11*, 287–299.

[6] Liao, G. F.; Fang, J. S.; Li, Q.; Li, S. H.; Xu, Z. S.; Fang, B. Z. Ag-based nanocomposites: Synthesis and applications in catalysis. *Nanoscale* **2019**, *11*, 7062–7096.

[7] Cheng, T. Y.; Zhang, D. C.; Li, H. X.; Liu, G. H. Magnetically recoverable nanoparticles as efficient catalysts for organic transformations in aqueous medium. *Green Chem.* **2014**, *16*, 3401–3427.

[8] Saran, S.; Manjari, G.; Devipriya, S. P. Synergistic eminently active catalytic and recyclable Ag, Cu and Ag-Cu alloy nanoparticles supported on TiO_2 for sustainable and cleaner environmental applications: A phytogenic mediated synthesis. *J. Clean. Prod.* **2018**, *177*, 134–143.

[9] Gangula, A.; Podila, R.; Ramakrishna, M.; Karanam, L.; Janardhana, C.; Rao, A. M. Catalytic reduction of 4-nitrophenol using biogenic gold and silver nanoparticles derived from *Breynia rhamnoides*. *Langmuir* **2011**, *27*, 15268–15274.

[10] Aswathy Aromal, S.; Philip, D. Green synthesis of gold nanoparticles using *Trigonella foenum-graecum* and its size-dependent catalytic activity. *Spectrochim. Acta A* **2012**, *97*, 1–5.

[11] Coccia, F.; Tonucci, L.; Bosco, D.; Bressan, M.; d'Alessandro, N. One-pot synthesis of lignin-stabilised platinum and palladium nanoparticles and their catalytic behaviour in oxidation and reduction reactions. *Green Chem.* **2012**, *14*, 1073–1078.

[12] Mourdikoudis, S.; Altantzis, T.; Liz-Marzan, L. M.; Bals, S.; Pastoriza-Santos, I.; Pérez-Juste, J. Hydrophilic Pt nanoflowers: Synthesis, crystallographic analysis and catalytic performance. *CrystEngComm* **2016**, *18*, 3422–3427.

[13] Kästner, C.; Thünemann, A. F. Catalytic reduction of 4-nitrophenol using silver nanoparticles with adjustable activity. *Langmuir* **2016**, *32*, 7383–7391.

[14] Zhao, P. X.; Feng, X. W.; Huang, D. S.; Yang, G. Y.; Astruc, D. Basic concepts and recent advances in nitrophenol reduction by gold- and other transition metal nanoparticles. *Coordin. Chem. Rev.* **2015**, *287*, 114–136.

[15] Cheng, Y. J.; Luo, G. F.; Zhu, J. Y.; Xu, X. D.; Zeng, X.; Cheng, D. B.; Li, Y. M.; Wu, Y.; Zhang, X. Z.; Zhuo, R. X. et al. Enzyme-induced and tumor-targeted drug delivery system based on multifunctional mesoporous silica nanoparticles. *ACS Appl. Mater. Interfaces* **2015**, *7*, 9078–9087.

[16] Tolaymat, T. M.; El Badawy, A. M.; Genaidy, A.; Scheckel, K. G.; Luxton, T. P.; Suidan, M. An evidence-based environmental perspective of manufactured silver nanoparticle in syntheses and applications: A systematic review and critical appraisal of peer-reviewed scientific papers. *Sci. Total Environ.* **2010**, *408*, 999–1006.

[17] Liao, G. F.; Zhao, W. Z.; Li, Q.; Pang, Q. H.; Xu, Z. S. Novel poly(acrylic acid)-modified tourmaline/silver composites for adsorption removal of Cu(II) ions and catalytic reduction of methylene blue in water. *Chem. Lett.* **2017**, *46*, 1631–1634.

[18] Mudassir, M. A.; Hussain, S. Z.; Rehman, A.; Zaheer, W.; Asma, S. T.; Jilani, A.; Aslam, M.; Zhang, H. F.; Ansari, T. M.; Hussain, I. Development of silver-nanoparticle-decorated emulsion-templated hierarchically porous poly(1-vinylimidazole) beads for water treatment. *ACS Appl. Mater. Interfaces* **2017**, *9*, 24190–24197.

[19] Wu, Z. L.; Liu, Q. G.; Yang, X. F.; Ye, X.; Duan, H. M.; Zhang, J.; Zhao, B.; Huang, Y. Q. Knitting aryl network polymers-incorporated Ag nanoparticles: A mild and efficient catalyst for the fixation of CO_2 as carboxylic acid. *ACS Sustainable Chem. Eng.* **2017**, *5*, 9634–9639.

[20] Li, N.; Zhao, P. X.; Astruc, D. Anisotropic gold nanoparticles: Synthesis, properties, applications, and toxicity. *Angew. Chem., Int. Ed.* **2014**, *53*, 1756–1789.

[21] Mathew, A.; Pradeep, T. Noble metal clusters: Applications in energy, environment, and biology. *Part. Part. Syst. Char.* **2014**, *31*, 1017–1053.

[22] Dang-Bao, T.; Pla, D.; Favier, I.; Gómez, M. Bimetallic nanoparticles in alternative solvents for catalytic purposes. *Catalysts* **2017**, *7*, 207.

[23] Pradhan, N.; Pal, A.; Pal, T. Catalytic reduction of aromatic nitro compounds by coinage metal nanoparticles. *Langmuir* **2001**, *17*, 1800–1802.

[24] Pradhan, N.; Pal, A.; Pal, T. Silver nanoparticle catalyzed reduction of aromatic nitro compounds. *Colloids Surf. A* **2002**, *196*, 247–257.

[25] Fang, G. C.; Bi, X. H. Silver-catalysed reactions of alkynes: Recent advances. *Chem. Soc. Rev.* **2015**, *44*, 8124–8173.

[26] Martin, D. J.; Liu, G. G.; Moniz, S. J. A.; Bi, Y. P.; Beale, A. M.; Ye, J. H.; Tang, J. W. Efficient visible driven photocatalyst, silver phosphate: Performance, understanding and perspective. *Chem. Soc. Rev.* **2015**, *44*, 7808–7828.

[27] Li, G. P.; Wang, Y. X.; Mao, L. Q. Recent progress in highly efficient Ag-based visible-light photocatalysts. *RSC Adv.* **2014**, *4*, 53649–53661.

[28] Wen, C.; Yin, A. Y.; Dai, W. L. Recent advances in silver-based heterogeneous catalysts for green chemistry processes. *Appl. Catal. B Environ.* **2014**, *160–161*, 730–741.

[29] Zheng, Q. Z.; Jiao, N. Ag-catalyzed C-H/C-C bond functionalization. *Chem. Soc. Rev.* **2016**, *45*, 4590–4627.

[30] Gu, S.; Wunder, S.; Lu, Y.; Ballauff, M.; Fenger, R.; Rademann, K.; Jaquet, B.; Zaccone, A. Kinetic analysis of the catalytic reduction of 4-nitrophenol by metallic nanoparticles. *J. Phys. Chem. C* **2014**, *118*, 18618–18625.

[31] Hervés, P.; Pérez-Lorenzo, M.; Liz-Marzán, L. M.; Dzubiella, J.; Lu, Y.; Ballauff, M. Catalysis by metallic nanoparticles in aqueous solution: Model reactions. *Chem. Soc. Rev.* **2012**, *41*, 5577–5587.

[32] Wunder, S.; Lu, Y.; Albrecht, M.; Ballauff, M. Catalytic activity of faceted gold nanoparticles studied by a model reaction: Evidence for substrate-induced surface restructuring. *ACS Catal.* **2011**, *1*, 908–916.

[33] Xu, W. L.; Kong, J. S.; Yeh, Y. T.; Chen, P. Single-molecule nanocatalysis reveals heterogeneous reaction pathways and catalytic dynamics. *Nat. Mater.* **2008**, *7*, 992–996.

[34] Wunder, S.; Polzer, F.; Lu, Y.; Mei, Y.; Ballauff, M. Kinetic analysis of catalytic reduction of 4-nitrophenol by metallic nanoparticles immobilized in spherical polyelectrolyte brushes. *J. Phys. Chem. C* **2010**, *114*, 8814–8820.

[35] Zhang, L.; Liu, Z.; Liu, L. Y.; Ju, X. J.; Wang, W.; Xie, R.; Chu, L. Y. Novel smart microreactors equipped with responsive catalytic nanoparticles on microchannels. *ACS Appl. Mater. Interfaces* **2017**, *9*, 33137–33148.

[36] Mei, Y.; Sharma, G.; Lu, Y.; Ballauff, M.; Drechsler, M.; Irrgang, T.; Kempe, R. High catalytic activity of platinum nanoparticles immobilized on spherical polyelectrolyte brushes. *Langmuir* **2005**, *21*, 12229–12234.

[37] Choi, H.; Lee, J. P.; Ko, S. J.; Jung, J. W.; Park, H.; Yoo, S.; Park, O.; Jeong, J. R.; Park, S.; Kim, J. Y. Multipositional silica-coated silver nanoparticles for high-performance polymer solar cells. *Nano Lett.* **2013**, *13*, 2204–2208.

[38] Murugan, E.; Rangasamy, R. Synthesis, characterization, and heterogeneous catalysis of polymer-supported poly(propyleneimine) dendrimer stabilized gold nanoparticle catalyst. *J. Polym. Sci. A Polym. Chem.* **2010**, *48*, 2525–2532.

[39] Li, Y. X.; Wu, Y.; Gao, Y.; Sha, S. S.; Hao, J. F.; Cao, G. Q.; Yang, C. A facile method to fabricate polystyrene/silver composite particles and their catalytic properties. *RSC Adv.* **2013**, *3*, 26361–26366.

[40] Mura, S.; Nicolas, J.; Couvreur, P. Stimuli-responsive nanocarriers for drug delivery. *Nat. Mater.* **2013**, *12*, 991–1003.

[41] Deng, Z. W.; Zhu, H. B.; Peng, B.; Chen, H.; Sun, Y. F.; Gang, X. D.; Jin, P. J.; Wang, J. L. Synthesis of PS/Ag nanocomposite spheres with catalytic and antibacterial activities. *ACS Appl. Mater. Interfaces* **2012**, *4*, 5625–5632.

[42] Cong, Y.; Xia, T.; Zou, M.; Li, Z. N.; Peng, B.; Guo, D. Z.; Deng, Z. W. Mussel-inspired polydopamine coating as a versatile platform for synthesizing polystyrene/Ag nanocomposite particles with enhanced antibacterial activities. *J. Mater. Chem. B* **2014**, *2*, 3450–3461.

[43] Liao, G. F.; Li, Q.; Zhao, W. Z.; Pang, Q. H.; Gao, H. Y.; Xu, Z. S. *In-situ* construction of novel silver nanoparticle decorated polymeric spheres as highly active and stable catalysts for reduction of methylene blue dye. *Appl. Catal. A Gen.* **2018**, *549*, 102–111.

[44] Liao, G. F.; Chen, J.; Zeng, W. G.; Yu, C. H.; Yi, C. F.; Xu, Z. S. Facile preparation of uniform nanocomposite spheres with loading silver nanoparticles on polystyrene-methyl acrylic acid spheres for catalytic reduction of 4-nitrophenol. *J. Phys. Chem. C* **2016**, *120*, 25935–25944.

[45] Peng, F.; Wang, Q.; Shi, R. J.; Wang, Z. Y.; You, X.; Liu, Y. H.; Wang, F. H.; Gao, J.; Mao, C. Fabrication of sesame sticks-like silver nanoparticles/polystyrene hybridnanotubes and their catalytic effects. *Sci. Rep.* **2016**, *6*,

39502.
[46] Xu, P. P.; Liao, G. F. A novel fluorescent biosensor for adenosine triphosphate detection based on a metal–organic framework coating polydopamine Layer. *Materials* **2018**, *11*, 1616.
[47] Zou, Y. B.; Jin, H. L.; Sun, F.; Dai, X. M.; Xu, Z. S.; Yang, S. L.; Liao, G. F. Design and synthesis of a lead sulfide based nanotheranostic agent for computer tomography/magnetic resonance dual-mode-bioimaging-guided photothermal therapy. *ACS Appl. Nano Mater.* **2018**, *1*, 2294–2305.
[48] Zhang, H.; Zhao, T. Y.; Newland, B.; Liu, W. G.; Wang, W.; Wang, W. X. Catechol functionalized hyperbranched polymers as biomedical materials. *Prog. Polym. Sci.* **2018**, *78*, 47–55.
[49] Li, Q.; Liao, G. F.; Tian, J.; Xu, Z. S. Preparation of novel fluorinated copolyimide/amine-functionalized *Sepia eumelanin* nanocomposites with enhanced mechanical, thermal, and UV-shielding properties. *Macromol. Mater. Eng.* **2018**, *303*, 1700407.
[50] Zou, Y. B.; Sun, F.; Liu, C. M.; Yu, C. H.; Zhang, M. J.; He, Q. Y.; Xiong, Y. X.; Xu, Z. S.; Yang, S. L.; Liao, G. F. A novel nanotheranostic agent for dual-mode imaging-guided cancer therapy based on europium complexes-grafted-oxidative dopamine. *Chem. Eng. J.* **2019**, *357*, 237–247.
[51] Zhang, M. J.; Zou, Y. B.; Zhong, Y. P.; Liao, G. F.; Yu, C. H.; Xu, Z. S. Polydopamine-based tumor-targeted multifunctional reagents for computer tomography/fluorescence dual-mode bioimaging-guided photothermal therapy. *ACS Appl. Bio Mater.* **2019**, *2*, 630–637.
[52] Liao, G. F.; Li, Q.; Xu, Z. S. The chemical modification of polyaniline with enhanced properties: A review. *Prog. Org. Coat.* **2019**, *126*, 35–43.
[53] Wang, B. W.; Zhang, J. J.; Xia, Z. G.; Fan, M. Q.; Lv, C. J.; Tian, G. L.; Li, X. N. Polyaniline-coated selenium/carbon composites encapsulated in graphene as efficient cathodes for Li-Se batteries. *Nano Res.* **2018**, *11*, 2460–2469.
[54] Liao, G. F.; Gong, Y.; Yi, C. F.; Xu, Z. S. Soluble, antibaterial, and anticorrosion studies of sulfonated polystyrene/polyaniline/silver nanocomposites prepared with the sulfonated polystyrene template. *Chin. J. Chem.* **2017**, *35*, 1157–1164.
[55] Tian, X. C.; Xiao, B.; Xu, X.; Xu, L.; Liu, Z. H.; Wang, Z. Y.; Yan, M. Y.; Wei, Q. L.; Mai, L. Q. Vertically stacked holey graphene/polyaniline heterostructures with enhanced energy storage for on-chip micro-supercapacitors. *Nano Res.* **2016**, *9*, 1012–1021.
[56] Liao, G. F.; Gong, Y.; Zhang, L.; Gao, H. Y.; Yang, G. J.; Fang, B. Z. Semiconductor polymeric graphitic carbon nitride photocatalysts: The "holy grail" for the photocatalytic hydrogen evolution reaction under visible light. *Energy Environ. Sci.* **2019**, DOI: 10.1039/c9ee00717b.
[57] Tian, G. Y.; Wang, W. B.; Mu, B.; Kang, Y. R.; Wang, A. Q. Ag(I)-triggered one-pot synthesis of Ag nanoparticles onto natural nanorods as a multifunctional nanocomposite for efficient catalysis and adsorption. *J. Colloid Interface Sci.* **2016**, *473*, 84–92.
[58] Bogdanović, U.; Pašti, I.; Ćirić-Marjanović, G.; Mitrić, M.; Ahrenkiel, S. P.; Vodnik, V. Interfacial synthesis of gold-polyaniline nanocomposite and its electrocatalytic application. *ACS Appl. Mater. Interfaces* **2015**, *7*, 28393–28403.
[59] Hien, H. T.; Giang, H. T.; van Hieu, N.; Trung, T.; van Tuan, C. Elaboration of Pd-nanoparticle decorated polyaniline films for room temperature NH_3 gas sensors. *Sens. Actuat. B Chem.* **2017**, *249*, 348–356.
[60] Guo, S. J.; Dong, S. J.; Wang, E. K. Polyaniline/Pt hybrid nanofibers: High-efficiency nanoelectrocatalysts for electrochemical devices. *Small* **2009**, *5*, 1869–1876.
[61] Han, J.; Liu, Y.; Guo, R. Reactive template method to synthesize gold nanoparticles with controllable size and morphology supported on shells of polymer hollow microspheres and their application for aerobic alcohol oxidation in water. *Adv. Funct. Mater.* **2009**, *19*, 1112–1117.
[62] Wang, H. Y.; Jiang, X. X.; Lee, S. T.; He, Y. Silicon nanohybrid-based surface-enhanced Raman scattering sensors. *Small* **2014**, *10*, 4455–4468.
[63] Stejskal, J. Conducting polymer-silver composites. *Chem. Papers* **2013**, *67*, 814–848.
[64] Han, J.; Wang, M. G.; Hu, Y. M.; Zhou, C. Q.; Guo, R. Conducting polymer-noble metal nanoparticle hybrids: Synthesis mechanism application. *Prog. Polym. Sci.* **2017**, *70*, 52–91.
[65] Yuan, C. H.; Xu, Y. T.; Zhong, L. N.; Zhang, L.; Yang, C. J.; Jiang, B. J.; Deng, Y. M.; Zeng, B. R.; He, N.; Luo, W. A. et al. Heterogeneous silver-polyaniline nanocomposites with tunable morphology and controllable catalytic properties. *Nanotechnology* **2013**, *24*, 185602.
[66] Mondal, S.; Rana, U.; Malik, S. Facile decoration of polyaniline fiber with Ag nanoparticles for recyclable SERS substrate. *ACS Appl. Mater. Interfaces* **2015**, *7*, 10457–10465.
[67] Zhang, L.; Liu, X. C.; Wang, Y. H.; Xing, S. X. Controllable silver embedding into polypyrrole. *J. Alloys Compd.* **2017**, *709*, 431–437.
[68] Balamurugan, A.; Ho, K. C.; Chen, S. M. One-pot synthesis of highly stable silver nanoparticles-conducting polymer nanocomposite and its catalytic application. *Synth. Met.* **2009**, *159*, 2544–2549.
[69] Xia, Y. Y.; Xu, L. Fabrication and catalytic property of an Ag@poly(3, 4-ethylenedioxythiophene) yolk/shell structure. *Synth. Met.* **2010**, *160*, 545–548.
[70] Seo, E.; Kim, J.; Hong, Y.; Kim, Y. S.; Lee, D.; Kim, B. S. Double hydrophilic block copolymer templated Au nanoparticles with enhanced catalytic activity toward nitroarene reduction. *J. Phys. Chem. C* **2013**, *117*, 11686–11693.
[71] Huang, X. J.; Xiao, Y.; Zhang, W.; Lang, M. D. *In-situ* formation of silver nanoparticles stabilized by amphiphilic star-shaped copolymer and their catalytic application. *Appl. Surf. Sci.* **2012**, *258*, 2655–2660.
[72] Zhang, Z. T.; Zhao, B.; Hu, L. M. PVP protective mechanism of ultrafine silver powder synthesized by chemical reduction processes. *J. Solid State Chem.* **1996**, *121*, 105–110.
[73] Koczkur, K. M.; Mourdikoudis, S.; Polavarapu, L.; Skrabalak, S. E. Polyvinylpyrrolidone (PVP) in nanoparticle synthesis. *Dalton Trans.* **2015**, *44*, 17883–17905.
[74] Cloud, J. E.; Taylor, L. W.; Yang, Y. A. A simple and effective method for controllable synthesis of silver and silver oxide nanocrystals. *RSC Adv.* **2014**, *4*, 24551–24559.
[75] Tuck, C. O.; Pérez, E.; Horváth, I. T.; Sheldon, R. A.; Poliakoff, M. Valorization of biomass: Deriving more value from waste. *Science* **2012**, *337*, 695–699.
[76] Song, J. L.; Birbach, N. L.; Hinestroza, J. P. Deposition of silver nanoparticles on cellulosic fibers via stabilization of carboxymethyl groups. *Cellulose* **2012**, *19*, 411–424.
[77] Ngo, Y. H.; Li, D.; Simon, G. P.; Garnier, G. Paper surfaces functionalized by nanoparticles. *Adv. Colloid Interface Sci.* **2011**, *163*, 23–38.
[78] Wu, J. J.; Zhao, N.; Zhang, X. L.; Xu, J. Cellulose/silver nanoparticles composite microspheres: Eco-friendly synthesis and catalytic application. *Cellulose* **2012**, *19*, 1239–1249.
[79] Kaushik, M.; Moores, A. Review: Nanocelluloses as versatile supports for metal nanoparticles and their applications in catalysis. *Green Chem.* **2016**, *18*, 622–637.
[80] Wu, X. Y.; Shi, Z. Q.; Fu, S. D.; Chen, J. L.; Berry, R. M.; Tam, K. C. Strategy for synthesizing porous cellulose nanocrystal supported metal nanocatalysts. *ACS Sustainable Chem. Eng.* **2016**, *4*, 5929–5935.
[81] Jiang, F.; Hsieh, Y. L. Synthesis of cellulose nanofibril bound silver nanoprism for surface enhanced Raman scattering. *Biomacromolecules* **2014**, *15*, 3608–3616.
[82] Wei, H. R.; Rodriguez, K.; Renneckar, S.; Vikesland, P. J. Environmental science and engineering applications of nanocellulose-based nanocomposites. *Environ. Sci.: Nano* **2014**, *1*, 302–316.
[83] Tang, J. T.; Shi, Z. Q.; Berry, R. M.; Tam, K. C. Mussel-inspired green metallization of silver nanoparticles on cellulose nanocrystals and their enhanced catalytic reduction of 4-nitrophenol in the presence of β-cyclodextrin. *Ind. Eng. Chem. Res.* **2015**, *54*, 3299–3308.
[84] Zhu, Y. J.; Chen, F. Microwave-assisted preparation of inorganic nanostructures in liquid phase. *Chem. Rev.* **2014**, *114*, 6462–6555.
[85] Yalçın, G.; Elmas, B.; Tuncel, M.; Tuncel, A. A low, particle-sized, nonporous support for enzyme immobilization: Uniform poly(glycidyl methacrylate) latex particles. *J. Appl. Polym. Sci.* **2006**, *101*, 818–824.
[86] Deng, Y. M.; Li, J. F.; Pu, Y. T.; Chen, Y. M.; Zhao, J. L.; Tang, J. N. Ultra-fine silver nanoparticles dispersed in mono-dispersed amino functionalized poly glycidyl methacrylate based microspheres as an effective anti-bacterial agent. *React. Funct. Polym.* **2016**, *103*, 92–98.
[87] Macková, H.; Oukacine, F.; Plichta, Z.; Hrubý, M.; Kučka, J.; Taverna, M.; Horák, D. Poly(glycidyl methacrylate)/silver nanocomposite microspheres as a radioiodine scavenger: Electrophoretic characterisation of carboxyl- and amine-modified particles. *J. Colloid Interface Sci.* **2014**, *421*, 146–153.
[88] Zhang, W. C.; Sun, Y.; Zhang, L. *In situ* synthesis of monodisperse silver nanoparticles on sulfhydryl-functionalized poly(glycidyl methacrylate) microspheres for catalytic reduction of 4-nitrophenol. *Ind. Eng. Chem. Res.* **2015**, *54*, 6480–6488.
[89] Zhang, W. C.; Sun, Y.; Zhang, L. Fabrication of high efficient silver nanoparticle catalyst supported on poly(glycidyl methacrylate)–polyacrylamide. *Ind. Eng. Chem. Res.* **2016**, *55*, 12398–12406.
[90] Panigrahi, R.; Srivastava, S. K. Ultrasound assisted synthesis of a

polyaniline hollow microsphere/Ag core/shell structure for sensing and catalytic applications. *RSC Adv*. **2013**, *3*, 7808–7815.
[91] Dang, G. F.; Shi, Y.; Fu, Z. F.; Yang, W. T. Polymer nanoparticles with dendrimer-Ag shell and its application in catalysis. *Particuology* **2013**, *11*, 346–352.
[92] Rajesh, R.; Venkatesan, R. Encapsulation of silver nanoparticles into graphite grafted with hyperbranched poly(amidoamine) dendrimer and their catalytic activity towards reduction of nitro aromatics. *J. Mol. Catal. A Chem* **2012**, *359*, 88–96.
[93] Murugadoss, A.; Chattopadhyay, A. A 'green' chitosan-silver nanoparticle composite as a heterogeneous as well as micro-heterogeneous catalyst. *Nanotechnology* **2008**, *19*, 015603.
[94] Baruah, B.; Gabriel, G. J.; Akbashev, M. J.; Booher, M. E. Facile synthesis of silver nanoparticles stabilized by cationic polynorbornenes and their catalytic activity in 4-nitrophenol reduction. *Langmuir* **2013**, *29*, 4225–4234.
[95] Nemanashi, M.; Meijboom, R. Synthesis and characterization of Cu, Ag and Au dendrimer-encapsulated nanoparticles and their application in the reduction of 4-nitrophenol to 4-aminophenol. *J. Colloid Interface Sci*. **2013**, *389*, 260–267.
[96] Crooks, R. M.; Zhao, M. Dendrimer-encapsulated Pt nanoparticles: Synthesis, characterization, and applications to catalysis. *Adv. Mater*. **1999**, *11*, 217–220.
[97] Chechik, V.; Crooks, R. M. Dendrimer-encapsulated Pd nanoparticles as fluorous phase-soluble catalysts. *J. Am. Chem. Soc*. **2000**, *122*, 1243–1244.
[98] Chechik, V.; Zhao, M. Q.; Crooks, R. M. Self-assembled inverted micelles prepared from a dendrimer template: Phase transfer of encapsulated guests. *J. Am. Chem. Soc*. **1999**, *121*, 4910–4911.
[99] Balogh, L.; Swanson, D. R.; Tomalia, D. A.; Hagnauer, G. L.; McManus, A. T. Dendrimer−silver complexes and nanocomposites as antimicrobial agents. *Nano Lett*. **2001**, *1*, 18–21.
[100] Rodríguez-reinoso, F. The role of carbon materials in heterogeneous catalysis. *Carbon* **1998**, *36*, 159–175.
[101] Zhang, J. T.; Dai, L. M. Heteroatom-doped graphitic carbon catalysts for efficient electrocatalysis of oxygen reduction reaction. *ACS Catal*. **2015**, *5*, 7244–7253.
[102] Cao, Y. L.; Mao, S. J.; Li, M. M.; Chen, Y. Q.; Wang, Y. Metal/porous carbon composites for heterogeneous catalysis: Old catalysts with improved performance promoted by N-doping. *ACS Catal*. **2017**, *7*, 8090–8112.
[103] Jiang, C. L.; Nie, J.; Ma, G. P. A polymer/metal core–shell nanofiber membrane by electrospinning with an electric field, and its application for catalyst support. *RSC Adv*. **2016**, *6*, 22996–23007.
[104] Cao, C.; Wei, L. L.; Su, M.; Wang, G.; Shen, J. Q. Template-free and one-pot synthesis of N-doped hollow carbon tube @ hierarchically porous carbon supporting homogeneous AgNPs for robust oxygen reduction catalyst. *Carbon* **2017**, *112*, 27–36.
[105] Ma, S. C.; Luo, R.; Gold, J. I.; Yu, A. Z.; Kim, B.; Kenis, P. J. A. Carbon nanotube containing Ag catalyst layers for efficient and selective reduction of carbon dioxide. *J. Mater. Chem. A* **2016**, *4*, 8573–8578.
[106] Allen, M. J.; Tung, V. C.; Kaner, R. B. Honeycomb carbon: A review of graphene. *Chem. Rev*. **2010**, *110*, 132–145.
[107] Wei, Y.; Zuo, X.; Li, X. Q.; Song, S. S.; Chen, L. W.; Shen, J.; Meng, Y. D.; Zhao, Y.; Fang, S. D. Dry plasma synthesis of graphene oxide–Ag nanocomposites: A simple and green approach. *Mater. Res. Bull*. **2014**, *53*, 145–150.
[108] Mao, A. Q.; Zhang, D. H.; Jin, X.; Gu, X. L.; Wei, X. Q.; Yang, G. J.; Liu, X. H. Synthesis of graphene oxide sheets decorated by silver nanoparticles in organic phase and their catalytic activity. *J. Phys. Chem. Solids* **2012**, *73*, 982–986.
[109] Li, Y. Z.; Cao, Y. L.; Xie, J.; Jia, D. Z.; Qin, H. Y.; Liang, Z. T. Facile solid-state synthesis of Ag/graphene oxide nanocomposites as highly active and stable catalyst for the reduction of 4-nitrophenol. *Catal. Commun*. **2015**, *58*, 21–25.
[110] Kamat, P. V. Graphene-based nanoarchitectures. Anchoring semiconductor and metal nanoparticles on a two-dimensional carbon support. *J. Phys. Chem. Lett*. **2010**, *1*, 520–527.
[111] Bai, W. S.; Nie, F.; Zheng, J. B.; Sheng, Q. L. Novel silver nanoparticle-manganese oxyhydroxide-graphene oxide nanocomposite prepared by modified silver mirror reaction and its application for electrochemical sensing. *ACS Appl. Mater. Interfaces* **2014**, *6*, 5439–5449.
[112] Wang, Z. M.; Xu, C. L.; Li, X.; Liu, Z. H. *In situ* green synthesis of Ag nanoparticles on tea polyphenols-modified graphene and their catalytic reduction activity of 4-nitrophenol. *Colloids Surf. A* **2015**, *485*, 102–110.
[113] Jeon, E. K.; Seo, E.; Lee, E.; Lee, W.; Um, M. K.; Kim, B. S. Mussel-inspired green synthesis of silver nanoparticles on graphene oxide nanosheets for enhanced catalytic applications. *Chem. Commun*. **2013**, *49*, 3392–3394.
[114] Panchakarla, L. S.; Subrahmanyam, K. S.; Saha, S. K.; Govindaraj, A.; Krishnamurthy, H. R.; Waghmare, U. V.; Rao, C. N. R. Synthesis, structure, and properties of boron- and nitrogen-doped graphene. *Adv. Mater*. **2009**, *21*, 4726–4730.
[115] Duan, J. J.; Chen, S.; Jaroniec, M.; Qiao, S. Z. Heteroatom-doped graphene-based materials for energy-relevant electrocatalytic processes. *ACS Catal*. **2015**, *5*, 5207–5234.
[116] Zhang, L. S.; Liang, X. Q.; Song, W. G.; Wu, Z. Y. Identification of the nitrogen species on N-doped graphene layers and Pt/NG composite catalyst for direct methanol fuel cell. *Phys. Chem. Chem. Phys*. **2010**, *12*, 12055–12059.
[117] Cheng, C.; Li, S.; Thomas, A.; Kotov, N. A.; Haag, R. Functional graphene nanomaterials based architectures: Biointeractions, fabrications, and emerging biological applications. *Chem. Rev*. **2017**, *117*, 1826–1914.
[118] Nair, A. K.; Elizabeth, I.; Gopukumar, S.; Thomas, S.; Kala, M. S.; Kalarikkal, N. Nitrogen doped graphene–silver nanowire hybrids: An excellent anode material for lithium ion batteries. *Appl. Surf. Sci*. **2018**, *428*, 1119–1129.
[119] Zhang, J. S.; Chen, Y.; Wang, X. C. Two-dimensional covalent carbon nitride nanosheets: Synthesis, functionalization, and applications. *Energy Environ. Sci*. **2015**, *8*, 3092–3108.
[120] Tian, Y.; Cao, Y. Y.; Pang, F.; Chen, G.-Q.; Zhang, X. Ag nanoparticles supported on N-doped graphene hybrids for catalytic reduction of 4-nitrophenol. *RSC Adv*. **2014**, *4*, 43204–43211.
[121] John, J.; Gravel, E.; Namboothiri, I. N. N.; Doris, E. Advances in carbon nanotube-noble metal catalyzed organic transformations. *Nanotechnol. Rev*. **2012**, *1*, 515–539.
[122] Pérez-Mayoral, E.; Calvino-Casilda, V.; Soriano, E. Metal-supported carbon-based materials: Opportunities and challenges in the synthesis of valuable products. *Catal. Sci. Technol*. **2016**, *6*, 1265–1291.
[123] Tasis, D.; Tagmatarchis, N.; Bianco, A.; Prato, M. Chemistry of carbon nanotubes. *Chem. Rev*. **2006**, *106*, 1105–1136.
[124] Sun, Y. P.; Fu, K. F.; Lin, Y.; Huang, W. J. Functionalized carbon nanotubes: Properties and applications. *Acc. Chem. Res*. **2002**, *35*, 1096–1104.
[125] Li, H. Q.; Jo, J. K.; Zhang, L. D.; Ha, C. S.; Suh, H.; Kim, I. A general and efficient route to fabricate carbon nanotube-metal nanoparticles and carbon nanotube-inorganic oxides hybrids. *Adv. Funct. Mater*. **2010**, *20*, 3864–3873.
[126] Li, H. Q.; Jo, J. K.; Zhang, L. D.; Ha, C. S.; Suh, H.; Kim, I. Hyperbranched polyglycidol assisted green synthetic protocols for the preparation of multifunctional metal nanoparticles. *Langmuir* **2010**, *26*, 18442–18453.
[127] Li, H. Q.; Cooper-White, J. J. Hyperbranched polymer mediated fabrication of water soluble carbon nanotube-metal nanoparticle hybrids. *Nanoscale* **2013**, *5*, 2915–2920.
[128] Sahoo, N. G.; Rana, S.; Cho, J. W.; Li, L.; Chan, S. H. Polymer nanocomposites based on functionalized carbon nanotubes. *Prog. Polym. Sci*. **2010**, *35*, 837–867.
[129] Alshehri, S. M.; Almuqati, T.; Almuqati, N.; Al-Farraj, E.; Alhokbany, N.; Ahamad, T. Chitosan based polymer matrix with silver nanoparticles decorated multiwalled carbon nanotubes for catalytic reduction of 4-nitrophenol. *Carbohyd. Polym*. **2016**, *151*, 135–143.
[130] Baker, S. N.; Baker, G. A. Luminescent carbon nanodots: Emergent nanolights. *Angew. Chem., Int. Ed*. **2010**, *49*, 6726–6744.
[131] Zheng, H. Z.; Wang, Q. L.; Long, Y. J.; Zhang, H. J.; Huang, X. X.; Zhu, R. Enhancing the luminescence of carbon dots with a reduction pathway. *Chem. Commun*. **2011**, *47*, 10650–10652.
[132] Bhattacharyya, S.; Ehrat, F.; Urban, P.; Teves, R.; Wyrwich, R.; Doblinger, M.; Feldmann, J.; Urban, A. S.; Stolarczyk, J. K. Effect of nitrogen atom positioning on the trade-off between emissive and photocatalytic properties of carbon dots. *Nat. Commun*. **2017**, *8*, 1401.
[133] Ehrat, F.; Bhattacharyya, S.; Schneider, J.; Löf, A.; Wyrwich, R.; Rogach, A. L.; Stolarczyk, J. K.; Urban, A. S.; Feldmann, J. Tracking the source of carbon dot photoluminescence: Aromatic domains versus molecular fluorophores. *Nano Lett*. **2017**, *17*, 7710–7716.
[134] Lim, S. Y.; Shen, W.; Gao, Z. Q. Carbon quantum dots and their applications. *Chem. Soc. Rev*. **2015**, *44*, 362–381.
[135] Essner, J. B.; Laber, C. H.; Baker, G. A. Carbon dot reduced bimetallic nanoparticles: Size and surface plasmon resonance tunability for enhanced

catalytic applications. *J. Mater. Chem. A* **2015**, *3*, 16354–16360.
[136] Guardia, L.; Paredes, J. I.; Villar-Rodil, S.; Rouzaud, J. N.; Martínez-Alonso, A.; Tascón, J. M. D. Discovery of effective solvents for platelet-type graphite nanofibers. *Carbon* **2013**, *53*, 222–230.
[137] Fernández-Merino, M. J.; Guardia, L.; Paredes, J. I.; Villar-Rodil, S.; Martínez-Alonso, A.; Tascón, J. M. D. Developing green photochemical approaches towards the synthesis of carbon nanofiber- and graphene-supported silver nanoparticles and their use in the catalytic reduction of 4-nitrophenol. *RSC Adv.* **2013**, *3*, 18323–18331.
[138] Tang, S.; Vongehr, S.; Meng, X. K. Carbon spheres with controllable silver nanoparticle doping. *J. Phys. Chem. C* **2009**, *114*, 977–982.
[139] Kao, L. H.; Chang, Y. C.; Hung, P. W.; Lee, H. T.; Chi, P. H. Coupled synthesis and encapsulation in one-pot method for fabricating size-tunable hollow carbon spheres containing encapsulated Ag microparticles. *Colloids Surf. A* **2012**, *410*, 170–177.
[140] Ji, T.; Chen, L.; Schmitz, M.; Bao, F. S.; Zhu, J. H. Hierarchical macrotube/mesopore carbon decorated with mono-dispersed Ag nanoparticles as a highly active catalyst. *Green Chem.* **2015**, *17*, 2515–2523.
[141] Ji, T.; Chen, L.; Mu, L. W.; Yuan, R. X.; Knoblauch, M.; Bao, F. S.; Zhu, J. H. *In-situ* reduction of Ag nanoparticles on oxygenated mesoporous carbon fabric: Exceptional catalyst for nitroaromatics reduction. *Appl. Catal. B Environ.* **2016**, *182*, 306–315.
[142] Bulushev, D. A.; Zacharska, M.; Lisitsyn, A. S.; Podyacheva, O. Y.; Hage, F. S.; Ramasse, Q. M.; Bangert, U.; Bulusheva, L. G. Single atoms of Pt-group metals stabilized by N-doped carbon nanofibers for efficient hydrogen production from formic acid. *ACS Catal.* **2016**, *6*, 3442–3451.
[143] Cui, X. L.; Li, H.; Yuan, M.; Yang, J.; Xu, D.; Li, Z. Y.; Yu, G. Q.; Hou, Y. M.; Dong, Z. P. Facile preparation of fluffy N-doped carbon modified with Ag nanoparticles as a highly active and reusable catalyst for catalytic reduction of nitroarenes. *J. Colloid Interface Sci.* **2017**, *506*, 524–531.
[144] Tzounis, L.; Contreras-Caceres, R.; Schellkopf, L.; Jehnichen, D.; Fischer, D.; Cai, C. Z.; Uhlmann, P.; Stamm, M. Controlled growth of Ag nanoparticles decorated onto the surface of SiO_2 spheres: A nanohybrid system with combined SERS and catalytic properties. *RSC Adv.* **2014**, *4*, 17846–17855.
[145] Pérez-Lorenzo, M.; Vaz, B.; Salgueiriño, V.; Correa-Duarte, M. A. Hollow-shelled nanoreactors endowed with high catalytic activity. *Chem.—Eur. J.* **2013**, *19*, 12196–12211.
[146] Jiang, S. D.; Song, L.; Zeng, W. R.; Huang, Z. Q.; Zhan, J.; Stec, A. A.; Hull, T. R.; Hu, Y.; Hu, W. Z. Self-assembly fabrication of hollow mesoporous silica@Co-Al layered double hydroxide@graphene and application in toxic effluents elimination. *ACS Appl. Mater. Interfaces* **2015**, *7*, 8506–8514.
[147] Li, W. Q.; Wang, G. Z.; Li, G. H.; Zhang, Y. X. "Ship-in-a-bottle" approach to synthesize Ag@hm-SiO_2 yolk/shell nanospheres. *Chin. J. Chem. Phys.* **2015**, *28*, 611–616.
[148] Li, W. Q.; Ge, X.; Zhang, H.; Ding, Q. Q.; Ding, H. L.; Zhang, Y. X.; Wang, G. Z.; Zhang, H. M.; Zhao, H. J. Hollow mesoporous SiO_2 sphere nanoarchitectures with encapsulated silver nanoparticles for catalytic reduction of 4-nitrophenol. *Inorg. Chem. Front.* **2016**, *3*, 663–670.
[149] Sun, Z. B.; Cui, G. J.; Li, H. Z.; Tian, Y. X.; Yan, S. Q. Multifunctional dendritic mesoporous silica nanospheres loaded with silver nanoparticles as a highly active and recyclable heterogeneous catalyst. *Colloids Surf. A* **2016**, *489*, 142–153.
[150] Dong, Z.; Le, X.; Li, X.; Zhang, W.; Dong, C.; Ma, J. Silver nanoparticles immobilized on fibrous nano-silica as highly efficient and recyclable heterogeneous catalyst for reduction of 4-nitrophenol and 2-nitroaniline. *Appl. Catal. B Environ.* **2014**, *158–159*, 129–135.
[151] Xing, Z.; Tay, S. W.; Ng, Y. H.; Hong, L. Porous SiO_2 hollow spheres as a solar reflective pigment for coatings. *ACS Appl. Mater. Interfaces* **2017**, *9*, 15103–15113.
[152] Rodrigues, T. S.; da Silva, A. G. M.; Gonçalves, M. C.; Fajardo, H. V.; Balzer, R.; Probst, L. F. D.; Camargo, P. H. C. AgPt hollow nanodendrites: Synthesis and uniform dispersion over SiO_2 support for catalytic applications. *ChemNanoMat* **2015**, *1*, 46–51.
[153] Shajkumar, A.; Nandan, B.; Sanwaria, S.; Albrecht, V.; Libera, M.; Lee, M. H.; Auffermann, G.; Stamm, M.; Horechyy, A. Silica-supported Au@hollow-SiO_2 particles with outstanding catalytic activity prepared via block copolymer template approach. *J. Colloid Interface Sci.* **2017**, *491*, 246–254.
[154] Xu, C. X.; Su, J. X.; Xu, X. H.; Liu, P. P.; Zhao, H. J.; Tian, F.; Ding, Y. Low temperature CO oxidation over unsupported nanoporous gold. *J. Am. Chem. Soc.* **2007**, *129*, 42–43.
[155] Wu, L.; Wang, Z. Y.; Zong, S. F.; Huang, Z.; Zhang, P. Y.; Cui, Y. P. A SERS-based immunoassay with highly increased sensitivity using gold/silver core-shell nanorods. *Biosensor. Bioelectron.* **2012**, *38*, 94–99.
[156] Xiao, Z. Y.; Huang, S. X.; Zhai, S. R.; Zhai, B.; Zhang, F.; An, Q. D. PMHS-reduced fabrication of hollow Ag–SiO_2 composite spheres with developed porosity. *J. Sol-Gel Sci. Technol.* **2015**, *75*, 82–89.
[157] Zhu, C. Z.; Du, D.; Eychmüller, A.; Lin, Y. H. Engineering ordered and nonordered porous noble metal nanostructures: Synthesis, assembly, and their applications in electrochemistry. *Chem. Rev.* **2015**, *115*, 8896–8943.
[158] Liong, M.; France, B.; Bradley, K. A.; Zink, J. I. Antimicrobial activity of silver nanocrystals encapsulated in mesoporous silica nanoparticles. *Adv. Mater.* **2009**, *21*, 1684–1689.
[159] Song, Y. Y.; Jiang, H. J.; Wang, B. B.; Kong, Y.; Chen, J. Silver-incorporated mussel-inspired polydopamine coatings on mesoporous silica as an efficient nanocatalyst and antimicrobial agent. *ACS Appl. Mater. Interfaces* **2018**, *10*, 1792–1801.
[160] Polshettiwar, V.; Luque, R.; Fihri, A.; Zhu, H. B.; Bouhrara, M.; Basset, J. M. Magnetically recoverable nanocatalysts. *Chem. Rev.* **2011**, *111*, 3036–3075.
[161] Zeng, H.; Sun, S. H. Syntheses, properties, and potential applications of multicomponent magnetic nanoparticles. *Adv. Funct. Mater.* **2008**, *18*, 391–400.
[162] Shen, M.; Chen, S. Q.; Jia, W. P.; Fan, G. D.; Jin, Y. X.; Liang, H. D. Facile synthesis of Ag@Fe_3O_4@C-Au core-shell microspheres for surface-enhanced Raman scattering. *Gold Bull.* **2016**, *49*, 103–109.
[163] Lin, T. R.; Wang, J.; Guo, L. Q.; Fu, F. F. Fe_3O_4@MoS_2 core–shell composites: Preparation, characterization, and catalytic application. *J. Phys. Chem. C* **2015**, *119*, 13658–13664.
[164] Sharma, G.; Jeevanandam, P. A facile synthesis of multifunctional iron oxide@Ag core-shell nanoparticles and their catalytic applications. *Eur. J. Inorg. Chem.* **2013**, *2013*, 6126–6136.
[165] Zhu, M. Y.; Wang, C. J.; Meng, D. H.; Diao, G. W. *In situ* synthesis of silver nanostructures on magnetic Fe_3O_4@C core–shell nanocomposites and their application in catalytic reduction reactions. *J. Mater. Chem. A* **2013**, *1*, 2118–2125.
[166] Karki, H. P.; Ojha, D. P.; Joshi, M. K.; Kim, H. J. Effective reduction of p-nitrophenol by silver nanoparticle loaded on magnetic Fe_3O_4/ATO nano-composite. *Appl. Surf. Sci.* **2018**, *435*, 599–608.
[167] Kaloti, M.; Kumar, A.; Navani, N. K. Synthesis of glucose-mediated Ag–γ-Fe_2O_3 multifunctional nanocomposites in aqueous medium–a kinetic analysis of their catalytic activity for 4-nitrophenol reduction. *Green Chem.* **2015**, *17*, 4786–4799.
[168] Yamazaki, K.; Kayama, T.; Dong, F.; Shinjoh, H. A mechanistic study on soot oxidation over CeO_2–Ag catalyst with "rice-ball" morphology. *J. Catal.* **2011**, *282*, 289–298.
[169] Mitsudome, T.; Matoba, M.; Mizugaki, T.; Jitsukawa, K.; Kaneda, K. Core-shell AgNP@CeO_2 nanocomposite catalyst for highly chemoselective reductions of unsaturated aldehydes. *Chem.—Eur. J.* **2013**, *19*, 5255–5258.
[170] Evangelista, V.; Acosta, B.; Miridonov, S.; Smolentseva, E.; Fuentes, S.; Simakov, A. Highly active Au-CeO_2@ZrO_2 yolk–shell nanoreactors for the reduction of 4-nitrophenol to 4-aminophenol. *Appl. Catal. B Environ.* **2015**, *166–167*, 518–528.
[171] Zhang, J.; Li, L. P.; Huang, X. S.; Li, G. S. Fabrication of Ag–CeO_2 core–shell nanospheres with enhanced catalytic performance due to strengthening of the interfacial interactions. *J. Mater. Chem.* **2012**, *22*, 10480–10487.
[172] Wang, Y. Y.; Shu, Y.; Xu, J.; Pang, H. Facile one-step synthesis of Ag@CeO_2 core–shell nanospheres with efficient catalytic activity for the reduction of 4-nitrophenol. *CrystEngComm* **2017**, *19*, 684–689.
[173] Shi, Y.; Zhang, X. L.; Zhu, Y. M.; Tan, H. L.; Chen, X. S.; Lu, Z. H. Core–shell structured nanocomposites Ag@CeO_2 as catalysts for hydrogenation of 4-nitrophenol and 2-nitroaniline. *RSC Adv.* **2016**, *6*, 47966–47973.
[174] Ji, Z. Y.; Shen, X. P.; Yang, J. L.; Zhu, G. X.; Chen, K. M. A novel reduced graphene oxide/Ag/CeO_2 ternary nanocomposite: Green synthesis and catalytic properties. *Appl. Catal. B Environ.* **2014**, *144*, 454–461.
[175] Liu, Q.; Wang, A. Q.; Wang, X. H.; Gao, P.; Wang, X. D.; Zhang, T. Synthesis, characterization and catalytic applications of mesoporous γ-alumina from boehmite sol. *Micropor. Mesopor. Mater.* **2008**, *111*, 323–333.

[176] Lesaint, C.; Kleppa, G.; Arla, D.; Glomm, W. R.; Øye, G. Synthesis and characterization of mesoporous alumina materials with large pore size prepared by a double hydrolysis route. *Micropor. Mesopor. Mater.* **2009**, *119*, 245–251.
[177] Naik, B.; Prasad, V. S.; Ghosh, N. N. Preparation of Ag nanoparticle loaded mesoporous γ-alumina catalyst and its catalytic activity for reduction of 4-nitrophenol. *Powder Technol.* **2012**, *232*, 1–6.
[178] Solanki, J. N.; Murthy, Z. V. P. Reduction of nitro aromatic compounds over Ag/Al_2O_3 nanocatalyst prepared in water-in-oil microemulsion: Effects of water-to-surfactant mole ratio and type of reducing agent. *Ind. Eng. Chem. Res.* **2011**, *50*, 7338–7344.
[179] Mori, K.; Kumami, A.; Tomonari, M.; Yamashita, H. A pH-induced size controlled deposition of colloidal Ag nanoparticles on alumina support for catalytic application. *J. Phys. Chem. C* **2009**, *113*, 16850–16854.
[180] Li, W.; Deng, Y. H.; Wu, Z. X.; Qian, X. F.; Yang, J. P.; Wang, Y.; Gu, D.; Zhang, F.; Tu, B.; Zhao, D. Y. Hydrothermal etching assisted crystallization: A facile route to functional yolk-shell titanate microspheres with ultrathin nanosheets-assembled double shells. *J. Am. Chem. Soc.* **2011**, *133*, 15830–15833.
[181] Hu, M.; Zhang, Z. W.; Luo, C. K.; Qiao, X. Q. One-pot green synthesis of Ag-decorated SnO_2 microsphere: An efficient and reusable catalyst for reduction of 4-nitrophenol. *Nanoscale Res. Lett.* **2017**, *12*, 435.
[182] Lei, M.; Wu, W.; Yang, S. L.; Zhang, X. G.; Xing, Z.; Ren, F.; Xiao, X. H.; Jiang, C. Z. Design of enhanced catalysts by coupling of noble metals (Au, Ag) with semiconductor SnO_2 for catalytic reduction of 4-nitrophenol. *Part. Part. Syst. Char.* **2016**, *33*, 212–220.
[183] Ma, J. Q.; Guo, X. H.; Zhang, Y. Y.; Ge, H. G. Catalytic performance of TiO_2@Ag composites prepared by modified photodeposition method. *Chem. Eng. J.* **2014**, *258*, 247–253.
[184] Shoaib, A.; Ji, M. W.; Qian, H. M.; Liu, J. J.; Xu, M.; Zhang, J. T. Noble metal nanoclusters and their *in situ* calcination to nanocrystals: Precise control of their size and interface with TiO_2 nanosheets and their versatile catalysis applications. *Nano Res.* **2016**, *9*, 1763–1774.
[185] Bao, Z. H.; Yuan, Y.; Leng, C. B.; Li, L.; Zhao, K.; Sun, Z. H. One-pot synthesis of noble metal/zinc oxide composites with controllable morphology and high catalytic performance. *ACS Appl. Mater. Interfaces* **2017**, *9*, 16417–16425.
[186] Zhang, Y. Y.; Guo, S. B.; Ma, J. Q.; Ge, H. G. Preparation, characterization, catalytic performance and antibacterial activity of Ag photodeposited on monodisperse ZnO submicron spheres. *J. Sol-Gel Sci. Technol.* **2014**, *72*, 171–178.
[187] Xu, Y.; Yan, X. F.; Fang, W. Z.; Daniele, S.; Zhang, J. L.; Wang, L. Z. SERS self-monitoring of Ag-catalyzed reaction by magnetically separable mesoporous Fe_3O_4@Ag@mSiO_2. *Micropor. Mesopor. Mater.* **2018**, *263*, 113–119.
[188] Shen, J. H.; Zhu, Y. H.; Yang, X. L.; Zong, J.; Li, C. Z. Multifunctional Fe_3O_4@Ag/SiO_2/Au core-shell microspheres as a novel SERS-activity label via long-range plasmon coupling. *Langmuir* **2013**, *29*, 690–695.
[189] Shin, K. S.; Cho, Y. K.; Choi, J. Y.; Kim, K. Facile synthesis of silver-deposited silanized magnetite nanoparticles and their application for catalytic reduction of nitrophenols. *Appl. Catal. A Gen.* **2012**, *413–414*, 170–175.
[190] Abbas, M.; Torati, S. R.; Kim, C. A novel approach for the synthesis of ultrathin silica-coated iron oxide nanocubes decorated with silver nanodots (Fe_3O_4/SiO_2/Ag) and their superior catalytic reduction of 4-nitroaniline. *Nanoscale* **2015**, *7*, 12192–12204.
[191] Chi, Y.; Yuan, Q.; Li, Y. J.; Tu, J. C.; Zhao, L.; Li, N.; Li, X. T. Synthesis of Fe_3O_4@SiO_2-Ag magnetic nanocomposite based on small-sized and highly dispersed silver nanoparticles for catalytic reduction of 4-nitrophenol. *J. Colloid Interface Sci.* **2012**, *383*, 96–102.
[192] Du, X. Y.; He, J.; Zhu, J.; Sun, L. J.; An, S. S. Ag-deposited silica-coated Fe_3O_4 magnetic nanoparticles catalyzed reduction of p-nitrophenol. *Appl. Surf. Sci.* **2012**, *258*, 2717–2723.
[193] Kokate, M.; Garadkar, K.; Gole, A. Zinc-oxide-silica-silver nanocomposite: Unique one-pot synthesis and enhanced catalytic and anti-bacterial performance. *J. Colloid Interface Sci.* **2016**, *483*, 249–260.
[194] Moon, H. R.; Lim, D. W.; Suh, M. P. Fabrication of metal nanoparticles in metal-organic frameworks. *Chem. Soc. Rev.* **2013**, *42*, 1807–1824.
[195] Rösler, C.; Fischer, R. A. Metal–organic frameworks as hosts for nanoparticles. *CrystEngComm* **2015**, *17*, 199–217.
[196] Yang, Q. H.; Xu, Q.; Jiang, H. L. Metal-organic frameworks meet metal nanoparticles: Synergistic effect for enhanced catalysis. *Chem. Soc. Rev.* **2017**, *46*, 4774–4808.
[197] Gu, X. J.; Lu, Z. H.; Jiang, H. L.; Akita, T.; Xu, Q. Synergistic catalysis of metal-organic framework-immobilized Au-Pd nanoparticles in dehydrogenation of formic acid for chemical hydrogen storage. *J. Am. Chem. Soc.* **2011**, *133*, 11822–11825.
[198] Islam, D. A.; Chakraborty, A.; Acharya, H. Fluorescent silver nanoclusters (Ag NCs) in the metal–organic framework MIL-101(Fe) for the catalytic hydrogenation of 4-nitroaniline. *New J. Chem.* **2016**, *40*, 6745–6751.
[199] Janiak, C.; Vieth, J. K. MOFs, MILs and more: Concepts, properties and applications for porous coordination networks (PCNs). *New J. Chem.* **2010**, *34*, 2366–2388.
[200] Zhang, L.; Wu, H. B.; Madhavi, S.; Hng, H. H.; Lou, X. W. Formation of Fe_2O_3 microboxes with hierarchical shell structures from metal-organic frameworks and their lithium storage properties. *J. Am. Chem. Soc.* **2012**, *134*, 17388–17391.
[201] Jiang, Z. F.; Jiang, D. L.; Showkot Hossain, A. M.; Qian, K.; Xie, J. M. *In situ* synthesis of silver supported nanoporous iron oxide microbox hybrids from metal-organic frameworks and their catalytic application in p-nitrophenol reduction. *Phys. Chem. Chem. Phys.* **2015**, *17*, 2550–2559.
[202] Rogge, S. M. J.; Bavykina, A.; Hajek, J.; Garcia, H.; Olivos-Suarez, A. I.; Sepúlveda-Escribano, A.; Vimont, A.; Clet, G.; Bazin, P.; Kapteijn, F. et al. Metal-organic and covalent organic frameworks as single-site catalysts. *Chem. Soc. Rev.* **2017**, *46*, 3134–3184.
[203] Wu, D. C.; Xu, F.; Sun, B.; Fu, R. W.; He, H. K.; Matyjaszewski, K. Design and preparation of porous polymers. *Chem. Rev.* **2012**, *112*, 3959–4015.
[204] Li, Q.; Liao, G. F.; Zhang, S. L.; Pang, L.; Tong, H.; Zhao, W. Z.; Xu, Z. S. Effect of adjustable molecular chain structure and pure silica zeolite nanoparticles on thermal, mechanical, dielectric, UV-shielding and hydrophobic properties of fluorinated copolyimide composites. *Appl. Surf. Sci.* **2018**, *427*, 437–450.
[205] Zeng, W. G.; Chen, J.; Yang, H.; Deng, L. D.; Liao, G. F.; Xu, Z. S. Robust coating with superhydrophobic and self-cleaning properties in either air or oil based on natural zeolite. *Surf. Coat. Technol.* **2017**, *309*, 1045–1051.
[206] Davis, M. E. Ordered porous materials for emerging applications. *Nature* **2002**, *417*, 813–821.
[207] Das, S.; Heasman, P.; Ben, T.; Qiu, S. L. Porous organic materials: Strategic design and structure-function correlation. *Chem. Rev.* **2017**, *117*, 1515–1563.
[208] Wang, R.; Gu, L. N.; Zhou, J. J.; Liu, X. L.; Teng, F.; Li, C. H.; Shen, Y. H.; Yuan, Y. P. Quasi-polymeric metal-organic framework UiO-66/g-C_3N_4 heterojunctions for enhanced photocatalytic hydrogen evolution under visible light irradiation. *Adv. Mater. Interfaces* **2015**, *2*, 1500037.
[209] Hasell, T.; Wood, C. D.; Clowes, R.; Jones, J. T. A.; Khimyak, Y. Z.; Adams, D. J.; Cooper, A. I. Palladium nanoparticle incorporation in conjugated microporous polymers by supercritical fluid processing. *Chem. Mater.* **2010**, *22*, 557–564.
[210] Cao, H. L.; Huang, H. B.; Chen, Z.; Karadeniz, B.; Lü, J.; Cao, R. Ultrafine silver nanoparticles supported on a conjugated microporous polymer as high-performance nanocatalysts for nitrophenol reduction. *ACS Appl. Mater. Interfaces* **2017**, *9*, 5231–5236.
[211] Waller, P. J.; Gándara, F.; Yaghi, O. M. Chemistry of covalent organic frameworks. *Acc. Chem. Res.* **2015**, *48*, 3053–3063.
[212] Shi, X. F.; Yao, Y. J.; Xu, Y. L.; Liu, K.; Zhu, G. S.; Chi, L. F.; Lu, G. Imparting catalytic activity to a covalent organic framework material by nanoparticle encapsulation. *ACS Appl. Mater. Interfaces* **2017**, *9*, 7481–7488.
[213] da Silva, A. G. M.; Rodrigues, T. S.; Wang, J. L.; Yamada, L. K.; Alves, T. V.; Ornellas, F. R.; Ando, R. A.; Camargo, P. H. C. The fault in their shapes: Investigating the surface-plasmon-resonance-mediated catalytic activities of silver quasi-spheres, cubes, triangular prisms, and wires. *Langmuir* **2015**, *31*, 10272–10278.
[214] Sadeghi, B.; Sadjadi, M. A. S.; Vahdati, R. A. R. Nanoplates controlled synthesis and catalytic activities of silver nanocrystals. *Superlattices Microstruct.* **2009**, *46*, 858–863.
[215] Maiyalagan, T. Synthesis, characterization and electrocatalytic activity of silver nanorods towards the reduction of benzyl chloride. *Appl. Catal. A Gen.* **2008**, *340*, 191–195.
[216] Kim, B. H.; Lee, J. S. One-pot photochemical synthesis of silver nanodisks using a conventional metal-halide lamp. *Mater. Chem. Phys.* **2015**, *149–150*, 678–685.
[217] Miao, Y. E.; Lee, H. K.; Chew, W. S.; Phang, I. Y.; Liu, T. X.; Ling, X. Y. Catalytic liquid marbles: Ag nanowire-based miniature reactors for

highly efficient degradation of methylene blue. *Chem. Commun.* **2014**, *50*, 5923–5926.
[218] Zhang, W.; Tan, F. T.; Wang, W.; Qiu, X. L.; Qiao, X. L.; Chen, J. G. Facile, template-free synthesis of silver nanodendrites with high catalytic activity for the reduction of p-nitrophenol. *J. Hazard. Mater.* **2012**, *217–218*, 36–42.
[219] Wei, G. D.; Nan, C. W.; Deng, Y.; Lin, Y. H. Self-organized synthesis of silver chainlike and dendritic nanostructures via a solvothermal method. *Chem. Mater.* **2003**, *15*, 4436–4441.
[220] Wen, X. G.; Xie, Y. T.; Mak, M. W.; Cheung, K. Y.; Li, X. Y.; Renneberg, R.; Yang, S. H. Dendritic nanostructures of silver: Facile synthesis, structural characterizations, and sensing applications. *Langmuir* **2006**, *22*, 4836–4842.
[221] Rashid, M. H.; Mandal, T. K. Synthesis and catalytic application of nanostructured silver dendrites. *J. Phys. Chem. C* **2007**, *111*, 16750–16760.
[222] Takahashi, M.; Mohan, P.; Nakade, A.; Higashimine, K.; Mott, D.; Hamada, T.; Matsumura, K.; Taguchi, T.; Maenosono, S. Ag/FeCo/Ag core/shell/shell magnetic nanoparticles with plasmonic imaging capability. *Langmuir* **2015**, *31*, 2228–2236.
[223] Mahmoud, M. A.; El-Sayed, M. A. Metallic double shell hollow nanocages: The challenges of their synthetic techniques. *Langmuir* **2012**, *28*, 4051–4059.
[224] Weng, G. J.; Mahmoud, M. A.; El-Sayed, M. A. Nanocatalysts can change the number of electrons involved in oxidation–reduction reaction with the nanocages being the most efficient. *J. Phys. Chem. C* **2012**, *116*, 24171–24176.
[225] Mahmoud, M. A.; El-Sayed, M. A. Time dependence and signs of the shift of the surface plasmon resonance frequency in nanocages elucidate the nanocatalysis mechanism in hollow nanoparticles. *Nano Lett.* **2011**, *11*, 946–953.
[226] Sun, Y. G.; Xia, Y. N. Shape-controlled synthesis of gold and silver nanoparticles. *Science* **2002**, *298*, 2176–2179.
[227] Mahmoud, M. A.; Narayanan, R.; El-Sayed, M. A. Enhancing colloidal metallic nanocatalysis: Sharp edges and corners for solid nanoparticles and cage effect for hollow ones. *Acc. Chem. Res.* **2013**, *46*, 1795–1805.
[228] Min, J. Z.; Wang, F.; Cai, Y. L.; Liang, S.; Zhang, Z. W.; Jiang, X. M. Azeotropic distillation assisted fabrication of silver nanocages and their catalytic property for reduction of 4-nitrophenol. *Chem. Commun.* **2015**, *51*, 761–764.
[229] Vadakkekara, R.; Chakraborty, M.; Parikh, P. A. Reduction of aromatic nitro compounds on colloidal hollow silver nanospheres. *Colloids Surf. A* **2012**, *399*, 11–17.
[230] Chng, L. L.; Erathodiyil, N.; Ying, J. Y. Nanostructured catalysts for organic transformations. *Acc. Chem. Res.* **2013**, *46*, 1825–1837.
[231] Liao, F. L.; Lo, T. W. B.; Tsang, S. C. E. Recent developments in palladium-based bimetallic catalysts. *ChemCatChem* **2015**, *7*, 1998–2014.
[232] Kaiser, J.; Leppert, L.; Welz, H.; Polzer, F.; Wunder, S.; Wanderka, N.; Albrecht, M.; Lunkenbein, T.; Breu, J.; Kümmel, S. et al. Catalytic activity of nanoalloys from gold and palladium. *Phys. Chem. Chem. Phys.* **2012**, *14*, 6487–6495.
[233] Jang, H. J.; Min, D. H. Spherically-clustered porous Au-Ag alloy nanoparticle prepared by partial inhibition of galvanic replacement and its application for efficient multimodal therapy. *ACS Nano* **2015**, *9*, 2696–2703.
[234] Zhang, J. W.; Winget, S. A.; Wu, Y. R.; Su, D.; Sun, X. J.; Xie, Z. X.; Qin, D. Ag@Au concave cuboctahedra: A unique probe for monitoring Au-catalyzed reduction and oxidation reactions by surface-enhanced Raman spectroscopy. *ACS Nano* **2016**, *10*, 2607–2616.
[235] Liu, H. L.; Nosheen, F.; Wang, X. Noble metal alloy complex nanostructures: Controllable synthesis and their electrochemical property. *Chem. Soc. Rev.* **2015**, *44*, 3056–3078.
[236] Sun, Y. G.; Xia, Y. N. Mechanistic study on the replacement reaction between silver nanostructures and chloroauric acid in aqueous medium. *J. Am. Chem. Soc.* **2004**, *126*, 3892–3901.
[237] Papagiannouli, I.; Aloukos, P.; Rioux, D.; Meunier, M.; Couris, S. Effect of the composition on the nonlinear optical response of Au_xAg_{1-x} nano-alloys. *J. Phys. Chem. C* **2015**, *119*, 6861–6872.
[238] Mallin, M. P.; Murphy, C. J. Solution-phase synthesis of sub-10 nm Au−Ag alloy nanoparticles. *Nano Lett.* **2002**, *2*, 1235–1237.
[239] Cortie, M. B.; McDonagh, A. M. Synthesis and optical properties of hybrid and alloy plasmonic nanoparticles. *Chem. Rev.* **2011**, *111*, 3713–3735.
[240] Rajendra, R.; Bhatia, P.; Justin, A.; Sharma, S.; Ballav, N. Homogeneously-alloyed gold–silver nanoparticles as per feeding moles. *J. Phys. Chem. C* **2015**, *119*, 5604–5613.
[241] Choi, Y.; Hong, S.; Liu, L. C.; Kim, S. K.; Park, S. Galvanically replaced hollow Au-Ag nanospheres: Study of their surface plasmon resonance. *Langmuir* **2012**, *28*, 6670–6676.
[242] Wu, H. X.; Wang, P.; He, H. L.; Jin, Y. D. Controlled synthesis of porous Ag/Au bimetallic hollow nanoshells with tunable plasmonic and catalytic properties. *Nano Res.* **2012**, *5*, 135–144.
[243] Liu, R. X.; Guo, J. H.; Ma, G.; Jiang, P.; Zhang, D. H.; Li, D. X.; Chen, L.; Guo, Y. T.; Ge, G. L. Alloyed crystalline Au-Ag hollow nanostructures with high chemical stability and catalytic performance. *ACS Appl. Mater. Interfaces* **2016**, *8*, 16833–16844.
[244] Roh, J.; Back, S. H.; Ahn, D. J. Shape-persistent replica synthesis of gold/silver bimetallic nanoplates using tailored silica cages. *Small* **2016**, *12*, 1322–1327.
[245] Xia, B. H.; He, F.; Li, L. D. Preparation of bimetallic nanoparticles using a facile green synthesis method and their application. *Langmuir* **2013**, *29*, 4901–4907.
[246] Lee, J.; Han, K.; Jang, D. J. Silica-coated silver/gold composite nanoboxes having enhanced catalytic performances and reusability. *Appl. Catal. A Gen.* **2014**, *469*, 380–386.
[247] Wang, Y.; Wang, X. C.; Antonietti, M. Polymeric graphitic carbon nitride as a heterogeneous organocatalyst: From photochemistry to multipurpose catalysis to sustainable chemistry. *Angew. Chem., Int. Ed.* **2012**, *51*, 68–89.
[248] Niknafs, Y.; Amirjani, A.; Marashi, P.; Fatmehsari, D. H. Synthesis of Ag-Cu and Ag-Cu_2O alloy nanoparticles using a seed-mediated polyol process, thermodynamic and kinetic aspects. *Mater. Chem. Phys.* **2017**, *189*, 44–49.
[249] Wu, W.; Lei, M.; Yang, S. L.; Zhou, L.; Liu, L.; Xiao, X. H.; Jiang, C. Z.; Roy, V. A. L. A one-pot route to the synthesis of alloyed Cu/Ag bimetallic nanoparticles with different mass ratios for catalytic reduction of 4-nitrophenol. *J. Mater. Chem. A* **2015**, *3*, 3450–3455.
[250] Jin, M. S.; Zhang, H.; Wang, J. G.; Zhong, X. L.; Lu, N.; Li, Z. Y.; Xie, Z. X.; Kim, M. J.; Xia, Y. N. Copper can still be epitaxially deposited on palladium nanocrystals to generate core-shell nanocubes despite their large lattice mismatch. *ACS Nano* **2012**, *6*, 2566–2573.
[251] Jin, M. S.; He, G. N.; Zhang, H.; Zeng, J.; Xie, Z. X.; Xia, Y. N. Shape-controlled synthesis of copper nanocrystals in an aqueous solution with glucose as a reducing agent and hexadecylamine as a capping agent. *Angew. Chem., Int. Ed.* **2011**, *50*, 10560–10564.
[252] Sevonkaev, I. V.; Herein, D.; Jeske, G.; Goia, D. V. Size control of noble metal clusters and metallic heterostructures through the reduction kinetics of metal precursors. *Nanoscale* **2014**, *6*, 9614–9617.
[253] Verma, A. D.; Pal, S.; Verma, P.; Srivastava, V.; Mandal, R. K.; Sinha, I. Ag-Cu bimetallic nanocatalysts for p-nitrophenol reduction using a green hydrogen source. *J. Environ. Chem. Eng.* **2017**, *5*, 6148–6155.
[254] Jiang, H. L.; Akita, T.; Ishida, T.; Haruta, M.; Xu, Q. Synergistic catalysis of Au@Ag core-shell nanoparticles stabilized on metal-organic framework. *J. Am. Chem. Soc.* **2011**, *133*, 1304–1306.
[255] Chuntonov, L.; Bar-Sadan, M.; Houben, L.; Haran, G. Correlating electron tomography and plasmon spectroscopy of single noble metal core-shell nanoparticles. *Nano Lett.* **2012**, *12*, 145–150.
[256] Liu, Y. T.; Zhou, J.; Wang, B. B.; Jiang, T.; Ho, H. P.; Petti, L.; Mormile, P. Au@Ag core-shell nanocubes: Epitaxial growth synthesis and surface-enhanced Raman scattering performance. *Phys. Chem. Chem. Phys.* **2015**, *17*, 6819–6826.
[257] Wang, R. J.; Yao, Y. F.; Shen, M.; Wang, X. S. Green synthesis of Au@Ag nanostructures through a seed-mediated method and their application in SERS. *Colloids Surf. A* **2016**, *492*, 263–272.
[258] Liu, F. K.; Huang, P. W.; Chang, Y. C.; Ko, F. H.; Chu, T. C. Combining optical lithography with rapid microwave heating for the selective growth of Au/Ag bimetallic core/shell structures on patterned silicon wafers. *Langmuir* **2005**, *21*, 2519–2525.
[259] Xue, C.; Millstone, J. E.; Li, S. Y.; Mirkin, C. A. Plasmon-driven synthesis of triangular core–shell nanoprisms from gold seeds. *Angew. Chem., Int. Ed.* **2007**, *46*, 8436–8439.
[260] Yoo, H.; Millstone, J. E.; Li, S. Z.; Jang, J. W.; Wei, W.; Wu, J. S.; Schatz, G. C.; Mirkin, C. A. Core-shell triangular bifrustums. *Nano Lett.* **2009**, *9*, 3038–3041.
[261] Wilson, O. M.; Scott, R. W.; Garcia-Martinez, J. C.; Crooks, R. M. Synthesis, characterization, and structure-selective extraction of 1–3-nm diameter AuAg dendrimer-encapsulated bimetallic nanoparticles. *J. Am.*

Chem. *Soc*. **2005**, *127*, 1015–1024.

[262] Tsao, Y. C.; Rej, S.; Chiu, C. Y.; Huang, M. H. Aqueous phase synthesis of Au-Ag core-shell nanocrystals with tunable shapes and their optical and catalytic properties. *J*. *Am*. *Chem*. *Soc*. **2014**, *136*, 396–404.

[263] Haldar, K. K.; Kundu, S.; Patra, A. Core-size-dependent catalytic properties of bimetallic Au/Ag core-shell nanoparticles. *ACS Appl*. *Mater*. *Interfaces* **2014**, *6*, 21946–21953.

[264] Li, T.; Chattopadhyay, S.; Shibata, T.; Cook, R. E.; Miller, J. T.; Suthiwangcharoen, N.; Lee, S.; Winans, R. E.; Lee, B. Synthesis and characterization of Au-core Ag-shell nanoparticles from unmodified apoferritin. *J*. *Mater*. *Chem*. **2012**, *22*, 14458–14464.

[265] Monga, A.; Pal, B. Improved catalytic activity and surface electro-kinetics of bimetallic Au–Ag core–shell nanocomposites. *New J*. *Chem*. **2015**, *39*, 304–313.

[266] Zhang, X.; Su, Z. H. Polyelectrolyte-multilayer-supported Au@Ag core-shell nanoparticles with high catalytic activity. *Adv*. *Mater*. **2012**, *24*, 4574–4577.

[267] Zhou, J. J.; Duan, B.; Fang, Z.; Song, J. B.; Wang, C. X.; Messersmith, P. B.; Duan, H. W. Interfacial assembly of mussel-inspired Au@Ag@ polydopamine core-shell nanoparticles for recyclable nanocatalysts. *Adv*. *Mater*. **2014**, *26*, 701–705.

[268] Gilroy, K. D.; Ruditskiy, A.; Peng, H. C.; Qin, D.; Xia, Y. N. Bimetallic nanocrystals: Syntheses, properties, and applications. *Chem*. *Rev*. **2016**, *116*, 10414–10472.

[269] Huang, J. F.; Vongehr, S.; Tang, S. C.; Lu, H. M.; Shen, J. C.; Meng, X. K. Ag dendrite-based Au/Ag bimetallic nanostructures with strongly enhanced catalytic activity. *Langmuir* **2009**, *25*, 11890–11896.

[270] Huang, J. F.; Vongehr, S.; Tang, S. C.; Lu, H. M.; Meng, X. K. Highly catalytic Pd–Ag bimetallic dendrites. *J*. *Phys*. *Chem*. *C* **2010**, *114*, 15005–15010.

[271] Kim, M.; Lee, K. Y.; Jeong, G. H.; Jang, J.; Han, S. W. Fabrication of Au–Ag alloy nanoprisms with enhanced catalytic activity. *Chem*. *Lett*. **2007**, *36*, 1350–1351.

[272] Jing, H.; Wang, H. Structural evolution of Ag–Pd bimetallic nanoparticles through controlled galvanic replacement: Effects of mild reducing agents. *Chem*. *Mater*. **2015**, *27*, 2172–2180.

[273] Zheng, T. T.; Zhang, Q. F.; Feng, S.; Zhu, J. J.; Wang, Q.; Wang, H. Robust nonenzymatic hybrid nanoelectrocatalysts for signal amplification toward ultrasensitive electrochemical cytosensing. *J*. *Am*. *Chem*. *Soc*. **2014**, *136*, 2288–2291.

[274] Zhang, W. Q.; Yang, J. Z.; Lu, X. M. Tailoring galvanic replacement reaction for the preparation of Pt/Ag bimetallic hollow nanostructures with controlled number of voids. *ACS Nano* **2012**, *6*, 7397–7405.

[275] Popa, A.; Samia, A. C. S. Effect of metal precursor on the growth and electrochemical sensing properties of Pt-Ag nanoboxes. *Chem*. *Commun*. **2014**, *50*, 7295–7298.

[276] Chen, C.; Kang, Y. J.; Huo, Z. Y.; Zhu, Z. W.; Huang, W. Y.; Xin, H. L.; Snyder, J. D.; Li, D. G.; Herron, J. A.; Mavrikakis, M. et al. Highly crystalline multimetallic nanoframes with three-dimensional electrocatalytic surfaces. *Science* **2014**, *343*, 1339–1343.

[277] Mahmoud, M. A.; Garlyyev, B.; El-Sayed, M. A. Controlling the catalytic efficiency on the surface of hollow gold nanoparticles by introducing an inner thin layer of platinum or palladium. *J*. *Phys*. *Chem*. *Lett*. **2014**, *5*, 4088–4094.

[278] Fang, Z. C.; Wang, Y. C.; Liu, C. X.; Chen, S.; Sang, W.; Wang, C.; Zeng, J. Rational design of metal nanoframes for catalysis and plasmonics. *Small* **2015**, *11*, 2593–2605.

[279] Snyder, J.; Livi, K.; Erlebacher, J. Oxygen reduction reaction performance of [MTBD][beti]-encapsulated nanoporous NiPt alloy nanoparticles. *Adv*. *Funct*. *Mater*. **2013**, *23*, 5494–5501.

[280] Xia, Y. N.; Yang, X. Toward cost-effective and sustainable use of precious metals in heterogeneous catalysts. *Acc*. *Chem*. *Res*. **2017**, *50*, 450–454.

[281] Li, J. M.; Liu, J. Y.; Yang, Y.; Qin, D. Bifunctional Ag@Pd-Ag nanocubes for highly sensitive monitoring of catalytic reactions by surface-enhanced Raman spectroscopy. *J*. *Am*. *Chem*. *Soc*. **2015**, *137*, 7039–7042.

[282] Li, J. M.; Sun, X. J.; Qin, D. Ag-enriched Ag-Pd bimetallic nanoframes and their catalytic properties. *ChemNanoMat* **2016**, *2*, 494–499.